A STUDY OF VIBRATION-INDUCED FRETTING CORROSION FOR

ELECTRICAL CONNECTORS

Except where reference is made to the work of others, the work described in this dissertation is my own or was done in collaboration with my advisory committee. This dissertation does not include proprietary or classified information

_____

Fei Xie

Certificate of Approval:

_____	_____
George T. Flowers, Co-Chair Alumni Professor Mechanical Engineering	R. Wayne Johnson, Co-Chair Ginn Professor Electrical and Computer Engineering
_____	_____
Thomas A. Baginski Professor Electrical and Computer Engineering	John L. Evans Associate Professor Industry and Systems Engineering

_____

Joe F. Pittman
Interim Dean
Graduate School

A STUDY OF VIBRATION-INDUCED FRETTING CORROSION FOR ELECTRICAL CONNECTORS

Fei Xie

A Dissertation

Submitted to

the Graduate Faculty of

Auburn University

in Partial Fulfillment of the

Requirements for the

Degree of

Doctor of Philosophy

Auburn, Alabama
May 10, 2007

A STUDY OF VIBRATION-INDUCED FRETTING CORROSION FOR

ELECTRICAL CONNECTORS

Fei Xie

Permission is granted to Auburn University to make copies of this dissertation at its discretion, upon request of individuals or institutions and at their expense. The author reserves all publication rights.

_____

Signature of Author

_____

Date of Graduation

VITA

Fei Xie, son of Zuogui Xie and Xiane Zhan, was born on February 5, 1968, in Hubei province, China. He entered the Beijing University of Aeronautics and Astronautics, Beijing, China, in September 1986 and four years later, he graduated with a Bachelor of Science degree in Electrical Engineering. He then worked in Beijing as an electrical engineer at the Institute of Railway Science from July 1990 to March 1993 and Beijing University of Aeronautics and Astronautics from April 1993 to August 1997. He entered the Graduate School of Beijing University of Aeronautics and Astronautics in September 1997 and graduated with a Master of Science degree in Systems Reliability Engineering in May 2000. In May 2002, he entered the Graduate School of Auburn University to work towards the degrees of Master of Science and Doctor of Philosophy in Electrical and Computer Engineering. He married Ying Jiang, daughter of Zixiong Jiang and Guizhi Yan, on April 22, 1997. Fei Xie and Ying Jiang have a son, Ramon P. Xie, who was born in Auburn on March 6, 2002.

DISSERTATION ABSTRACT

A STUDY OF VIBRATION-INDUCED FRETTING CORROSION FOR ELECTRICAL CONNECTORS

Fei Xie

Doctor of Philosophy, May 10, 2007
(M.S., Auburn University, 2003)
(M.S., Beijing University of Aeronautics and Astronautics, 2000)
(B.S., Beijing University of Aeronautics and Astronautics, 1990)

188 Typed Pages

Directed by George T. Flowers and R. Wayne Johnson

Vibration induced fretting degradation is a widely recognized failure phenomenon. However, the basic mechanisms that control the onset and progression of such fretting behavior are not well understood and are a topic of considerable interest in the electrical connector community. In this dissertation, four research projects on this topic are described.

The first two projects examined the physical characteristics of vibration-induced fretting corrosion and focused on PC-type connectors and automotive-type connectors respectively. The influence of connector design, wire tie-off length, vibration profile, and lubrication were considered. It was found that both connector designs exhibited self-

consistent relative displacement amplitude thresholds for the onset of fretting corrosion regardless of the excitation frequency. Also, there was a general linear dependency upon the g-level with regard to fretting rates for single frequency excitation. A mathematical model was developed that related the early stage fretting corrosion rate to the threshold vibration levels for the connectors. Additionally, a connector lubricant was tested and observed to inhibit fretting over the amplitude and frequency ranges, as expected.

The third project examined the influence of normal force and finish characteristics for vibration-induced fretting degradation. Two finish types and three normal force levels for each finish type were considered, with the objective of determining which created a larger fretting degradation. Once again, a threshold vibration level and a linear fashion resistance change of fretting were found. The relative motion transfer function was also shown to provide a good measure of the tendency to fret. Finally, a comparison of the fretting performance between two commercial connectors was performed as an application of this fretting study.

The fourth and final project considered the application of FEA simulation techniques to the prediction of vibration-induced fretting degradation. A single blade/receptacle contact pair was analyzed both experimentally and with an FEA model. The same transfer functions for one type of contact pair were obtained from both simulation and experiment, and the same x-axis relative motions were observed in the simulation when the threshold fretting displacements from the experiment were used. Generally, the results from the simulation matched those from the experiment very well. The results showed that for this limited system, finite element modeling and analysis have great potential for evaluating the influence of design variations on fretting behavior.

ACKNOWLEDGEMENTS

The author would like to express his deep appreciation and sincere thanks to his co-advisors, Dr. George T. Flowers, Department of Mechanical Engineering, and Dr. R. Wayne Johnson, Department of Electrical and Computer Engineering, for their instruction, guidance, encouragement and patience in the completion of this research and dissertation. Their advice has been invaluable and their suggestions and exchanges of ideas have contributed immensely to this dissertation.

Thanks are also extended to the other advisory committee members, Dr. Thomas A. Baginski, professor, Department of Electrical and Computer Engineering, and Dr. John L. Evans, associate professor, Department of Industry and Systems Engineering, for their academic guidance, time and generous assistance.

The author also thanks his friends, Dr. Roland Horvath and Dr. Xin Hai, for their help during this research.

Finally, the author would like to thank his wife, Ying Jiang, and other family members, for their consideration, support and patience during the completion of this degree (Doctor of Philosophy in Electrical and Computer Engineering) at Auburn University.

Style manual or journal used: Auburn University Guide to Preparation and Submission of Thesis and Dissertation, and Transactions of the Institute of Electrical and Electronics Engineers

Computer software used: Microsoft Word 2003, MATLAB 7.0 and ANSYS 9.0

TABLE OF CONTENTS

LIST OF FIGURES……xiii

LIST OF TABLES……xix

CHAPTER 1 INTRODUCTION AND LITERATURE REVIEW 1

1.1 Fretting Corrosion 1

1.2 Mechanism of Fretting Corrosion 3

1.3 Literature Review of Fretting Corrosion in Electrical Contacts 4

1.4 Overview of Current Work 12

CHAPTER 2 A STUDY OF THE PHYSICAL CHARACTERISTICS OF VIBRATION-INDUCED FRETTING CORROSION 14

2.1 Purpose of This Study 14

2.2 Description of Experimental Testing 16

2.2.1 Experimental Samples 16

2.2.2 Experimental Equipment 18

2.2.2.1 KEITHLEY Model 2010 Multimeter 19

2.2.2.2 HP 35665A Dynamic Signal Analyzer 19

2.2.2.3 POLYTEC Laser Vibrometer 20

2.2.2.4 Vibration System 21

2.2.3 Experimental Setup 23

2.3 Test Results 25

2.3.1 PC Connector 26
2.3.1.1 Short Tie-off Configuration 26
2.3.1.2 Middle Tie-off Configuration 29
2.3.1.3 Long Tie-off Configuration 31
2.3.1.4 Transfer Function and Relative Motion 33
2.3.2 Automotive Connector 39
2.3.2.1 Middle tie-off Configuration 39
2.3.2.2 Long-Cable Configuration 41
2.3.2.3 Transfer Function and Relative Motion 44
2.3.3 Lubricated Connector 46
2.4 Result Analysis 49
2.5 Modeling the Early Stage Fretting Rate 53
2.6 Summary and Conclusions 57
CHAPTER 3 THE INFLUENCE OF CONTACT INTERFACE CHARACTERISTICS ON VIBRATION-INDUCED FRETTING DEGRADATION 60
3.1 Purpose of This Study 60
3.2 Experimental Details 62
3.2.1 Experimental Samples 62
3.2.2 Experimental Equipment 66
3.2.3 Experimental Setup 71
3.3 Experimental Result and Analysis 75
3.4 Summary and Conclusions 85

CHAPTER 4 THE APPLICATION OF FEA SIMULATION TECHNIQUES TO THE PREDICTION OF VIBRATION-INDUCED FRETTING DEGRADATION: ANALYSIS OF A BLADE/RECEPTACLE PAIR... 87
4.1 Introduction to This Study ... 87
4.2 Experimental Description ... 89
4.2.1 Experimental Samples ... 89
4.2.2 Experimental Equipment ... 90
4.2.3 Electromagnetic Interference During Resistance Measurements ... 90
4.2.4 Experimental Setup ... 94
4.3 Experimental Results ... 97
4.4 Generation of the FEA Model ... 103
4.4.1 Geometric model ... 104
4.4.2 Material Properties ... 106
4.4.3 Meshing ... 107
4.4.4 Creating the Contact Pair ... 108
4.4.5 Boundary Conditions ... 109
4.5 Vibration Process Simulation ... 111
4.6 FEA Simulation Results and Comparison with the Experimental Results ... 113
4.7 Summary and Conclusions ... 123
CHAPTER 5 CONCLUSIONS AND FUTURE WORK ... 125
REFERENCES ... 128
APPENDIX A MATLAB CODE EXAMPLE FOR REGRESSING THE EARLY-STAGE FRETTING CURVES ... 135

APPENDIX B MATLAB CODE EXAMPLE FOR CALCULATING THE TRANSFER FUNCTIONS AND RELATIVE MOTIONS 138

APPENDIX C ANSYS LOG FILE FOR GENERATING THE FEA MODEL OF THE BLADE/RECEPTACLE PAIR..... 141

APPENDIX D ANSYS LOG FILE FOR THE TRANSIENT ANALYSIS OF THE FEA MODEL 165

APPENDIX E ANSYS LOG FILE FOR THE HARMONIC ANALYSIS OF THE FEA MODEL 167

LIST OF FIGURES

Figure 1-1 Idealized model of fretting action at a metallic surface 3

Figure 2-1 Photograph of the PC connector 16

Figure 2-2 Modified PC connector allowing visual access near the contact interface 17

Figure 2-3 Photograph of the original automotive connector 18

Figure 2-4 Modified automotive connector used in the study 18

Figure 2-5 Four-wire resistance measurements 19

Figure 2-6 HP 35665A Dynamic Signal Analyzer 20

Figure 2-7 POLYTEC Laser Vibrometer 21

Figure 2-8 Typical Vibration System 22

Figure 2-9 PA 500L Amplifier 23

Figure 2-10 V408 Shaker 23

Figure 2-11 PC connector vibration setup for middle tie-off configuration 24

Figure 2-12 Automotive connector vibration setup for short tie-off configuration 24

Figure 2-13 Measurement of the frequency response of displacement 25

Figure 2-14 Typical fretting curves in sine vibration test 26

Figure 2-15 PC connector resistance change for 20 Hz, short tie-off configuration 27

Figure 2-16 PC connector resistance change for 30 Hz, short tie-off configuration 27

Figure 2-17 PC connector resistance change for 40 Hz, short tie-off configuration 28

Figure 2-18 PC connector resistance change for 200 Hz, short tie-off configuration 28

Figure 2-19 Summary of early stage fretting for short tie-off, PC connector..... 29

Figure 2-20 PC connector resistance change for 50 Hz, middle tie-off configuration..... 30

Figure 2-21 PC connector resistance change for 100 Hz, middle tie-off configuration... 30

Figure 2-22 Summary of early stage fretting rates for middle tie-off, PC connector..... 31

Figure 2-23 PC connector resistance change for 50 Hz, long tie-off configuration..... 32

Figure 2-24 PC connector resistance change for 200 Hz, long tie-off configuration..... 32

Figure 2-25 Summary of early stage fretting rates for long tie-off, PC connector..... 33

Figure 2-26 Relative motions between the plug housing and interface, PC short cable .. 34

Figure 2-27 Relative motions between the plug housing and interface, PC middle cable 35

Figure 2-28 Relative motions between the plug housing and interface, PC long cable ... 35

Figure 2-29 Transfer functions over a long frequency range for three tie-off cables..... 37

Figure 2-30 Relative motions over a long frequency range for three tie-off cables..... 37

Figure 2-31 PC relative displacement at interfaces to a constant g-level at the shaker head 38

Figure 2-32 Auto connector resistance change for 60 Hz, middle tie-off configuration.. 39

Figure 2-33 Auto connector resistance change for 110 Hz, middle tie-off configuration 40

Figure 2-34 Auto connector resistance change for 140 Hz, middle tie-off configuration 40

Figure 2-35 Summary of early stage fretting rates for middle tie-off, Auto connector.... 41

Figure 2-36 Auto connector resistance change for 50 Hz, long tie-off configuration..... 42

Figure 2-37 Auto connector resistance change for 100 Hz, long tie-off configuration.... 42

Figure 2-38 Auto connector resistance change for 140 Hz, long tie-off configuration.... 43

Figure 2-39 Summary of early stage fretting rates for long tie-off, Auto connector..... 43

Figure 2-40 Transfer function in 200Hz for three tie-off length, automotive connectors 44

Figure 2-41 Relative motion in 200Hz for three tie-off length, automotive connectors .. 45

Figure 2-42 Auto relative displacement at interfaces to a constant g-level at shaker head..... 45

Figure 2-43 Auto relative displacement at interfaces in 800Hz frequency range..... 46

Figure 2-44 Resistance change of un-lubricated samples for 50Hz, middle cable testing 47

Figure 2-45 Resistance change of lubricated samples for 50Hz, middle cable testing..... 47

Figure 2-46 Resistance change of un-lubricated samples for 30Hz, short cable testing .. 48

Figure 2-47 Resistance change of lubricated samples for 30Hz, short cable testing..... 48

Figure 2-48 Threshold displacement at the shaker head and the relative motion, PC short 52

Figure 2-49 Threshold displacement at the shaker head and relative motion, Auto middle 52

Figure 2-50 Threshold displacement at the shaker head and the relative motion, Auto long 53

Figure 2-51 Conceptual diagram for predicting vibration induced fretting corrosion..... 53

Figure 3-1 Original automotive sample 62

Figure 3-2 Automotive sample with viewing slots 64

Figure 3-3 Comparison of the effect of viewing slots on transfer function..... 64

Figure 3-4 A different connector from another manufacturer 66

Figure 3-5 Viewing slots in the comparison connector 66

Figure 3-6 LDS vibration test system 69

Figure 3-7 LDS 350 vibration shaker 70

Figure 3-8 DACTRON vibration control system and SPAK amplifier 70

Figure 3-9 Photograph of the experimental setup..... 71

Figure 3-10 Measurement of the transfer function 72

Figure 3-11 Transfer functions with or without supplementary mass 73

Figure 3-12 Ohmmeter reading with and without circuit loops in cable 73

Figure 3-13 Connector resistance measurement with circuit loops minimized 74

Figure 3-14 Setup for the unmodified Auto connector in the comparison experiment 75

Figure 3-15 Setup for the unmodified alternative connector in the comparison experiment 75

Figure 3-16 Transfer function for type 1 specimens..... 76

Figure 3-17 Transfer function for type 2 specimens..... 77

Figure 3-18 Relative motion function for type 1 specimens..... 77

Figure 3-19 Relative motion function for type 2 specimens..... 78

Figure 3-20 Threshold g-level for type 1 samples 79

Figure 3-21 Threshold g-level for type 2 samples 79

Figure 3-22 Fretting rate for type 1 samples..... 81

Figure 3-23 Fretting rate for type 2 samples..... 81

Figure 3-24 Relative threshold g-level as a function of normal force 82

Figure 3-25 SEM examination of the fretting degradation zone for type 1 receptacle..... 83

Figure 3-26 SEM examination of the fretting degradation zone for type 1 blade 83

Figure 3-27 Transfer functions for the automotive connector and the alternative connector..... 84

Figure 3-28 Relative motions for the automotive connector and the alternative connector..... 84

Figure 3-29 Fretting for the automotive connector and the alternative connector 85

Figure 4-1 photograph of the blade and receptacle..... 89

Figure 4-2 mated blade/receptacle pair..... 89

Figure 4-3 Method 1: sample setup for the electromagnetic interference test..... 91
Figure 4-4 Method 1: resistance measurement in the electromagnetic interference test.. 91
Figure 4-5 Method 2: sample setup for the electromagnetic interference test..... 92
Figure 4-6 Method 2: resistance measurement in the electromagnetic interference test.. 92
Figure 4-7 Comparison of the measured resistances for the two experimental setup 93
Figure 4-8 Photograph of the experimental setup for the blade/receptacle pair..... 94
Figure 4-9 Resistance measurement for the blade/receptacle pair..... 95
Figure 4-10 Transfer function measurement for the blade/receptacle pair..... 95
Figure 4-11 Measurement of the side-motion transfer function 96
Figure 4-12 Side-motion transfer function below 50Hz for the setup 97
Figure 4-13 Identification of the threshold displacement (or g-level)..... 98
Figure 4-14 Transfer function of type 1 and type 2 contact pairs with a 0.43mm gap..... 99
Figure 4-15 Transfer function of type 1 and type 2 contact pairs with a 0.48mm gap... 100
Figure 4-16 Transfer function of type 1 and type 2 contact pairs with a 0.53mm gap... 100
Figure 4-17 Relative motion of type 1 and type 2 contact pairs with a 0.53mm gap..... 101
Figure 4-18 Comparison of type 2 transfer functions for three gap widths..... 101
Figure 4-19 Relationship between the threshold displacement and the relative motion 103
Figure 4-20 Full geometric model 105
Figure 4-21 Blade/receptacle section of the geometric model..... 105
Figure 4-22 Meshed blade/receptacle model 108
Figure 4-23 Creating the contact pair 109
Figure 4-24 Boundary conditions for the model..... 110
Figure 4-25 Sinusoidal vibration excitation with the load substeps 110

Figure 4-26 Full model motion at time 1 during vibration 111

Figure 4-27 Full model motion at time 2 during vibration 112

Figure 4-28 Motion of the blade and the receptacle at time 1 112

Figure 4-29 Motion of the blade and the receptacle at time 2 113

Figure 4-30 Node locations for the transfer function simulation..... 114

Figure 4-31 Transfer functions for the 0.53mm gap contact pair from the simulation .. 115

Figure 4-32 Comparison of the transfer functions from the simulation and experiment 115

Figure 4-33 Simulated relative motion locations between the blade and the receptacle 116

Figure 4-34 Simulated X-axis relative motion at position 1..... 117

Figure 4-35 Simulated X-axis relative motion at position 2..... 118

Figure 4-36 Simulated X-axis relative motion at position 3..... 118

Figure 4-37 Simulated Y-axis relative motion at position 1..... 119

Figure 4-38 Simulated Y-axis relative motion at position 2..... 119

Figure 4-39 Simulated Y-axis relative motion at position 3..... 120

Figure 4-40 FFT analysis for the simulated X-axis relative motion at position2 120

Figure 4-41 Threshold displacement comparison between the simulation and experiment 121

Figure 4-42 Transfer function simulation for three kinds of gaps for type 2 contact pair..... 122

LIST OF TABLES

Table 2-1 Displacement decoder specification of the Laser vibrometer system 21

Table 2-2 Threshold vibration level at the shaker head for the PC short tie-off length ... 29

Table 2-3 Threshold vibration level at the shaker head for the PC middle tie-off length 31

Table 2-4 Threshold vibration level at the shaker head for the PC long tie-off length 33

Table 2-5 Threshold vibration level at the shaker head for the Auto middle tie-off length..... 41

Table 2-6 Threshold vibration level at the shaker head for the Auto long tie-off length . 44

Table 2-7 Product of $G_{threshold}$ and Relative Motion/ ω^2 for PC short tie-off length..... 50

Table 2-8 Product of $G_{threshold}$ and Relative Motion/ ω^2 for PC middle tie-off length 50

Table 2-9 Product of $G_{threshold}$ and Relative Motion/ ω^2 for PC long tie-off length 50

Table 2-10 Product of $G_{threshold}$ and Relative Motion/ ω^2 for Auto middle tie-off length 51

Table 2-11 Product of $G_{threshold}$ and Relative Motion/ ω^2 for Auto long tie-off length 51

Table 2-12 Modeling results for the PC-type connector in low frequencies 56

Table 2-13 Modeling results for the PC-type connector in higher frequencies..... 56

Table 2-14 Modeling results for the Automotive-type connector in low frequencies..... 57

Table 2-15 Modeling results for the Automotive-type connector in higher frequencies.. 57

Table 3-1 Types of Specimens..... 63

Table 3-2 Summary of fretting test results 80

Table 4-1 Threshold displacements for type1 and type2 (0.53mm gap) contact pair..... 99

Table 4-2 Relationship analysis for 0.53mm gap type 1 contact pair..... 102

Table 4-3 Relationship analysis for 0.53mm gap type 2 contact pair..... 102

Table 4-4 Thicknesses of the components in the geometry model..... 106

Table 4-5 Material properties of the components in the FEA model 107

CHAPTER 1 INTRODUCTION AND LITERATURE REVIEW

It is now well established that fretting corrosion is one of the major degradation mechanisms in electrical contacts. Much of the previous research work has focused on the causes of fretting corrosion, the mechanism of this phenomenon, and its prevention. In this dissertation, four research projects conducted by the author and concerned with the fretting corrosion of electrical connectors are described. Because the first two projects are related but the third and fourth are independent and separate, the first two projects are combined into one chapter and the other two projects are given a chapter each. The objectives and meaning of each project will be discussed in the introduction for each chapter. However, it is first necessary to pose the questions: What is meant by the term "fretting corrosion"? How does fretting corrosion happen and what is the mechanism of the fretting corrosion? And, what is the present status of research on this topic? This introductory material, as well as the major contents and structure of this dissertation, are discussed in turn in the following sections.

1.1 Fretting Corrosion

Fretting corrosion is a phenomenon that occurs because of mechanical stresses. In extreme cases it may lead to failure. It is defined as accelerated damage that occurs at the interface of two contacting surfaces, one or both being metal, that are subject to slight relative slip. Slip is usually a series of oscillatory movements, and can be produced by

mechanical vibrations, differential thermal expansion of the contacting metals, load relaxation, and junction heating as the power is switched on and off. Continuous slip, when one rolling surface moves slightly faster than another rolling surface in contacts, leads to a similar damage. Wear corrosion or friction oxidation are other terms that are sometimes applied to this kind of damage.

Damage due to fretting corrosion is characterized by discoloration of the metal surface and, in the case of oscillatory motion, by the formation of pits. It is at such pits on the surface of the material that fatigue cracks eventually nucleate. The rapid conversion of metal to metal oxide may in itself cause machines to malfunction, either because dimensional accuracy is lost or because corrosion products cause clogging or seizing.

Fretting corrosion is a frequent cause of failure of suspension springs, bolt and rivet heads, king pins in auto steering mechanisms, jewel bearings, variable-pitch propellers, shrink fits, contacts of electrical relays, connecting rods, and other parts of vibrating machinery. It may also cause discoloration of stacked metal sheets during shipment. One of the first documented examples of fretting corrosion was recognized when automobiles were being shipped some years ago by railroad from Detroit to the West Coast. Because of vibration, the ball-bearing races of the wheels became badly pitted by fretting corrosion, so that the automobiles were not operable on arrival. Damage was worse in winter than in summer, but could be avoided if the load on the wheels was relieved during shipment.

Laboratory experiments have shown that fretting corrosion of steel against steel requires oxygen but not moisture. Also, damage is less in moist air compared to dry air and is markedly less in a nitrogen atmosphere. Damage increases as the temperature

decreases, so the mechanism is clearly not electrochemical in nature. Increasing the load increases the damage. Fretting corrosion is also worsened by increased slip, provided the surface is not lubricated. Increases in frequency for the same number of cycles tend to decrease damage, but in nitrogen no frequency effect is observed [1].

1.2 Mechanism of Fretting Corrosion

When two surfaces touch, contact occurs only at relatively few sites, called asperities, where the surfaces protrude. Relative slip of the surfaces causes asperities on the surface to rub a clean track on the opposite surface. In the case of a metal, the track may oxidize superficially. The next asperity wipes off the oxide; or it may mechanically activate a reaction of adsorbed oxygen with the metal to form an oxide, which in turn is wiped off, forming another fresh metal track. Figure 1-1 shows such fretting action [1]. This is the chemical factor of fretting damage. In addition, asperities plow into the surface, causing a certain amount of wear by welding or shearing action due to metal particles rubbing against themselves or against adjacent surfaces. Also, the metal surface after an initial run-in period is fretted by oxide particles moving relative to the metal surface rather than by the mating opposite surface originally in contact. Hence, electrical resistance between the surfaces is at first low, then becomes high and remains so.

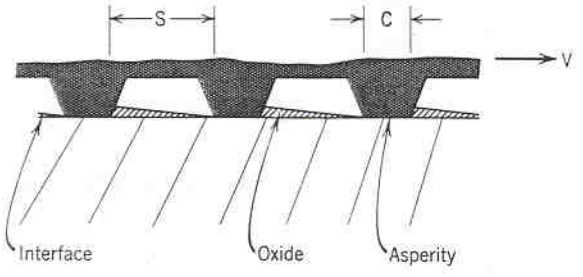

Figure 1-1 Idealized model of fretting action at a metallic surface

Some investigators have proposed that only small-size metallic particles are dislodged (worn off) during the fretting process and that these are subsequently oxidized spontaneously in air. However, the decreased damage in a nitrogen atmosphere, even if the surface is initially covered with oxide, and the lack of spontaneous oxidation of particles fretted in nitrogen and later exposed to air suggest that this mechanism does not apply.

Others have maintained that the high temperature produced by friction oxidizes the metal and the oxide is subsequently rubbed off. However, although local high temperatures are undoubtedly produced by friction, the damage caused by fretting is not solely a high-temperature oxidation phenomenon. This is demonstrated by the increased damage observed at below-room temperatures; by the reduction in damage at high frequencies, where surface temperatures are higher; by the fact that the oxide produced in the fretting corrosion of iron is αFe_2O_3 and not the high-temperature form Fe_3O_4; and finally, by the observation that steel is badly fretted in contact with polymethacrylate plastic, which melts at 80 °C. So the surface could have reached temperatures of this order, but no higher [2].

1.3 Literature Review of Fretting Corrosion in Electrical Contacts

Fretting corrosion is a common problem with significant practical importance, affecting a wide range of electrical and electronic equipment that contains costly components and leading to expensive replacements. However, the deleterious effect of fretting was not widely recognized as a serious factor in the degradation of electrical connections until 1974, when Bock and Whitley [3] clearly demonstrated its importance.

Since then, systematic studies of the phenomenon of fretting corrosion in electronic connectors have been conducted [4][5][6][7][8]. A comprehensive review of fretting corrosion was provided by Antler in 1984 [9], who systematically discussed the mechanisms such as transfer, wear, oxidation, and frictional polymerization that apply to the fretting of contacts; the effect of operational parameters such as the cycle rate and force on contact resistance change; a survey of materials whose fretting behavior has been characterized; and an analysis of the different roles that lubricants play in controlling fretting according to the contact materials. He pointed out that the connector designs, the expected connector lifetimes, and their reliability requirements determine whether contact materials will be satisfactory for a given application. Hardware tests, such as shock and vibration, should be employed before new contact materials and designs are incorporated in connectors. Antler concluded that contact resistance is determined by the composition of the interface and this composition may change during fretting with dissimilar metals due to transfer, wear, and film formation. For fretting corrosion and friction polymerizing systems, the longer the wipe, the more unstable the contact resistance becomes. Contact resistance transients during fretting may be significantly higher than contact resistance at rest. Finally, lubricants may stabilize contact resistance by retarding the rate of wear of thin noble metals on film-forming substrates by dispersing frictional polymers, and with base metals by shielding the surfaces and wear debris from the environment, thereby reducing the oxidation rate.

Studies of fretting corrosion in automotive connector systems were also underway during the same period [10][11][12]. In 1987, a study on the fretting corrosion of tin-plated copper alloy was reported by Lee and Mamrick [11] in which the relative motion

between the contacts was provided by a stepping motor/precision stage assembly. This research attempted to clarify the physical phenomena of electrical conduction using tin-plated contacts subjected to fretting corrosion and the influence of electric load on the fretting corrosion process. They studied the rise in contact resistance of tin-plated copper-alloy under minute cyclical motion and found that over the range of circuit voltage and current investigated, the electrical conduction through slightly corroded contacts was not affected by the electrical load. For moderately corroded contacts, the resistance characteristic showed a sustained plateau near the melting voltage of Sn, and for severely corroded contacts, a plateau occurred in the resistance range corresponding to the voltage range of the melting, sublimation, and decomposition of the oxides and vaporization of tin. They concluded that these resistance plateaus were consistent with the view that the current passing through the contact constriction caused the contact spots to thermally run-away until melting of the tin occurred. With further corrosion giving higher resistance and more heating, the temperature could rise further, resulting in the melting, sublimation, and decomposition of the oxides and eventually reaching the vaporization of tin, collectively forming the second contact resistance or voltage plateau.

In other application fields, such as IC devices, the phenomenon of fretting corrosion also occurs and there have been substantial efforts devoted to its study [13][14]. In 1984, Mottine and Reagor [14] investigated fretting corrosion at dissimilar metal interfaces in socketed IC device applications. This study was conducted on a variety of dissimilar metal (socket device) interfaces under conditions of mild vibration. The static resistance behavior of the samples was studied for a ten-month period. The samples were then disassembled and the contact surfaces examined using scanning electron microscope

(SEM) and scanning Auger microprobe (SAM) techniques. They concluded that under conditions of mild vibration similar to those encountered in minicomputer systems using a disk drive and cooling fan, DIP/socket interfaces composed of tin or solder mated to themselves or to gold would undergo fretting corrosion and, ultimately, contact resistance failures. Laboratory results confirmed that the mechanism of failure was the build-up of tin-oxide particulate deposits in the contact mating area. The results for the lubricated DIP/socket systems indicated that only similar metal interfaces (Au-Au and SnPb-SnPb) were reliable for applications where low-level vibration was present.

A very difficult task in the field of fretting corrosion is to develop models to predict contact resistance behavior under fretting corrosion. In 1994, Bryant [15] proposed a comprehensive model to predict the contact resistance during the n^{th} fretting cycle and the ultimate usable lifetime of the contact. This model took into account contact wipe, fretting vibration amplitude and frequency, contaminant chemistry, material properties, plating thickness, asperity deformations, normal load, electrical load, and surface topography. It was based upon two corrosive fretting failure mechanisms: one involving the filling of surface valleys with wear debris generated by fretting, and the other involving the contamination of surface asperities by the corrosion product. Both mechanisms gave estimates that were within an order of magnitude of the observed values for fretting tests and field failures. The model assumed that as fretting motions pull the exposed corroded asperities back together, a mismatch in size occurs and some of the corrosive products are scraped off and deposited in the valleys. Eventually, the valleys are filled and the a-spots are separated, resulting in ultimate failure. In contrast, a material balance between the amounts produced and scraped off was used to estimate the

amount of corrosive product dragged into the contact. Shifting of molecules via plastic deformation mixes particles of corrosive product into the asperity metal. This model calculated the amount of corrosive product produced on the exposed surfaces during the separation phase of a cycle of fretting. Assumptions that correlate mixing to plastic flow and the use of modern composite theory led to an estimate of the conductivity within the contaminated asperity. Integration over the asperity volume gave the asperity resistance, and then Greenwood's theory was used to estimate the total contact resistance.

In the early 1990s, Malucci [16][17] refined and combined two previously developed models dealing with contact resistance and oxide build-up under fretting conditions, respectively, into a single analytical model. This model was then used to predict the average effects of contact force and fretting amplitude on contact degradation. The results from fretting tests on specially prepared tin plated contacts were explained within the framework of this model. This study found that decreasing contact force or increasing fretting amplitude produced increased degradation and this was explained in terms of an increase in oxide buildup due to either asperity deformation (lower forces) or an increase in the number of asperity deformations per cycle (longer fretting amplitude). In addition, the data from thermal shock experiments were analyzed to determine the relationship between the temperature swing (ΔT) and acceleration factor. Malucci concluded that the assumed connection between the temperature swing and fretting amplitude was consistent with both the fretting probe data and the thermal shock tests. These results provided a basis for modeling the degradation rate in terms of fretting cycles and the temperature swing. Consequently, this model was developed sufficiently

to estimate the acceleration factor for a given set of laboratory test parameters to simulate field degradation.

Relatively few researchers have studied the vibration threshold of fretting corrosion in electrical connectors. In 2002, Flowers and co-workers [18] investigated the relationship between applied excitation levels and fretting rates using single frequency vibration tests. Their results revealed a threshold level of excitation for the fretting corrosion, below which fretting corrosion did not occur. For excitation levels above this threshold, fretting rates increased in a monotonic fashion. They also found that the threshold g-level varies as a function of the dynamic behavior of the connector, the tie-off conditions and its mass or stiffness properties. In this study, a correlation of the experimental results with simulated behavior showed that for the primary mode of connector interface motion (rocking-type motion), the relative moment at that location served as a good indicator of the expected fretting rate. It also showed that the moment applied as the result of a given excitation level and frequency could reasonably be predicted via simulation. Finally, a transfer matrix model was used to analyze the study results. An empirical fit of the data correlated well with the model when damping was used. The analysis revealed the importance of the bending moment induced at the contact interface as a result of excitation levels and tie-off configurations. The researchers concluded that the dynamic response of the mechanical system under various g-levels and tie-off configurations could greatly impact the performance of a connector system subject to vibration stresses.

Another method for measuring the relative motion that causes fretting corrosion was reported recently. In 2005, Lam and co-workers [19] used a novel thick film sensor

to measure the displacement at the connector interface to test for environmental influences on electrical contact fretting. The sensor was assembled into a connector sample, replacing the male component. When the interface experienced movement, the relative displacement of the contact point caused a corresponding linear change in the resistance measured across the male and female connection. The sensors were validated by a series of experiments and subsequently used in a field test to establish the relationships between the fretting effects and temperature, humidity and differential pressure. The group found that the variation in differential pressure dominated the movement behavior at the contact interface of the well-sealed connector sample, while temperature and humidity had negligible influences on the measured relative displacement.

In the last ten years, computer simulations have found many new applications in the studies of fretting corrosion in electrical contacts. Many companies and their researchers have used this technology to assist or guide their experiments and analyses. ANSYS and ABAQUS are the two tools that are generally used for this simulation. For instance, in 1996 Villeneuve and co-workers [20] at the Ford Motor Company used finite element analysis to simulate the terminal crimping process for a vehicle connector. In this study, the terminal grip cross section, the punch tooling and the wire strands were modeled. The grip was forced into the punch while sitting on an anvil, mimicking the real life application. The results of the study showed that the friction between the grip surface and the punch surface is crucial to the formation of a “good” crimp. The model also showed that the crimping process is a combination of both the plane stress and plane strain conditions. In 2005, Monnier and co-workers [21] used finite element analysis to

simulate the behavior of a sphere-plane electrical contact when a high current flowed through it, taking into account the mechanical, electrical and thermal coupling involved. Several analytical expressions were used in the simulation and the model validity was confirmed by experimental results. The simulation also gave the contact terminal voltage, the contact resistance of the system and the solid temperature, which are impossible to measure experimentally.

Today, many universities and companies around the world are conducting important research on the issues involved in electrical contacts. These universities include Purdue University, the University of Maryland, Auburn University, Drexel University (USA), Beijing University of Posts and Telecommunications, Beijing University of Technology, Harbin Institute of Technology (China), the University of Manchester, the University of Southampton (England), Uppsala University, Linkoping University (Sweden), the University of Rennes (France), Vienna University of Technology (Austria), the University of Aarhus (Denmark), Nanyang Technology University (Singapore), Tver State University of Technology (Russia), the University of Tokyo, Keio University, Nippon Institute of Technology, Shizuoka University (Japan), and so on. The large companies and research centers include Eaton Corporation, Molex Incorporated, AMI Doduco, Checon Corporation, Chugai USA, Rockwell Automation, MOOG Components Group, Delphi Research Labs, Sandia National Laboratories, and so on. The research fields covered include arc materials [22], arc interruption [23], power [24], connector fretting corrosion [25], modeling [26], MEMS in contacts [27], fundamental research [28], sliding [29], automotive contacts [30] and safety issues [31].

1.4 Overview of Current Work

This dissertation continues the author's previous research and continues to be funded by Molex Incorporated. It discusses four research projects on the topic of fretting corrosion for electrical connectors. The first and the second projects are combined into one chapter. The third project is introduced in the next chapter and the fourth project is introduced by another chapter. In total, there are five chapters in this dissertation. The contents of each chapter are as follows:

Chapter one is the introduction and literature review. It introduces the concept of fretting corrosion, the mechanism of fretting corrosion, and discusses the progress of research concerned with fretting corrosion of electrical contacts.

Chapter two describes two research projects. The first project focuses on a PC connector and the second on an automotive connector. Both of them are studies of the physical characteristics of vibration-induced fretting corrosion. The chapter opens with a discussion of the purpose of this work, followed by the experimental details (such as the experimental samples, test approach, equipment, setup, etc.). The results of the experiment are then given, along with an analysis of the data. Finally, a mathematical model describing the early-stage fretting of the electrical connector is developed based on the experimental results and the analysis.

Chapter three describes the third project, which examines the influence of connector interface characteristics on vibration-induced fretting degradation. Two different interface coating materials are used, with the objective of determining which one creates the larger fretting degradation in the connector. This chapter discusses the

purpose of this project, and then provides a description of the experiment and its results. Based upon these results, some conclusions are presented.

Chapter four describes the fourth project: Finite Element Analysis (FEA) modeling for electrical connectors. There are two parts to this project, namely the experimental part and the FEA modeling part. This chapter first introduces the experiment and the testing results, including the experiment samples and setup. Then the details of the generation of the FEA modeling will be introduced, including the geometry model, element type, material properties, meshing, and boundary conditions, etc. Finally, the results from the simulation are introduced and compared with the results from the experimental part of this study.

Chapter five summarizes the work presented in this dissertation. It also provides some recommendations for further avenues of research on the topic of fretting corrosion in electrical connectors.

CHAPTER 2 A STUDY OF THE PHYSICAL CHARACTERISTICS OF VIBRATION-INDUCED FRETTING CORROSION

2.1 Purpose of This Study

Fretting corrosion, induced either by thermal cycling or vibration, is a primary failure mode for base metal connector systems. In order to ensure that a product will work reliably in the field, it is typically subjected to qualification tests. However, there is always a concern as to whether the acceleration factors that have been selected are realistic. If the stresses utilized during testing exceed those that will be experienced in the field, there is the risk that irrelevant / inactive failure modes will be induced during testing. This is particularly true if a threshold exists below which no detectable degradation of the connector system occurs. Thus, a product can be improperly engineered simply to meet the demands of a qualification test rather than the true performance requirements of the field. An alternative approach, comparing the stress levels at which a product fails to the stress levels that will be experienced in the field, can be exceedingly costly and time consuming. Only through the development of empirically based models and a better comprehension of the behaviors of connector systems when subjected to environmental stresses, such as thermal or vibration induced fretting, will an opportunity exist for reconciling the limitations of accelerated testing and test to failure methodologies.

Although there has been a great deal of work in recent years with regard to understanding the mechanisms of fretting corrosion in environments subjected to thermal cycling [3][9][12][17], the present work focuses on the less heavily studied field of vibration induced fretting degradation [32][33]. Previous investigations by the author have demonstrated several interesting fretting behaviors [18][34], specifically the existence of a threshold vibration level for the onset of fretting and a strong relationship between the vibration level above the threshold and the rate of fretting degradation at the contact interface. However, a greater understanding of these behaviors is still required in order to develop more generalized models of vibration induced fretting corrosion. Such models would then provide a basis for the development of appropriate accelerated life tests and efficient test to failure methodologies. Furthermore, with the apparent existence of well-defined thresholds for the onset of fretting degradation, the development of connector system application design guidelines to avoid fretting degradation may be possible. Therefore, building upon the results from the previous studies, the present investigation seeks to answer the following questions: 1). What influence do vibration amplitude, frequency, wire tie-off length, connector design, and contact interface lubrication have on the threshold vibration level and the rate of fretting degradation at a contact interface? 2). What is the relationship between the connector vibration response measured at the housing and the actual motion of the terminals inside of the connector housing? and 3). Can the model developed in earlier investigations be extended beyond a single type of connector? In order to answer these questions, two types of connectors were used in this study: PC connectors and automotive connectors.

2.2 Description of Experimental Testing

2.2.1 Experimental Samples

A series of studies were conducted using a single-row, pin and socket PC-type connector that is similar to the test article used in the author's previous work [18][34]. For the purposes of this study, the housing was modified to allow the connector halves to move more freely under vibration excitation, as shown in Figure 2-1. This was found to be necessary as the original (as received) product did not readily exhibit fretting degradation.

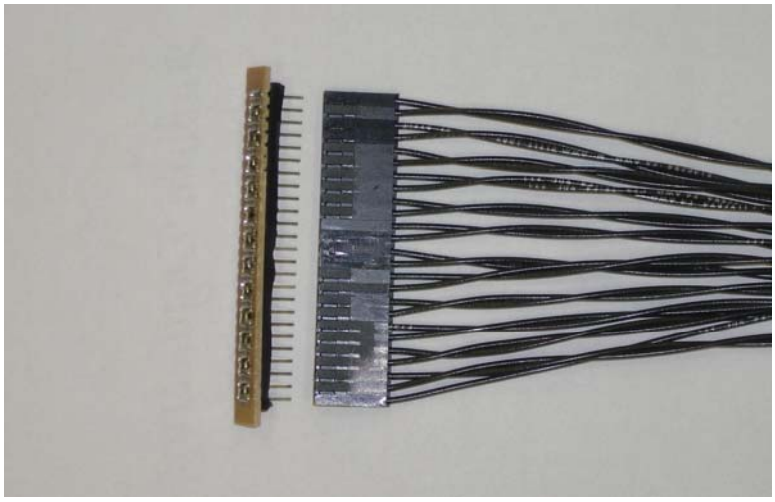

Figure 2-1 Photograph of the PC connector

In the author's previous work, the transfer functions related the motion at the connector header (which was attached to the shaker head) to the motion of the plug housing [18][34]. It was unclear whether this procedure gave an adequate measure of the relative motion occurring at the contact interface, which is after all the location where the fretting occurs. In order to address this question, a set of the PC connectors was further modified to allow visual observation of the terminal, as shown in Figure 2-2. This was

done so that direct measurements of the terminal motion could be made using a laser displacement measuring system.

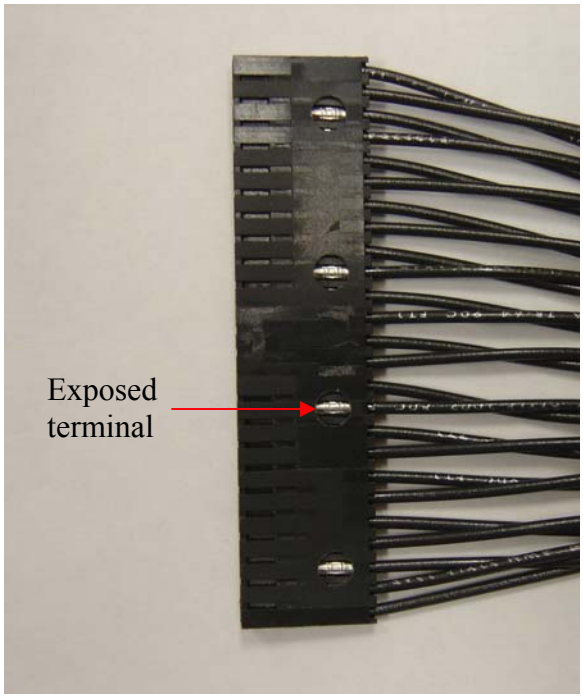

Figure 2-2 Modified PC connector allowing visual access near the contact interface

After the testing of the PC connectors was completed, a matter of concern was the more general applicability of these results to other connector types. In order to address this question, a series of studies with an automotive connector were conducted. The original Auto connector is shown in Figure 2-3. Again, a single row connector was utilized, but this design was much more rugged than that of the PC-type connector. A series of experiments and transfer function evaluations were done, and it was determined that the connector did not readily fret in its as-received condition. Therefore, the original unit was modified by the removal of a portion of the housing between the plug and the socket. A photograph of the modified configuration used for testing is shown in Figure 2-4.

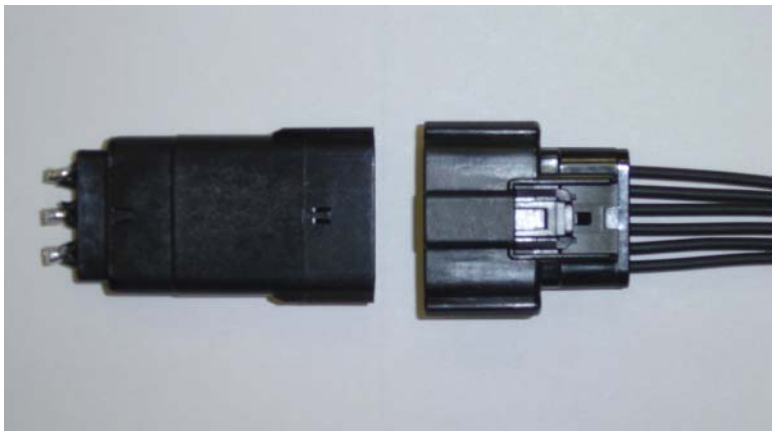

Figure 2-3 Photograph of the original automotive connector

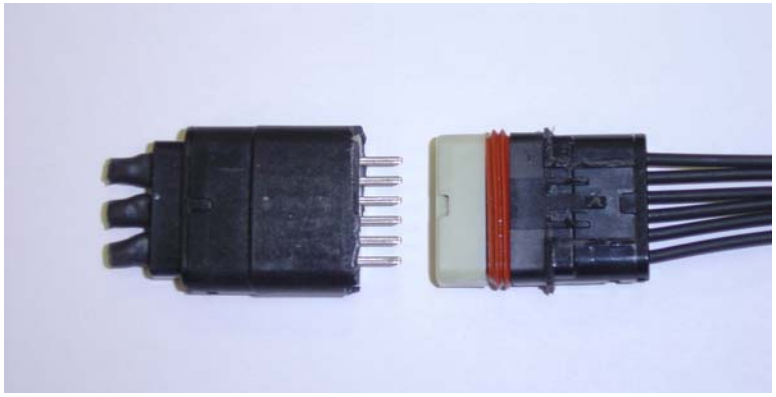

Figure 2-4 Modified automotive connector used in the study

2.2.2 Experimental Equipment

The experimental equipment in this research consisted of a Keithley Model 2010 multimeter, which was used for measuring the samples' resistance values; an HP 35665A Dynamic Signal Analyzer, which generated a random signal for the shaker and measured the frequency response; a POLYTEC laser vibrometer, which measured the transfer function for the connector samples; and a vibration system, which consisted of a DACTRON Vibration Control System, PA500L Amplifier and V408 Shaker. The major components are described in detail below.

2.2.2.1 KEITHLEY Model 2010 Multimeter

The Model 2010 is a $7^1/_2$-digit high-performance digital multimeter [35]. It has 0.0018% basic DV voltage accuracy and 0.0032% basic resistance accuracy. The meter is used to measure the contact resistance in four-wire mode. In this mode, it can measure the resistance from 1uΩ to 120MΩ. The circuit used for connecting test leads to the resistance is shown in Figure 2-5.

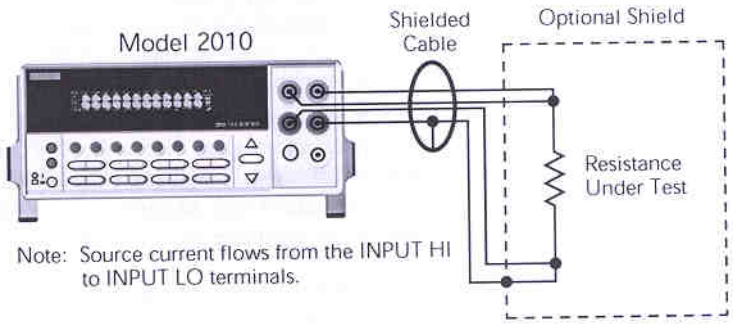

Figure 2-5 Four-wire resistance measurements

The key condition of the measurement for the contact resistance is dry circuit testing. Many low resistance measurements are made on contact devices such as switches and relay contacts. The purpose of this testing is to determine whether oxidation has increased the resistance of the contacts. If the voltage across the contacts during the test is too high, the oxidation will be punctured and render the test meaningless. Dry circuit testing limits the measurement voltage to 20mV or less.

2.2.2.2 HP 35665A Dynamic Signal Analyzer

Shown as Figure 2-6, the HP 35665A Dynamic Signal Analyzer [36] is a two-channel Fast Fourier Transform (FFT) spectrum/network analyzer with a frequency range that extends from 0.19531 Hz to 102.4 kHz in single channel mode and from 0.097656 to

51.2 kHz in its two channel mode. The analyzer has a built-in signal source providing random noise, burst random noise, periodic chirp, pink noise, and fixed sine. Measurements can be saved to an internal 3.5-inch flexible disk drive, or an external HP SS-80 disk drive, or can be directly printed out. It main characteristics that are important for this study are listed as follows:

Figure 2-6 HP 35665A Dynamic Signal Analyzer

Input Noise Level: < -140 db

Full Span FFT Noise Floor: < -76db (-85db typical)

FFT Cross-Channel Gain Accuracy: ± 0.04 db (0.46%)

FFT Cross-Channel Phase Accuracy: ± 0.5 degree

Minimum Frequency Resolution: 122 μ Hz (Two Channel Mode)

2.2.2.3 POLYTEC Laser Vibrometer

The Laser Vibrometer [37], shown in Figure 2-7, provides the means for a displacement measurement according to the fringe counter principle. An analog voltage signal is available at its output that is proportional to the vibration amplitude of the

measurement object. This signal can be visualized with an oscilloscope or can be entered into a data acquisition and processing system, such as the HP 35665A Dynamic Signal Analyzer. Table 2-1 shows its displacement decoder specifications.

Figure 2-7 POLYTEC Laser Vibrometer

Table 2-1 Displacement decoder specification of the Laser vibrometer system

Measurement Range	Full Scale Output (Peak-to-Peak)	Resolution	Max. Vibration Frequency	Max. Velocity	Max. Acceleration
µm/V	mm	µm	kHz	m/s	g
20	0.32	0.08	20	1.6	20,000
80	1.3	0.32	20	1.6	20,000
320	5.2	1.3	20	1.6	20,000
1280	20.5	5	20	1.6	20,000
5120	82	20	20	1.6	20,000

2.2.2.4 Vibration System

The connection of a typical vibration system [38][39] is shown as Figure 2-8. This is a closed-loop control system. Its working mechanism is described below.

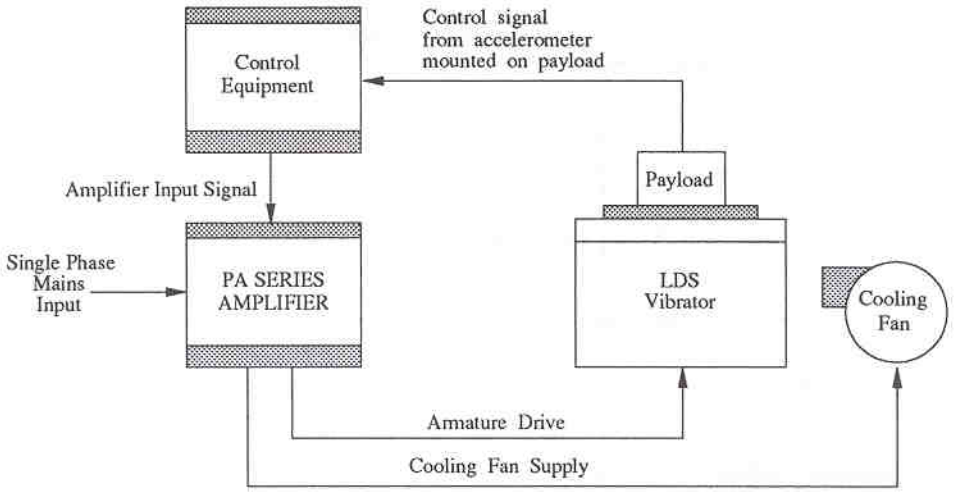

Figure 2-8 Typical Vibration System

A vibration control system generates time-domain signals that contain the required frequency-domain characters or profile and sends them to the amplifier. The powerful amplified signal, with a larger current and voltage, then drives the shaker to vibrate. The accelerometer mounted on the payload senses the vibration on the shaker and converts it into an electrical signal, which is sent back to the vibration control system. The vibration control system deals with this time-domain signal and transfers into the frequency domain by FFT. It then compares the frequency-domain characteristics of this signal with the original setting. If they are different, the vibration control system will adjust its output signal accordingly. This process repeats until the frequency-domain characteristics of the signal on the shaker match the required characteristics specified by the original setting.

Two elements of the vibration system used in this study, the PA 500L amplifier and V408 shaker, are shown as Figure 2-9 and Figure 2-10, respectively.

Figure 2-9 PA 500L Amplifier

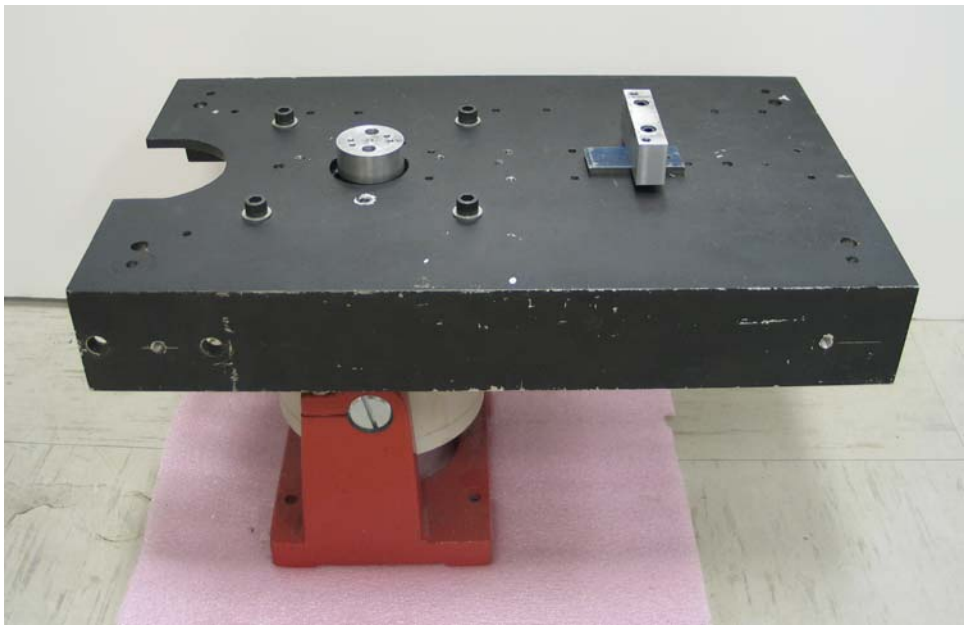

Figure 2-10 V408 Shaker

2.2.3 Experimental Setup

The basic test setup is shown in Figure 2-11 and Figure 2-12 for the PC connector and the automotive connector, respectively. The connector header was attached to the

head of a vibratory shaker. The opposite end of the test sample was clamped to a fixed table. The location of the clamp could be adjusted to produce a variety of tie-off lengths for the wiring.

Figure 2-11 PC connector vibration setup for middle tie-off configuration

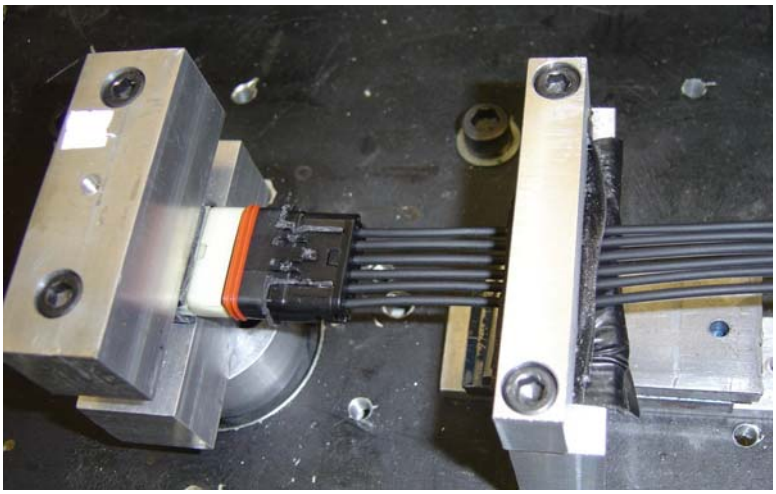

Figure 2-12 Automotive connector vibration setup for short tie-off configuration

The motion of the shaker head was measured using either an accelerometer or a laser displacement system. The accelerometer was used by the feedback vibration control system and the laser displacement system was used to measure the frequency response of

the displacement between the two halves of the connector samples. Figure 2-13 shows the setup used for the measurement of the frequency response.

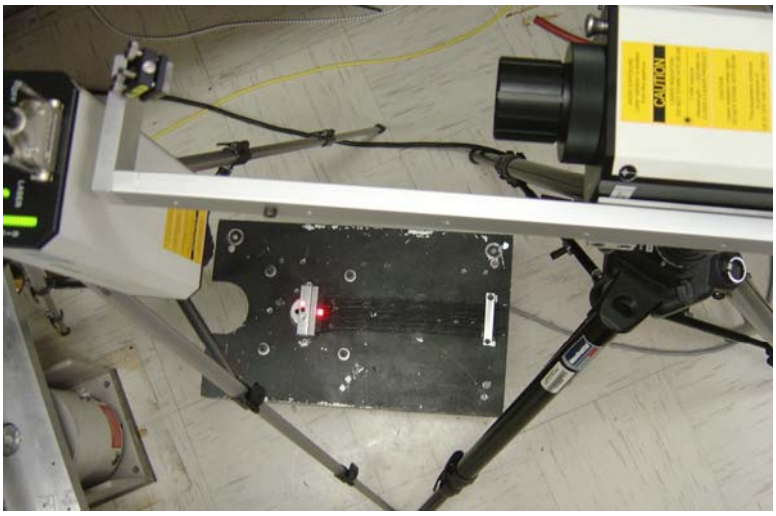

Figure 2-13 Measurement of the frequency response of displacement

2.3 Test Results

Sinusoid vibrations with specific frequencies and amplitudes were used in this study. The relationship between the g-level of the sinusoid vibration and its frequency and peak-to-peak amplitude is defined by the following equation:

$$g_{rms} = \frac{0.707 \times \frac{amplitude(mm)_{peak-peak}}{2} \times (2 \times \pi \times f)^2}{9.81 \times 1000} \quad (g) \qquad (1)$$

Figure 2-14 shows the curves typically obtained in the author's previous research on fretting in electrical connectors [40]. In this extension of the original research, two different types of connectors, and three tie-off configurations (3 inch, 8 inch and 12 inch cable lengths) were used, and the testing results for all of these factors will be introduced individually.

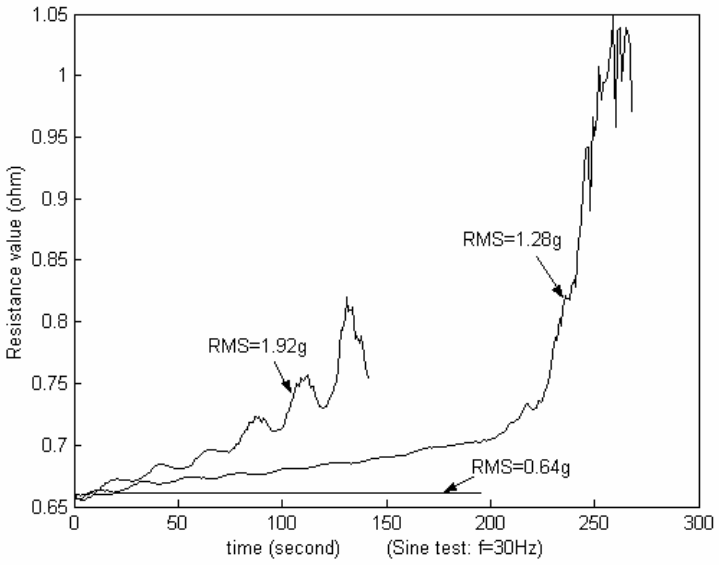

Figure 2-14 Typical fretting curves in sine vibration test

2.3.1 PC Connector

2.3.1.1 Short Tie-off Configuration

Frequencies of 20Hz, 30Hz, 40Hz, and 200Hz were used in the short tie-off configuration. The resistance changes for these frequencies in the early stage of the vibration are shown as Figure 2-15, Figure 2-16, Figure 2-17, and Figure 2-18, respectively. Figure 2-19 summarizes the early stage fretting rates for these 4 cases of single frequency vibrations.

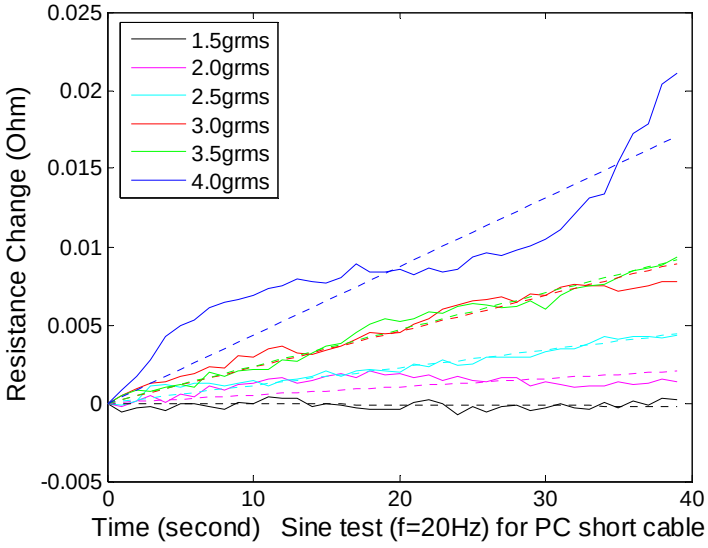

Figure 2-15 PC connector resistance change for 20 Hz, short tie-off configuration

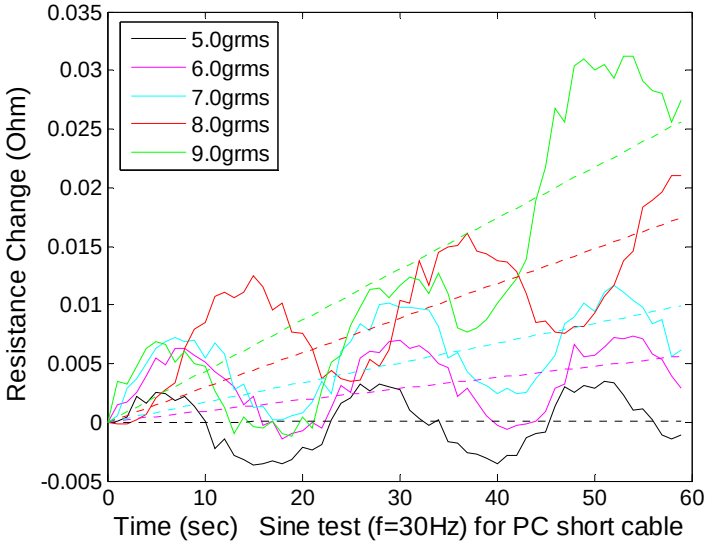

Figure 2-16 PC connector resistance change for 30 Hz, short tie-off configuration

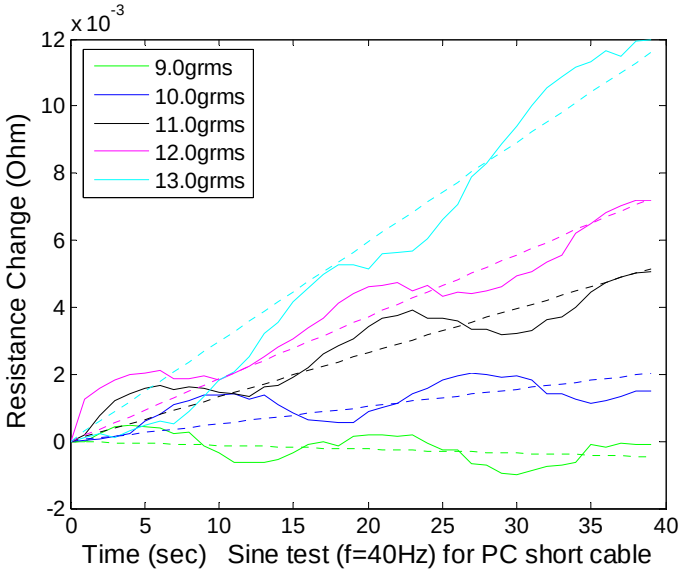

Figure 2-17 PC connector resistance change for 40 Hz, short tie-off configuration

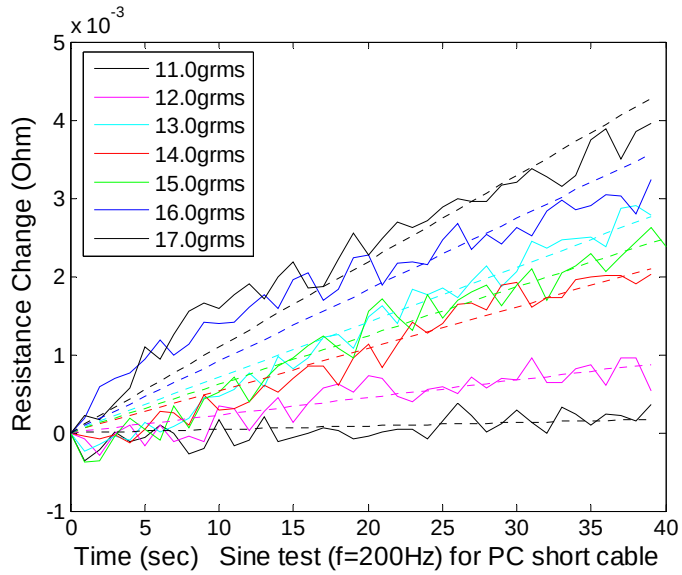

Figure 2-18 PC connector resistance change for 200 Hz, short tie-off configuration

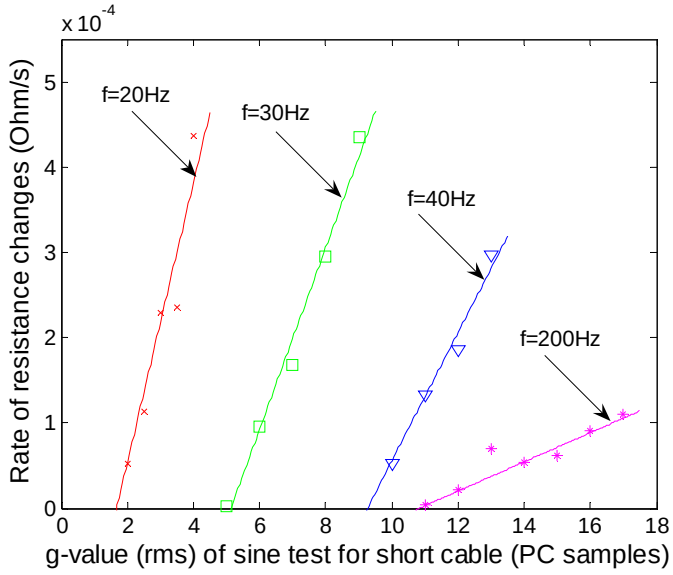

Figure 2-19 Summary of early stage fretting for short tie-off, PC connector

The above results reveal that as the G-level at the shaker head is increased for a given frequency, the rate of resistance change increases in a relatively linear fashion. Also, as the respective frequencies are increased, the G-level at the shaker head required to initiate fretting, which is the threshold G-level, tends to rise. Table 2-2 lists the threshold G-value at the shaker head for the short tie-off configuration.

Table 2-2 Threshold vibration level at the shaker head for the PC short tie-off length

Input Vibration Frequency (Hz)	Threshold Input Vibration level at Shaker Head $G_{threshold}$ (rms)
20	1.52
30	4.9
40	9.0
200	11.0

2.3.1.2 Middle Tie-off Configuration

Frequencies of 50Hz, 100Hz were used in the middle tie-off configuration. The resistance changes for these frequencies in the early stage of the vibration are shown as

Figure 2-20 and Figure 2-21, respectively. Figure 2-22 summarizes the early stage fretting rates for these 2 single frequency vibrations. Table 2-3 lists the threshold G-value at the shaker head for the middle tie-off configuration.

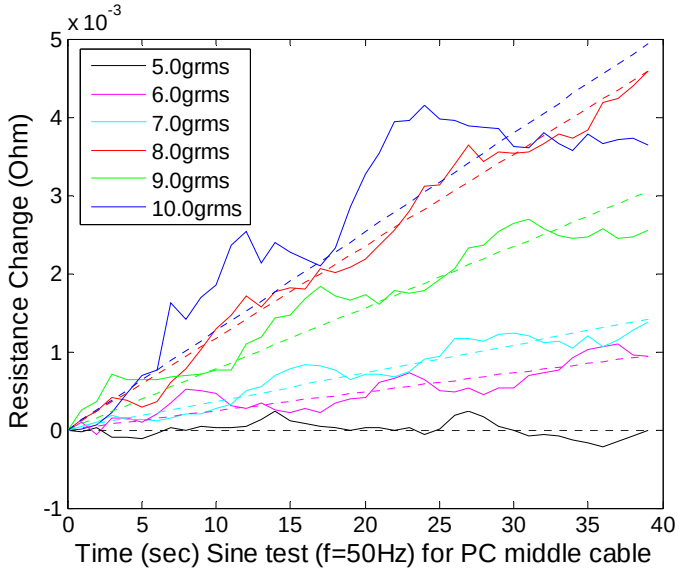

Figure 2-20 PC connector resistance change for 50 Hz, middle tie-off configuration

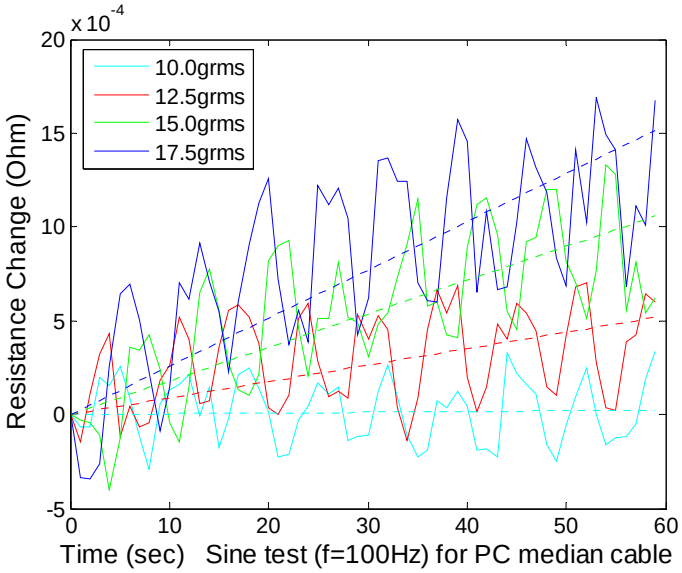

Figure 2-21 PC connector resistance change for 100 Hz, middle tie-off configuration

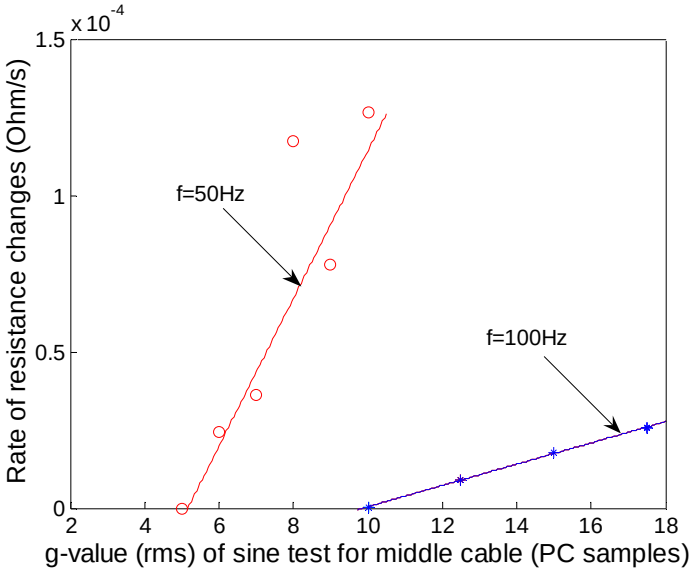

Figure 2-22 Summary of early stage fretting rates for middle tie-off, PC connector

Table 2-3 Threshold vibration level at the shaker head for the PC middle tie-off length

Input Vibration Frequency (Hz)	Threshold Input Vibration level at Shaker Head $G_{threshold}$ (rms)
50	5.2
100	10.0

2.3.1.3 Long Tie-off Configuration

As with the middle tie-off configuration, two frequencies, 50Hz and 200Hz, were used in the long tie-off configuration. The resistance changes for these frequencies in the early stage of the vibration are shown as Figure 2-23 and Figure 2-24, respectively.

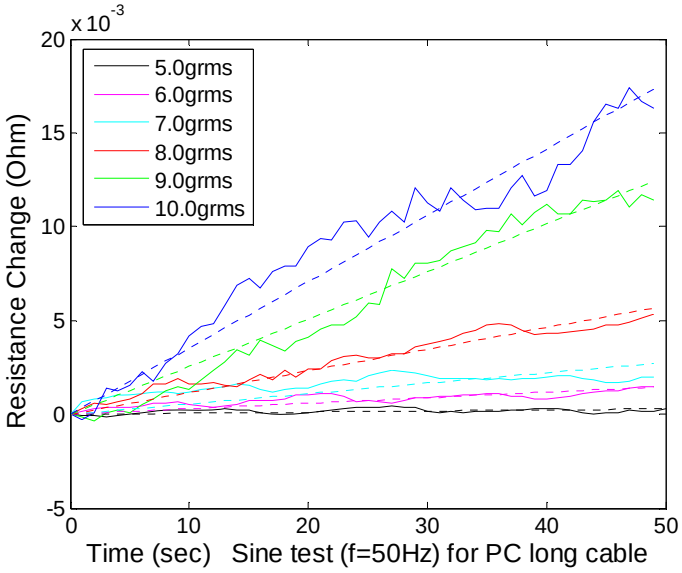

Figure 2-23 PC connector resistance change for 50 Hz, long tie-off configuration

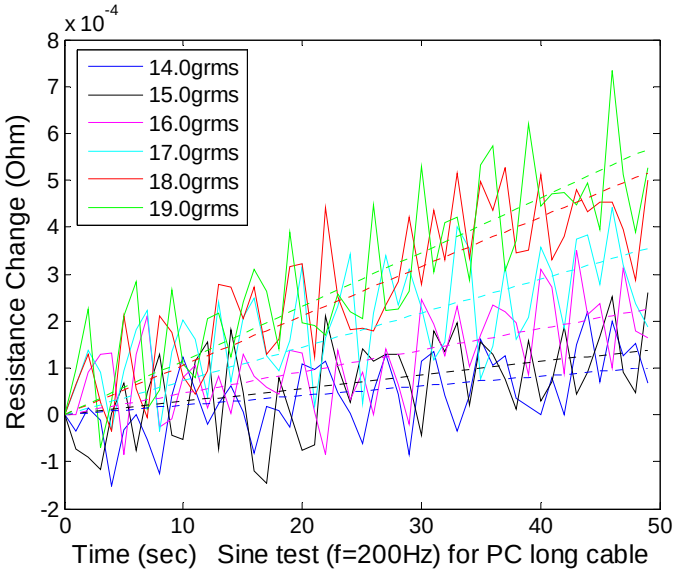

Figure 2-24 PC connector resistance change for 200 Hz, long tie-off configuration

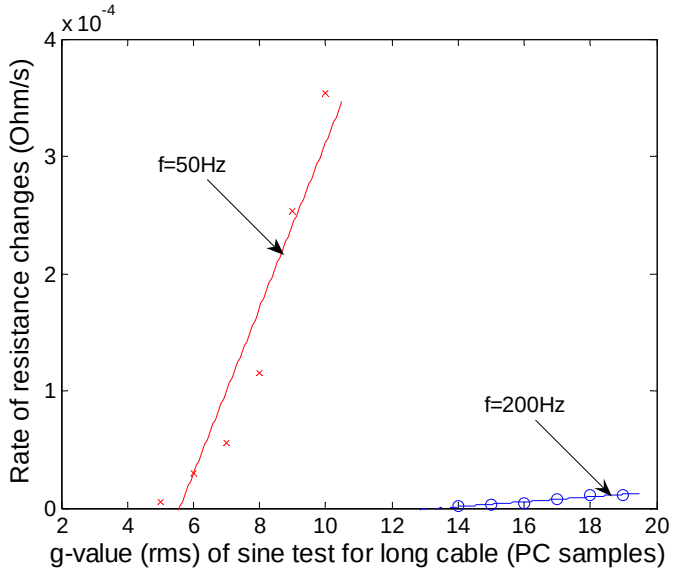

Figure 2-25 Summary of early stage fretting rates for long tie-off, PC connector

Figure 2-25 summarizes the early stage fretting rates for these 2 single frequency vibrations, and Table 2-4 lists the threshold input vibration level at the shaker head for this long tie-off configuration.

In the cases of the middle and long tie-off configurations for the PC connector, similar linear trends for the rate of resistance change and the threshold trends were found.

Table 2-4 Threshold vibration level at the shaker head for the PC long tie-off length

Input Vibration Frequency (Hz)	Threshold Input Vibration level at Shaker Head $G_{threshold}$ (rms)
50	5.6
200	13.4

2.3.1.4 Transfer Function and Relative Motion

The transfer function is defined by the ratio of the output displacement from the back-half connector interface and the input displacement from the front-half connector interface. Because the front-half connecter interface is fixed at the shaker head, its input

displacement is the same as for the shaker head. The transfer function can be expressed by the following equation:

$$\text{Transfer Function} = M*\cos(ø) + i*M*\sin(ø) \text{ or } M\angle ø \quad (2)$$

Based on the above transfer function, the relative motion between the two-half interfaces is defined by:

$$Z_F = \sqrt{[1 - M\cos(\phi)]^2 + [M\sin(\phi)]^2} \quad (3)$$

As mentioned in Chapter 2.2.1, the description of the experimental samples used in this dissertation, PC connector samples with slots were also used in this study to compare the effects of different relative motions between the plug housing and contact interface.

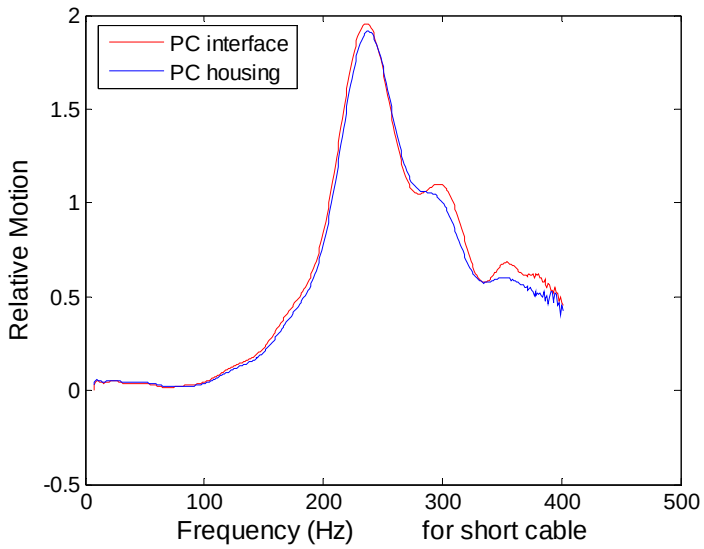

Figure 2-26 Relative motions between the plug housing and interface, PC short cable

Figure 2-26 shows the measured relative motion relations for the short (3 inch) cable tie-off length. Overall, the two plots are very similar and are almost identical for frequencies below the first resonance peaks at about 230 Hz. Above this value, the

relative motion of the interface is typically slightly higher than that of the plug housing alone, particularly for frequencies near each of the resonance peaks.

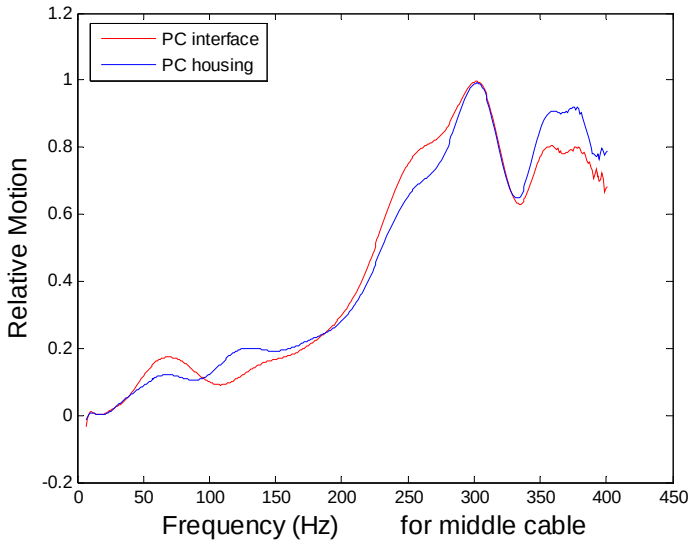

Figure 2-27 Relative motions between the plug housing and interface, PC middle cable

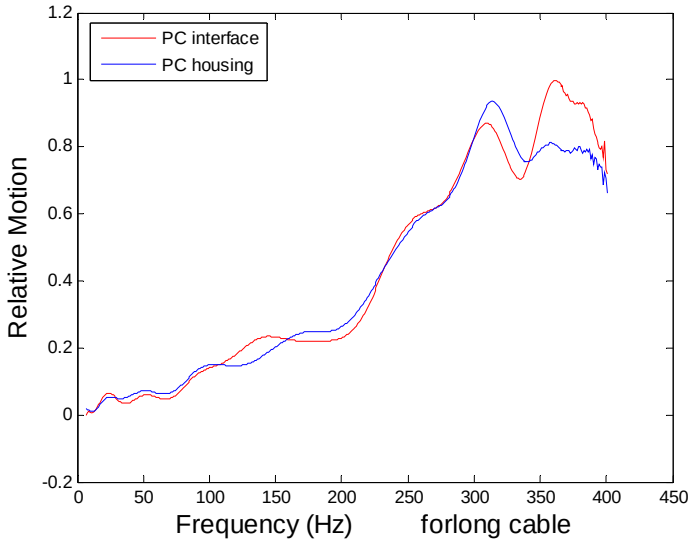

Figure 2-28 Relative motions between the plug housing and interface, PC long cable

Figure 2-27 shows the measured relative motion relations for the middle (8 inch) cable tie-off length. Again, the two plots are quite similar overall. However, the two plots show small differences starting at a frequency of about 40 Hz.

Figure 2-28 shows the measured relative motion relations for the long or 12 inch cable tie-off length. For this case, the two plots are again similar in overall shape but small differences can be observed starting at a frequency of about 40 Hz.

From a physical perspective, these results certainly make sense. As the wiring tie-off length is increased, the resonant frequencies of the test sample (connector and wiring) are lowered. This results in a higher amplitude vibration of the wiring, which in turn drives the connector plug and terminals to vibrate. The plug housing, being more rigid, tends to have a lower response than the terminals. So, it is reasonable to conclude that for low frequencies, the relative motion relations measured at the housing will be representative of the actual motion of the terminal. For higher driving frequencies, the housing motion provides a reasonably accurate overall trend, but the actual relative motion at the terminal could differ somewhat. This may be particularly important for driving frequencies near the various resonant peaks. It is important to note that the terminal measurements were made in the vicinity of, yet at a finite distance away from, the contact interface. Thus, the transfer functions represent the relative motion of the two halves of the contact interface multiplied by some constant scaling factor.

The transfer function and relative motion over a large frequency range (800Hz) were also measured for the short, middle, and long tie-off configuration. Figure 2-29 and Figure 2-30 show the transfer function and relative motion over the long frequency range

for the three tie-off configuration. The results indicate that there is a general tendency toward a leveling off of the relative amplitude as the driving frequency increases.

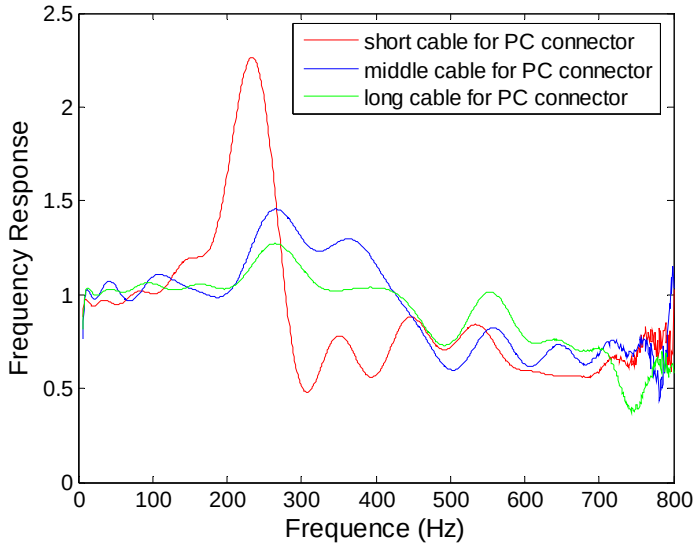

Figure 2-29 Transfer functions over a long frequency range for three tie-off cables

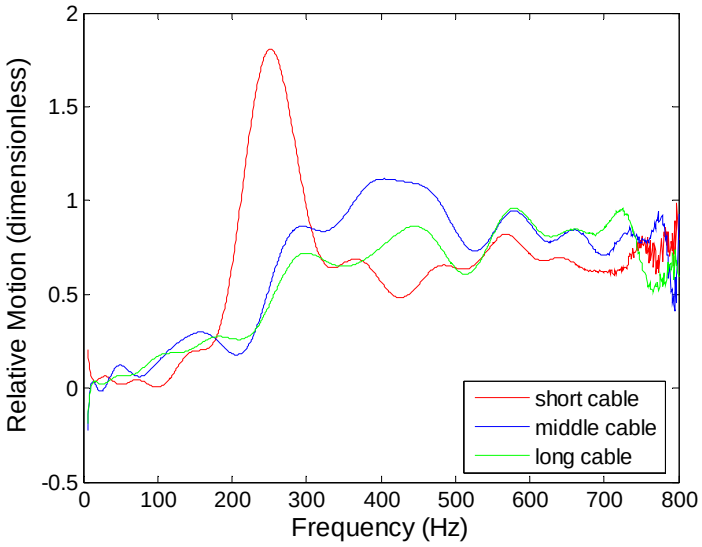

Figure 2-30 Relative motions over a long frequency range for three tie-off cables

Figure 2-31 shows, as a function of frequency, the relative displacement at the terminals for a constant G-level applied at the shaker head. This is a reasonable

perspective with regard to the relative motion during mechanically induced fretting since the excitation is usually specified in terms of the G-level. As can be seen from the trends in this figure, the absolute displacement associated with a given G-level decreases with the square of the driving frequency. For the middle (8 inch) and long (12 inch) cable tie-off lengths, the shaker and interface displacements thus become quite small (relative to the displacement at lower frequencies) for driving frequencies above about 150 Hz. The short (3 inch) configuration is a little more dynamic due to the presence of a resonance peak at about 230 Hz. However, for higher frequencies the displacement amplitude behaves in a fashion similar to that observed for the longer cable lengths. This observation is quite important. It is well known that fretting is a strong function of absolute displacement at the contact interface [32]. For even moderately high driving frequencies, the displacement amplitude may be below the fretting threshold if the applied G-level is not sufficiently high.

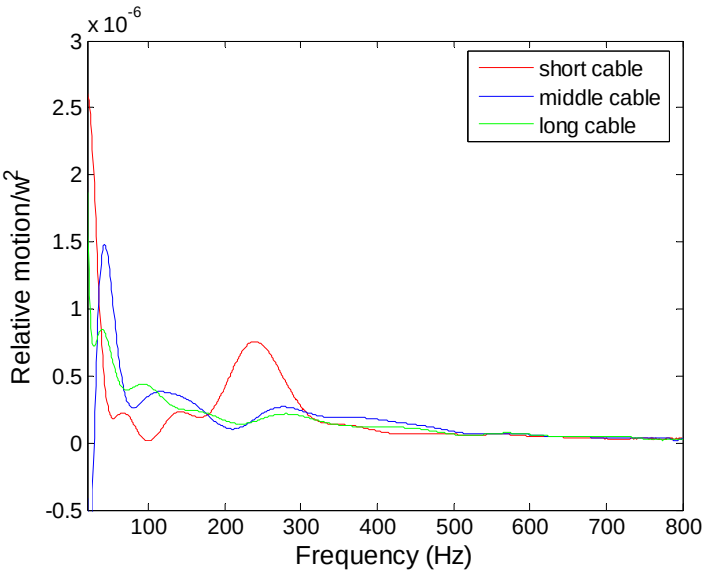

Figure 2-31 PC relative displacement at interfaces to a constant g-level at the shaker head

In the followed section, the data from these figures and the test results for the fretting thresholds, which were previously introduced in chapter 2.3.1.1-3, will be used to analyze their relationship.

2.3.2 Automotive Connector

A series of fretting degradation studies for the automotive connector were carried out using various single frequency vibration levels. Two of the same wiring tie-off lengths as those used in the PC-type connector study were used, namely the middle and long tie-off configuration.

2.3.2.1 Middle tie-off Configuration

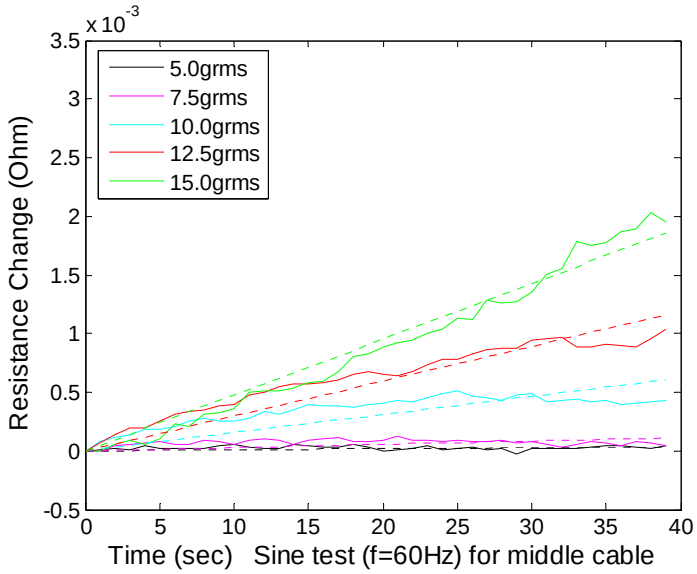

Figure 2-32 Auto connector resistance change for 60 Hz, middle tie-off configuration

Frequencies of 60Hz, 110Hz, and 140Hz were used in the middle tie-off configuration. The resistance changes for these frequencies in the early stage of the vibration are shown as Figure 2-32, Figure 2-33, and Figure 2-34, respectively. Figure

2-35 summarizes the early stage fretting rates for these 3 cases of single frequency vibration. Table 2-5 lists the threshold G-value at the shaker head for the middle tie-off configuration.

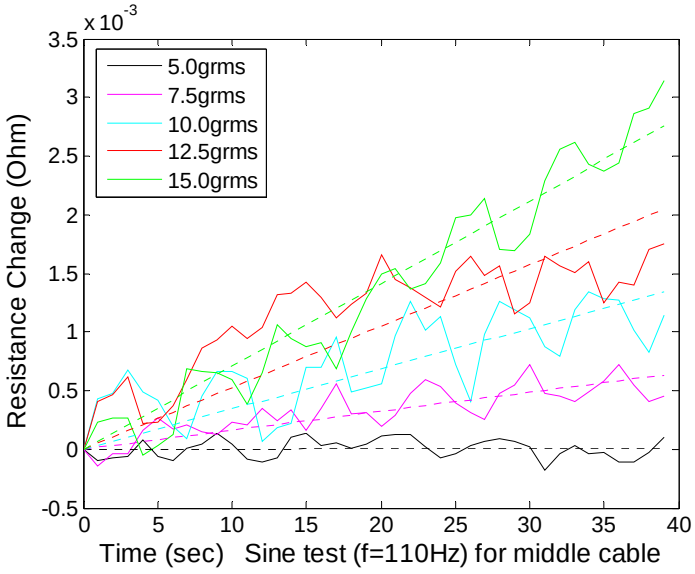

Figure 2-33 Auto connector resistance change for 110 Hz, middle tie-off configuration

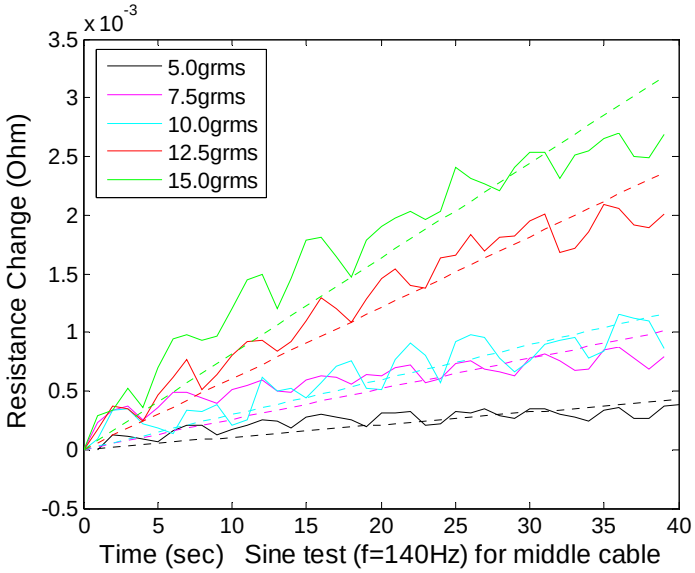

Figure 2-34 Auto connector resistance change for 140 Hz, middle tie-off configuration

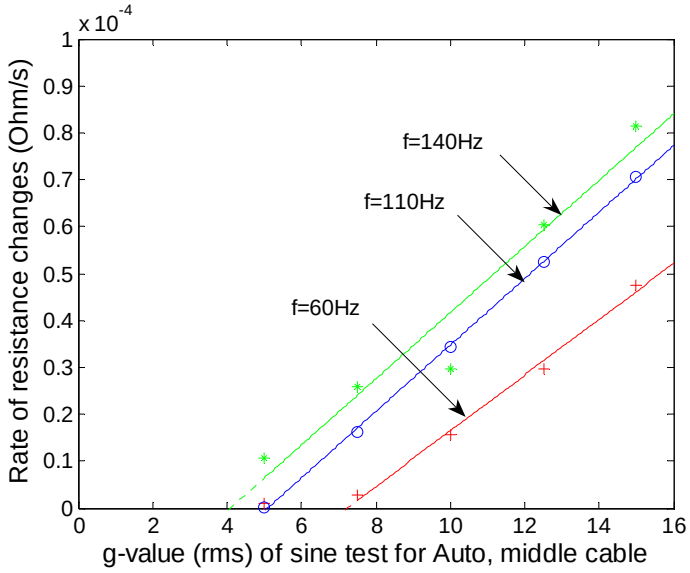

Figure 2-35 Summary of early stage fretting rates for middle tie-off, Auto connector

Table 2-5 Threshold vibration level at the shaker head for the Auto middle tie-off length

Input Vibration Frequency (Hz)	Threshold Input Vibration level at Shaker Head $G_{threshold}$ (rms)
60	7.2
110	5.1
140	4.0

2.3.2.2 Long-Cable Configuration

Frequencies of 50Hz, 100Hz, and 140Hz were used in the long tie-off configuration. The resistance changes for these frequencies in the early stage of the vibration are shown as Figure 2-36, Figure 2-37 and Figure 2-38, respectively.

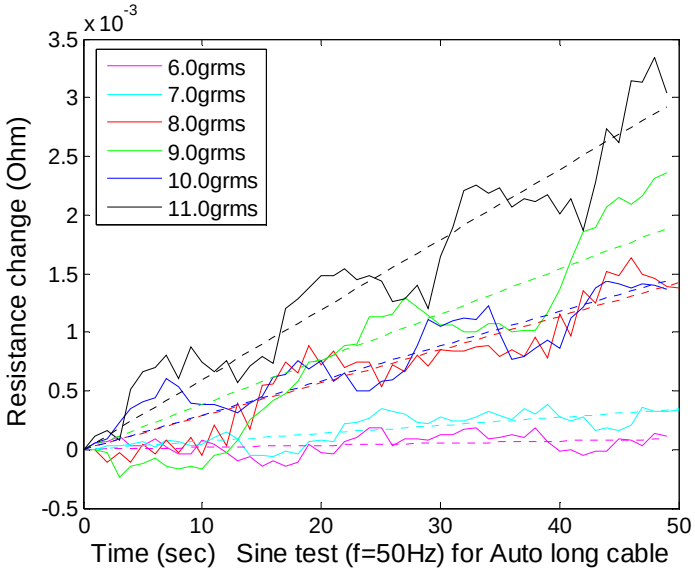

Figure 2-36 Auto connector resistance change for 50 Hz, long tie-off configuration

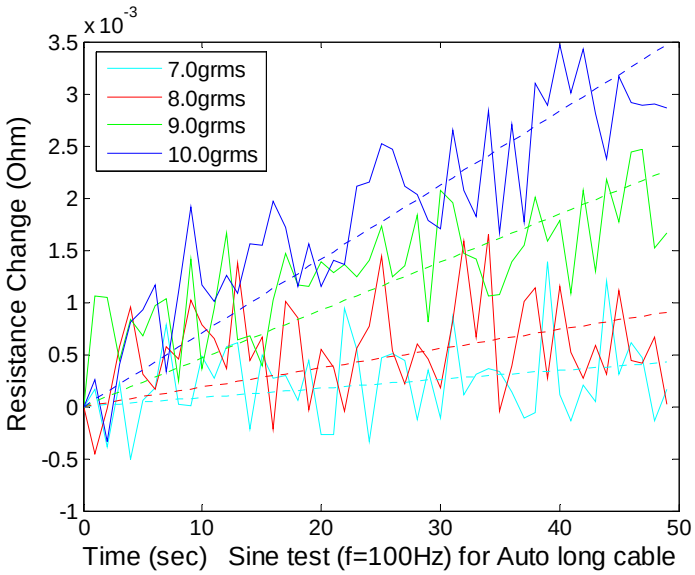

Figure 2-37 Auto connector resistance change for 100 Hz, long tie-off configuration

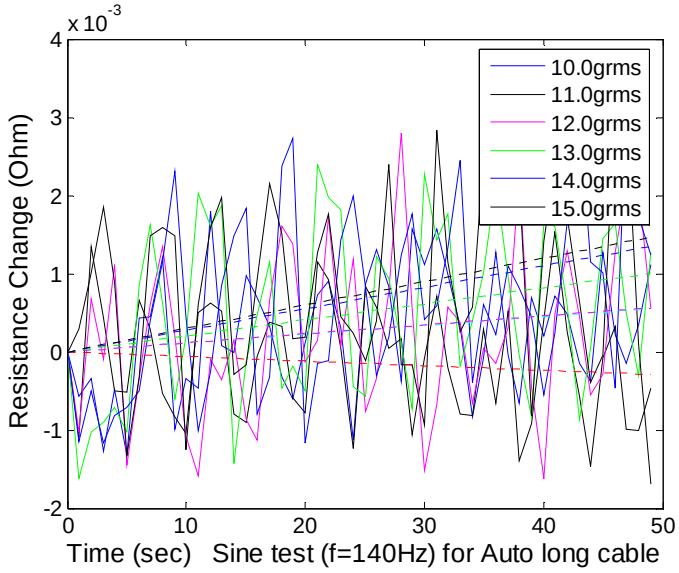

Figure 2-38 Auto connector resistance change for 140 Hz, long tie-off configuration

Figure 2-39 summarizes the early stage fretting rates for these 3 cases of single frequency vibration. Table 2-6 lists the threshold G-value at the shaker head for this long tie-off configuration.

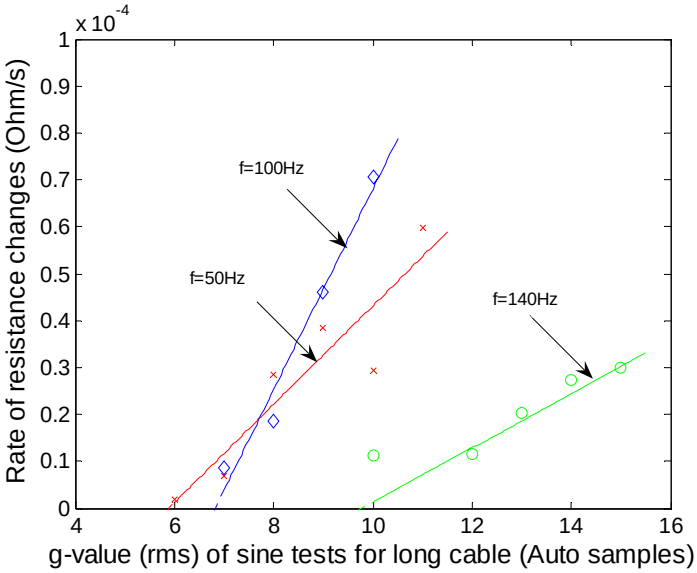

Figure 2-39 Summary of early stage fretting rates for long tie-off, Auto connector

Table 2-6 Threshold vibration level at the shaker head for the Auto long tie-off length

Input Vibration Frequency (Hz)	Threshold Input Vibration level at Shaker Head $G_{threshold}$ (rms)
50	6.0
100	6.8
140	10.0

For the automotive connector, the observed behavior was generally very similar to that of the PC connector. The rates of resistance change also increased in a relatively linear fashion and as the respective frequencies increased, the threshold g-level also rose.

2.3.2.3 Transfer Function and Relative Motion

Figure 2-40 shows the 200Hz frequency-range transfer function or frequency response for each of the three tie-off configurations for the automotive connector. Figure 2-41 and Figure 2-42 are the corresponding 200Hz frequency-range relative motion and the relative motion/ ω^2, which is also the relative displacement at the interfaces for a constant g-level at the shaker head.

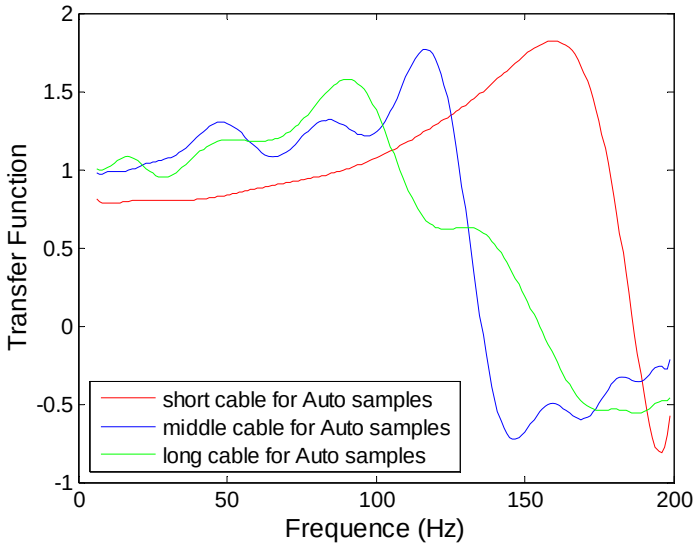

Figure 2-40 Transfer function in 200Hz for three tie-off length, automotive connectors

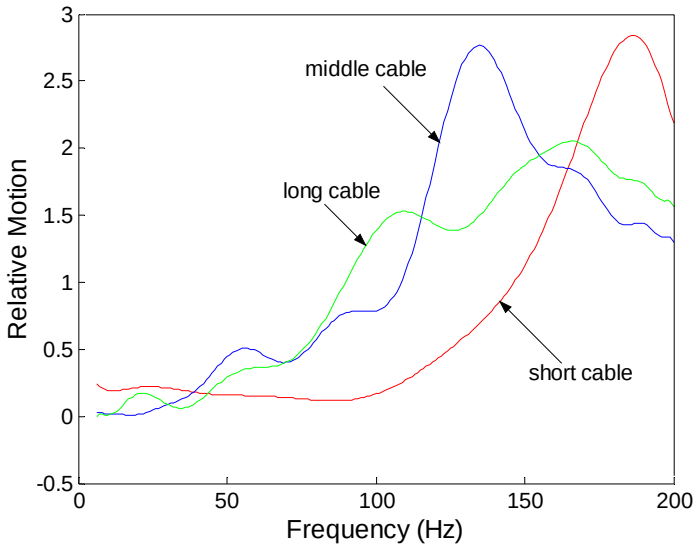

Figure 2-41 Relative motion in 200Hz for three tie-off length, automotive connectors

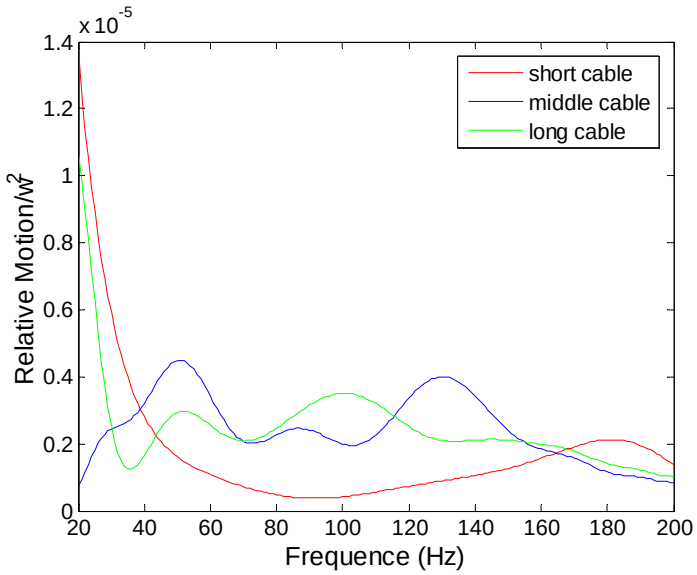

Figure 2-42 Auto relative displacement at interfaces to a constant g-level at shaker head

Figure 2-43 shows the 800Hz frequency-range relative displacement at the interfaces for the automotive connector. The basic form of this trace is similar to that for the PC connector. Once again, the absolute displacement associated with a given g-level

decreases with the square of the driving frequency, which is consistent with the finding that fretting is a strong function of absolute displacement at the contact interface.

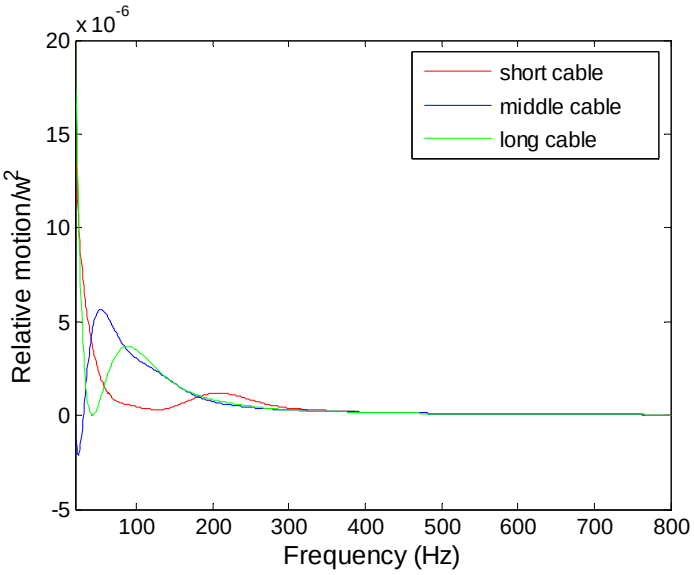

Figure 2-43 Auto relative displacement at interfaces in 800Hz frequency range

The data from these figures and the experimental results for the automotive connector will be analyzed in section 2.4 to discuss their relationship and this relationship will be compared with that of the PC connector. The consistence of this relationship will also be checked.

2.3.3 Lubricated Connector

Lubricated PC connector samples were also tested for the case of early stage fretting. The purpose of this testing was to identify the effect of adding lubricant and whether it could be used to eliminate or prevent fretting. The samples are the same PC samples as those used in the previous PC connector study but pre-lubricated with a proprietary lubricant. Figure 2-44 shows the non-lubricated connector resistance behavior when the experiment sequentially progressed from 5.0g to 11.0g for the 50Hz, middle

cable configuration. The connector resistance continued to rise as the testing progressed, which indicates that fretting was occurring.

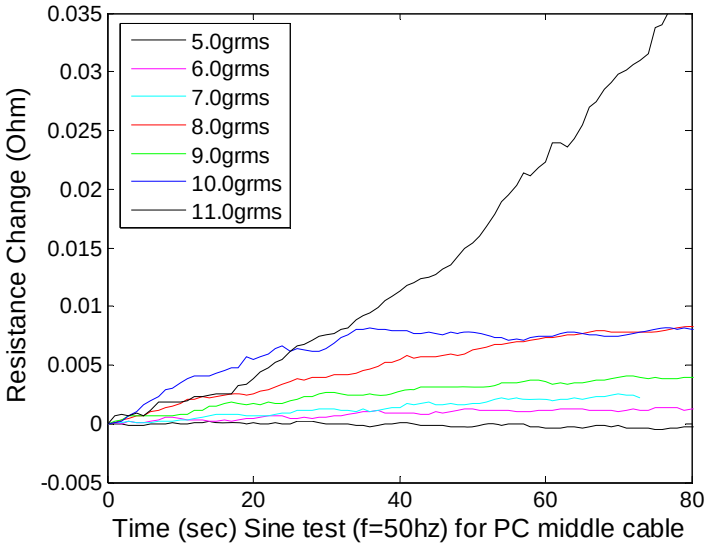

Figure 2-44 Resistance change of un-lubricated samples for 50Hz, middle cable testing

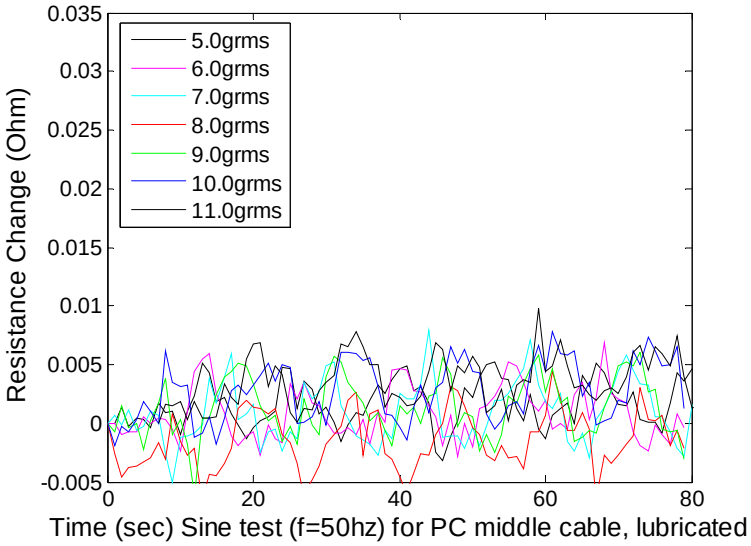

Figure 2-45 Resistance change of lubricated samples for 50Hz, middle cable testing

In contrast, for the same experimental conditions, the resistance of a connector with lubricant maintained the same average value and no longer increased. This is shown

in Figure 2-45, which has the same coordinate scale as that in Figure 2-44. Clearly, the lubricant prevented the occurrence of fretting in this test.

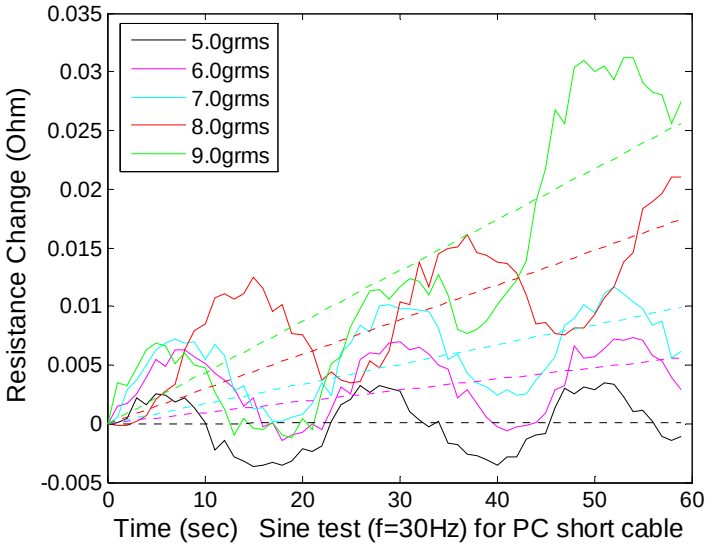

Figure 2-46 Resistance change of un-lubricated samples for 30Hz, short cable testing

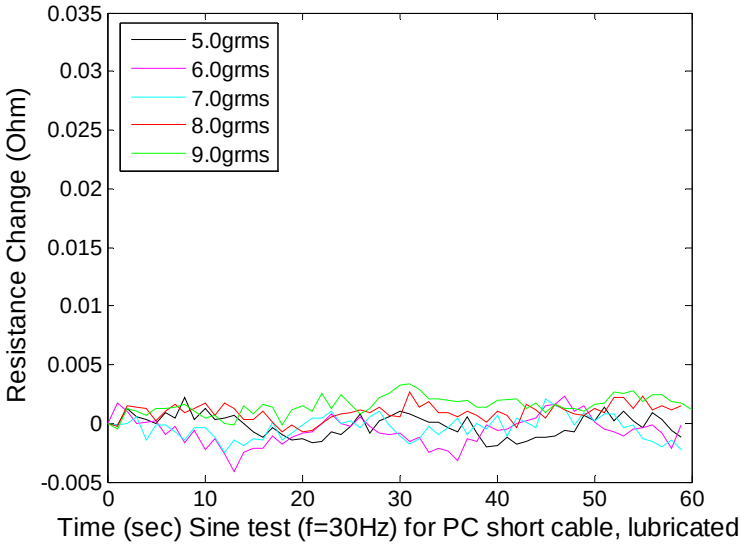

Figure 2-47 Resistance change of lubricated samples for 30Hz, short cable testing

A series of experiments were performed to confirm the effect of the lubricant. Figure 2-46 and Figure 2-47, which also use the same coordinate scale, compared the

resistance change (Δ R) of un-lubricated and lubricated samples for the same 30Hz, short tie-off configuration. The same phenomenon was observed for this test scenario. The results of other tests also confirmed that use of a lubricant successfully prevented fretting.

2.4 Result Analysis

From equation 1, equation 4 and equation 5 can be derived to calculate the amplitude of vibration if the vibration g-level is given.

$$amplitude_{peak-peak} = \frac{9.81 \times 1000 \times 2 \times \frac{g_{rms}}{(2 \times \pi \times f)^2}}{0.707} \quad (mm) \qquad (4)$$

Or

$$amplitude_{peak-peak} = 27751.06 \times \frac{g_{rms}}{\omega^2} \quad (mm) \qquad (5)$$

Where $\omega = 2 \times \pi \times f$

To identify the rule which determines the threshold of connector fretting, the threshold displacements or amplitudes of the input vibration are multiplied with the corresponding relative motion of the two contact halves of the PC connector and automotive connector for the short, middle and long tie-off configurations. Because amplitude (which corresponds to the displacement in the shaker head) = k * (g_{rms}/ ω^2), where g_{rms} is the vibration level at the shaker head, the displacement * relative motion = k * (g_{rms}/ ω^2) * relative motion = k * g_{rms} * (relative motion/ ω^2), where k is a constant.

In order to simplify the calculation, only g_{rms} * (relative motion/ ω^2) was calculated. Table 2-7 through Table 2-11 list the product values for the PC and automotive connectors in all three tie-off configurations.

Table 2-7 Product of $G_{threshold}$ and Relative Motion/ ω^2 for PC short tie-off length

Input Vibration Frequency (Hz)	Threshold Input Vibration level at Shaker Head $G_{threshold}$ (rms)	Value of Relative Motion/ω^2 Between two Connector Halves	Product of $G_{threshold}$ and Relative Motion/ω^2
20	1.52	4.0e-6	6.08e-6
30	4.9	1.69e-6	8.28e-6
40	9.0	0.87e-6	7.83e-6
200	11.0	0.57e-6	6.27e-6

Table 2-8 Product of $G_{threshold}$ and Relative Motion/ ω^2 for PC middle tie-off length

Input Vibration Frequency (Hz)	Threshold Input Vibration level at Shaker Head $G_{threshold}$ (rms)	Value of Relative Motion/ω^2 Between two Connector Halves	Product of $G_{threshold}$ and Relative Motion/ω^2
50	5.2	1.07e-6	5.56e-6
100	10.0	0.36e-6	3.6e-6

Table 2-9 Product of $G_{threshold}$ and Relative Motion/ ω^2 for PC long tie-off length

Input Vibration Frequency (Hz)	Threshold Input Vibration level at Shaker Head $G_{threshold}$ (rms)	Value of Relative Motion/ω^2 Between two Connector Halves	Product of $G_{threshold}$ and Relative Motion/ω^2
50	5.6	0.5e-6	2.8e-6
200	13.4	0.22e-6	2.95e-6

Table 2-10 Product of $G_{threshold}$ and Relative Motion/ ω^2 for Auto middle tie-off length

Input Vibration Frequency (Hz)	Threshold Input Vibration level at Shaker Head $G_{threshold}$ (rms)	Value of Relative Motion/ω^2 Between two Connector Halves	Product of $G_{threshold}$ and Relative Motion/ω^2
60	7.2	3.41e-6	2.46e-5
110	5.1	2.26e-6	1.15e-5
140	4.0	3.43e-6	1.37e-5

Table 2-11 Product of $G_{threshold}$ and Relative Motion/ ω^2 for Auto long tie-off length

Input Vibration Frequency (Hz)	Threshold Input Vibration level at Shaker Head $G_{threshold}$ (rms)	Value of Relative Motion/ω^2 Between two Connector Halves	Product of $G_{threshold}$ and Relative Motion/ω^2
50Hz	6.0	2.94e-6	1.76e-5
100Hz	6.8	3.5e-6	2.38e-5
140Hz	10.0	2.11e-6	2.11e-5

From the above tables, it is observed that the products of $G_{threshold}$ and Relative Motion/ω^2 for each type of connector and tie-off configuration are almost the same, less than 20% difference experimentally. Thus, the threshold displacement at the shaker head * relative motion between two connector halves, which is the threshold relative displacement between two connector halves, remains almost the same, regardless of the input vibration frequency.

This relationship can also be illustrated by Figure 2-48, Figure 2-49, and Figure 2-50, which show the threshold displacements at the shaker head and the scaled inverse relative motion curve for the PC, short tie-off configuration and the Auto, middle and long tie-off configurations, respectively. If the product of the threshold displacement at the shaker head * relative motion between two connector halves is a constant, then the

threshold displacement at the shaker head must match the inversed relative motion curve, with a scaling factor.

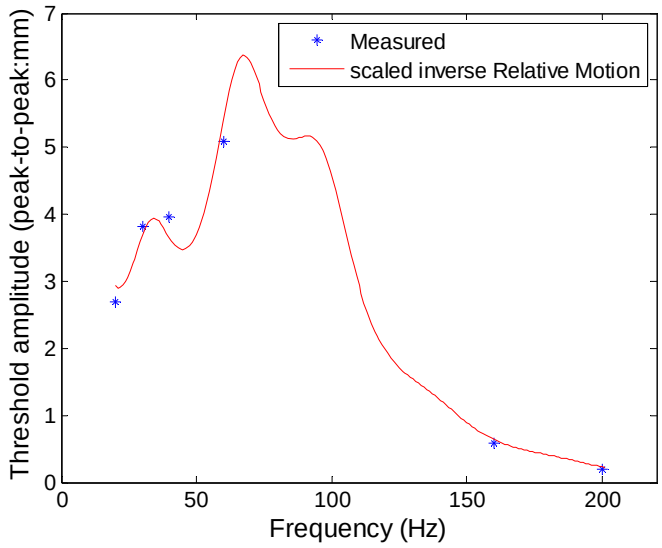

Figure 2-48 Threshold displacement at the shaker head and the relative motion, PC short

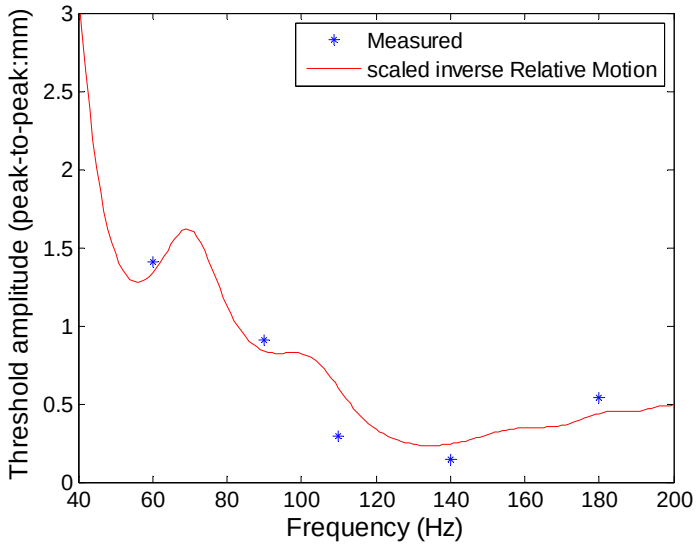

Figure 2-49 Threshold displacement at the shaker head and relative motion, Auto middle

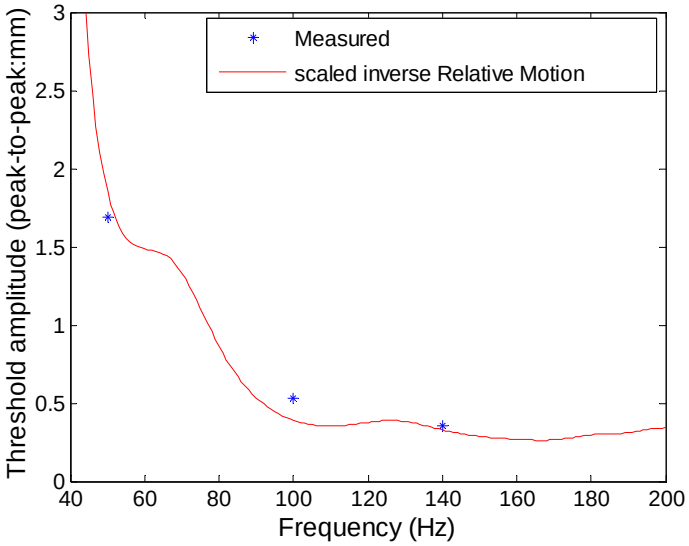

Figure 2-50 Threshold displacement at the shaker head and the relative motion, Auto long

2.5 Modeling the Early Stage Fretting Rate

In order to further analyze the data resulting from the experimental test and to develop some predictive capability, a simple model was developed. The diagram shown in Figure 2-51 outlines the basic modeling philosophy utilized. The gross excitation at the shaker head produces motion in the wiring and connector assembly that, in-turn, causes relative motion at the connector interface, resulting in the resistance increases associated with fretting corrosion.

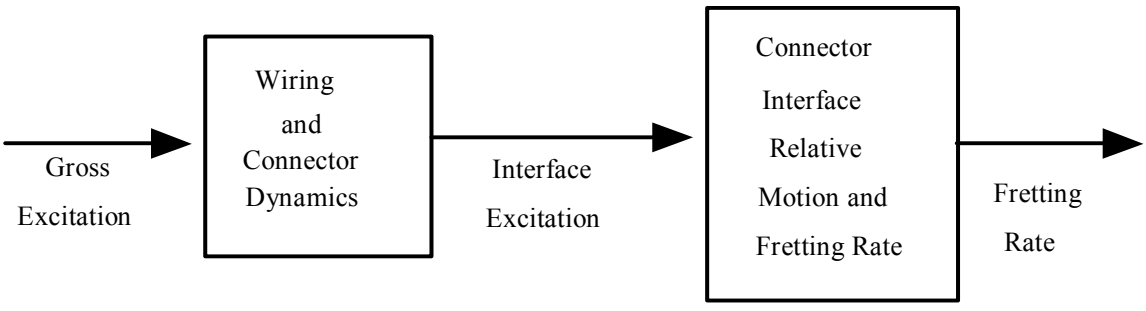

Figure 2-51 Conceptual diagram for predicting vibration induced fretting corrosion

For the purposes of this modeling exercise, it was assumed that the resistance change, ΔR, due to fretting depends on the number of cycles, C, and the amplitude of the vibration displacement above the threshold displacement. Functionally it was assumed that this relation could be expressed as follows:

$$\Delta R = D(A_x - A_{x,threshhold})^M (C)^P \tag{6}$$

where A_x is the relative displacement of the excitation that is actually seen at the connector interface, $A_{x,threshold}$ is the threshold relative displacement that will cause the connector fretting and D is the coefficient associated with the excitation frequency.

The relative displacement of the excitation that is actually seen at the connector interface, A_x, has the following relationship with the displacement of the excitation at the shaker head, A_F, where Z_F is the relative motion between the two connector halves at a given excitation frequency.

$$A_x = Z_F A_F \tag{7}$$

Equation 7 transforms equation 6 into:

$$\Delta R = DZ_F^M (A_f - A_{f,threshhold})^M (C)^P \tag{8}$$

Based upon the linearity of the contact resistance change in these early stages of fretting, P was assumed to be 1 in the model. Thus, substituting C = t/T = ft (where f is the excitation frequency, T is the period for one cycle and t is time) with P=1 produces:

$$\frac{d\Delta R}{dt} = DZ_F^M (A_f - A_{f,threshhold})^M f \tag{9}$$

Because g_{rms} amplitude has a linear relationship with the displacement amplitude at a given frequency, shown in equation 1, comparing the form of equation 9 with the data of Figure 2-19, Figure 2-22, Figure 2-25, Figure 2-35, and Figure 2-39 led to the selection of M=1, implying a linear response with respect to g_{rms} amplitude. This gives:

$$\frac{d\Delta R}{dt} = DZ_F (A_f - A_{f,threshhold}) f \tag{10}$$

According to equation 5, the displacement amplitude A = k * g_{rms}/ω^2, and because a vibration level is normally specified by g-level, equation 10 can be changed into the following format:

$$\frac{d\Delta R}{dt} = E \frac{Z_F}{f^2} (G_f - G_{f,threshhold}) f \tag{11}$$

where G_f is the G-level acceleration of the shaker head, $G_{threshold}$ is the vibration level of the shaker head at the threshold (the onset of fretting), and E is a new scaling factor with the excitation frequency. The f^2 term in the denominator of equation 11 accounts for the frequency relationship between the G-level and the displacement amplitude for a single frequency vibration.

Table 2-12 and Table 2-13 provide a summary of the basic results for PC connector tests for all three cable lengths in low frequencies and higher frequencies, respectively. The threshold displacements match reasonably well, but there appears to be a definite dependency on the cable length, with the values consistently decreasing as the cable length increases. The scaling factor E changed for higher frequencies because the motion mode of the connector halves had changed in higher frequencies.

Table 2-12 Modeling results for the PC-type connector in low frequencies

Wiring Tie-off Length (inches)	Input Vibration Frequency (Hz)	Threshold Input Vibration Level at Shaker Head $G_{threshold}$ (rms)	Scaling Factor Z_F/f^2	Threshold Relative Displacement at the Terminal (mm)	Scaling Factor, E
3.0 (short)	20	1.52	1.6e-4	0.06	0.05
3.0 (short)	30	4.9	6.7e-5	0.08	0.06
3.0 (short)	40	9.0	3.4e-5	0.08	0.06
3.0 (short)	60	25.2	1.3e-5	0.09	0.06
8.0 (middle)	50	5.2	4.2e-5	0.06	0.04
12.0 (long)	50	5.6	2.0e-5	0.03	0.07

Table 2-13 Modeling results for the PC-type connector in higher frequencies

Wiring Tie-off Length (inches)	Input Vibration Frequency (Hz)	Threshold Input Vibration Level at Shaker Head $G_{threshold}$ (rms)	Scaling Factor Z_F/f^2	Threshold Relative Displacement at the Terminal (mm)	Scaling Factor, E
3.0 (short)	160	18.1	1.8e-5	0.07	0.002
3.0 (short)	200	11.0	2.3e-5	0.06	0.006
8.0 (middle)	100	10.0	1.4e-5	0.04	0.003
12.0 (long)	200	13.4	0.87e-5	0.03	0.002

Table 2-14 and Table 2-15 provide a summary of the basic results for the auto connector tests for two cable lengths. Again, the threshold amplitude and the relative motion relationship correlate reasonably well and the scaling factor E changed because of the same reason as for the PC-type connector.

Table 2-14 Modeling results for the Automotive-type connector in low frequencies

Wiring Tie-off Length (inches)	Input Vibration Frequency (Hz)	Threshold Input Vibration Level at Shaker Head $G_{threshold}$ (rms)	Scaling Factor Z_F/f^2	Threshold Relative Displacement at the Terminal (mm)	Scaling Factor, E
8.0 (middle)	60	7.2	1.35e-4	0.25	0.032
8.0 (middle)	90	11.8	6.3e-5	0.19	0.031
8.0(middle)	110	5.1	8.92e-5	0.12	0.028

Table 2-15 Modeling results for the Automotive-type connector in higher frequencies

Wiring Tie-off Length (inches)	Input Vibration Frequency (Hz)	Threshold Input Vibration Level at Shaker Head $G_{threshold}$ (rms)	Scaling Factor Z_F/f^2	Threshold Relative Displacement at the Terminal (mm)	Scaling Factor, E
8.0(middle)	140	5.4	1.35e-4	0.14	0.016
8.0(middle)	180	3.5	2.1e-4	0.13	0.013
12.0(long)	140	10.0	8.33e-5	0.21	0.02

2.6 Summary and Conclusions

An investigation of the basic characteristics of vibration-induced fretting was conducted. The influence of connector design, wire tie-off length, vibration profile, and lubrication were considered. Two different connector designs were evaluated: a single-row, PC-type connector and a single-row, automotive-type connector. The "as-delivered" configuration of both connector types showed little or no tendency to fret, but with modification of the connectors, substantial fretting was induced.

Both connector designs exhibited self-consistent relative displacement amplitude thresholds for the onset of fretting corrosion. Also, there was a general linear dependency upon the G-level with regard to fretting rates over the G-levels and frequency ranges that were tested for single frequency excitation. This is probably because for single frequency vibration, the G-level and displacement amplitude are proportional. Based on the findings in the present work, the model describing the fretting corrosion rate constructed in earlier work [40] was extended by incorporating the role of displacement amplitude in governing the response of the system. Consequently, when considering the design of vibration tests, these factors must be taken into account. It is therefore necessary to consider how the expected field vibration stresses are related to the accelerated tests through the relation of threshold amplitudes and g-levels and how the frequency spectrum impacts these parameters.

Additionally, the relationship between the housing motion and the actual relative motion at the connector interface was evaluated using PC-type connector samples that were specially modified to allow direct measurement access to the terminal. The relative motion of the plug housing/header and the terminal/header tended to be quite similar except for small differences at vibration frequencies near the respective resonance peaks. Particular care must be taken to properly determine the transfer function relations if this information is to be used to make analytical predictions.

A connector lubricant was tested using the modified versions of the PC-type connectors. As expected, this lubricant was observed to inhibit fretting over the amplitude and frequency ranges that were tested.

After synthesizing the experimental results, modeling work and summary, the following conclusions can be obtained for the present research:

- The experimental results indicated that there is a linear relationship between the rate of the contact resistance change in the early stage of fretting corrosion and the amplitude or g-level at the input shaker's head in the sinusoidal single-frequency vibration tests.
- An input threshold g-level at the shaker's head can be observed in all vibration tests. This threshold g-level is related to the relative motion of the connector interface at different frequencies.
- Regardless of the excitation frequency applied to the overall system, the existence of a relative displacement threshold that caused fretting at the connector interface was observed.
- The use of a connector lubricant was observed to inhibit fretting.
- A model was developed that related the early stage fretting corrosion rate to the threshold vibration levels for the connector, the dynamic characteristics of the connector / wiring configuration, and the vibration frequency.
- A reasonable level of consistency between this model and the experimental data was demonstrated.

CHAPTER 3 THE INFLUENCE OF CONTACT INTERFACE CHARACTERISTICS ON VIBRATION-INDUCED FRETTING DEGRADATION

3.1 Purpose of This Study

Fretting degradation has long been recognized as a major failure mechanism, having been first identified as such over 65 years ago [41] and has continued to be a topic of considerable research interest even since. One of the earliest studies on fretting degradation in electrical connectors was reported by Whitley and Bock [3] in 1974. A detailed survey of research up to 1984 is provided by Antler [9] and more recent work is described by Malucci [33].

Fretting damage is caused by relative motion at the contact interface, which leads to material displacement and transfer. Due to the small relative displacements, this motion cannot effectively clean away the wear particles and oxidized material that is formed in the interface. This results in the localized buildup of an insulating layer, which leads to substantial and rapid increases in contact resistance [42]. This motion can be induced by thermal expansion/contraction, vibration, or by a combination of these two mechanisms. It is generally recognized that fretting is a complex phenomenon, as was noted by Malucci [17]. For example, the localized wiping action that occurs as the contacting surfaces move relative to each other can produce oscillations in the contact

resistance and even temporary reductions. The susceptibility of a particular connector to fretting depends upon a variety of factors, including the material and tribological properties of the finish and the dynamic characteristics of the connector design.

There has been considerable recent work on this topic, including experimental investigations (for example Maul, McBride, and Swingler [43]) and model development work (such as Bryant [15]). However, the basic mechanisms are not yet completely understood. At present, studies of vibration-induced fretting degradation in connectors often do not correlate well with laboratory studies of similar contact materials [43]. Subtle variations in specimen geometry and contact interfaces can considerably alter fretting behaviors for different pins, even when assembled into the same type of connector housing. Consequently, there is considerable current interest in developing a better understanding of the basic physical causes of fretting degradation.

Previous investigations of vibration-induced fretting degradation have demonstrated some interesting behaviors, specifically a threshold vibration level for the onset of fretting and a strong relationship between vibration amplitude (beyond the threshold level) and the rate of resistance change [18][34][44]. However, there were a number of questions that remained after these earlier studies that need to be resolved. One specific issue is the need for a more detailed understanding of the mechanisms controlling fretting degradation. In particular, how do changes in the design characteristics of the contact interface influence the observed fretting behavior?

The present study addresses these questions and develops answers based on the results from a series of experimental tests of sample connectors, which are subjected to single-frequency vibration profiles at room temperature. These test specimens consisted

of a series of dual-row 16-circuit automotive connectors in which the plating finish / base material combination and contact normal force were varied.

3.2 Experimental Details

3.2.1 Experimental Samples

A series of samples were fabricated based upon a commercially available automotive connector design, shown as Figure 3-1. These samples had two different plating finish / base metal configurations and three contact normal force levels. Table 3-1 summarizes the sample profiles. Both finishes were based upon a pure tin system, although the type 2 finish structure had been modified to produce a coefficient of friction approximately half of the coefficient for the type 1 finish. The thicknesses of the metal strips used to fabricate the terminals were the same, and the elastic modulus of the samples were very similar. Thus, the spring rates would nominally have been equivalent.

Figure 3-1 Original automotive sample

Table 3-1 Types of Specimens

Specimen Type	Finish	Normal Force (N)
1a	1	4.7
1b	1	6.0
1c	1	6.5
2a	2	4.3
2b	2	5.3
2c	2	6.3

A matter of critical interest in the present study was the measurement of the relative motion at the contact interface. However, it is not possible to measure the motion directly without altering the contact relationship. An alternative approach was therefore adapted to indirectly monitor the motion at the contact interface by measuring the relative motion between the male and female sides of the housing, which was an approach used in previous work [34]. This approach assumes that the housing motion is directly related to the motion at the contact interface.

In order to address this assumption, transfer functions were measured and compared for a housing system with viewing slots machined through its surface to allow direct access to the mating terminal pairs in each half of the connector housing, as shown in Figure 3-2. The slots were positioned so as not to alter any features of the housing that constrained terminal motion. The displacements at each location were measured using a non-contacting laser displacement measurement system. The resulting transfer functions are shown in Figure 3-3.

Comparing the housing-to-housing transfer function to the pin-to-pin transfer function for a sample with a 1.0 cm viewing slot shows that the resonant frequencies are approximately the same, although, the amplitude at the resonant frequency is higher for

the pin-to-pin transfer function. Away from the resonant peak, the differences appear to be quite small. Hence, for most testing and evaluation purposes, the housing-to-housing transfer function can be taken to be a reasonable approximation.

Figure 3-2 Automotive sample with viewing slots

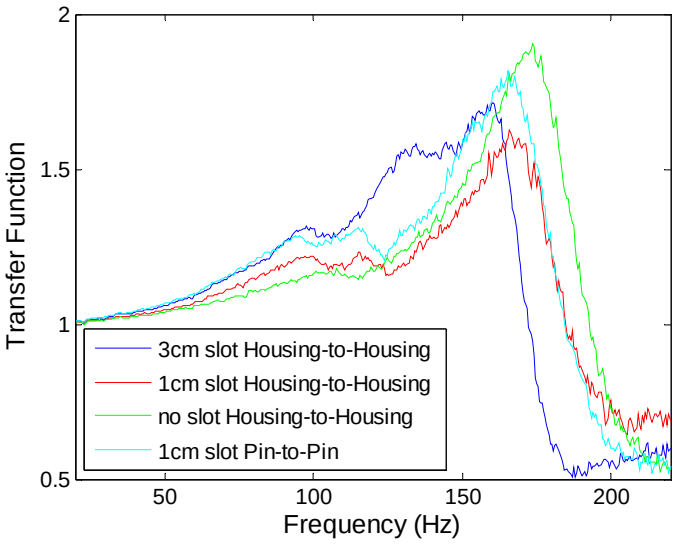

Figure 3-3 Comparison of the effect of viewing slots on transfer function

Another issue of concern with regard to the transfer functions is the effect on system performance of machining the slots. In order to obtain a qualitative measure of this effect, a comparison was made of the housing-to-housing transfer functions for housings with two different slot lengths, 3.0 cm and 1.0 cm, and housings with no viewing slots (Figure 3-3). The results show that the lengths of the slots can have a significant impact on the transfer function. The 1.0 cm slot was selected for use in this testing as it produced a minimal impact on the transfer function, while still permitting sufficient access for laser monitoring of the terminal motion.

Another kind of connector sample was used in this study to compare its fretting corrosion with that of the automotive samples. This alternative connector, shown as Figure 3-4, is produced by another connector manufacturer. It has a different housing structure, but the same connector wires and mating pairs as the automotive connectors used in this study. The only difference between these two kinds of connectors is their structure design. Again, as shown in Figure 3-5, viewing slots were machined through the housing surface to allow direct access for the transfer function measurement of the mating terminal pairs.

Figure 3-4 A different connector from another manufacturer

Figure 3-5 Viewing slots in the comparison connector

3.2.2 Experimental Equipment

In this study, most of the experimental equipment was the same as that used in the previous two projects and was described in the last chapter, including the Keithley Model 2010 multimeter, the HP 35665A Dynamic Signal Analyzer, and the POLYTEC laser

vibrometer. The only significant difference is the vibration system, which incorporated a bigger shaker and amplifier with an enhanced power-supply and excitation ability.

The vibration system used for this experiment consisted of the LDS 350 vibrator [45], LDS SPAK amplifier, KISTLER charge amplifier, DACTRON LASER vibration control equipment [46] and a cooling fan. Figure 3-6 shows how they were assembled to create the LDS vibration system. The main characteristics of the LDS shaker, SPAK amplifier and DACTRON vibration control system are listed below and indicate their suitability for this study. Figure 3-7 and Figure 3-8 show photographs of these three components.

LDS 350 vibrator:

- Useful frequency range: DC~3000Hz
- Velocity, sine, peak: 2.0m/s (78.7in/s)
- Acceleration, sine, peak: 5888.4m/s^2 (60.0g_n)
- Displacement peak-peak: 50.8mm (2.0in)

SPAK Amplifier:

- Power range: 5-50kVA in 5kVA increments
- Rated output voltage: 100V rms

An amplifier's self-protection capability is very important for safety reasons during vibration tests. The amplifier system is protected by the following interlocks:

- Output over-voltage
- Amplifier over-temperature

- Vibrator over-travel
- Slip Table over-travel
- Vibrator cooling system failure
- Input overdrive
- Power module failure

DACTRON LASER Vibration control system:

- Frequency range: Up to 42 kHz analysis frequency.
- Frequency accuracy: Within 0.01%
- Dynamic range: 120 dBfs.

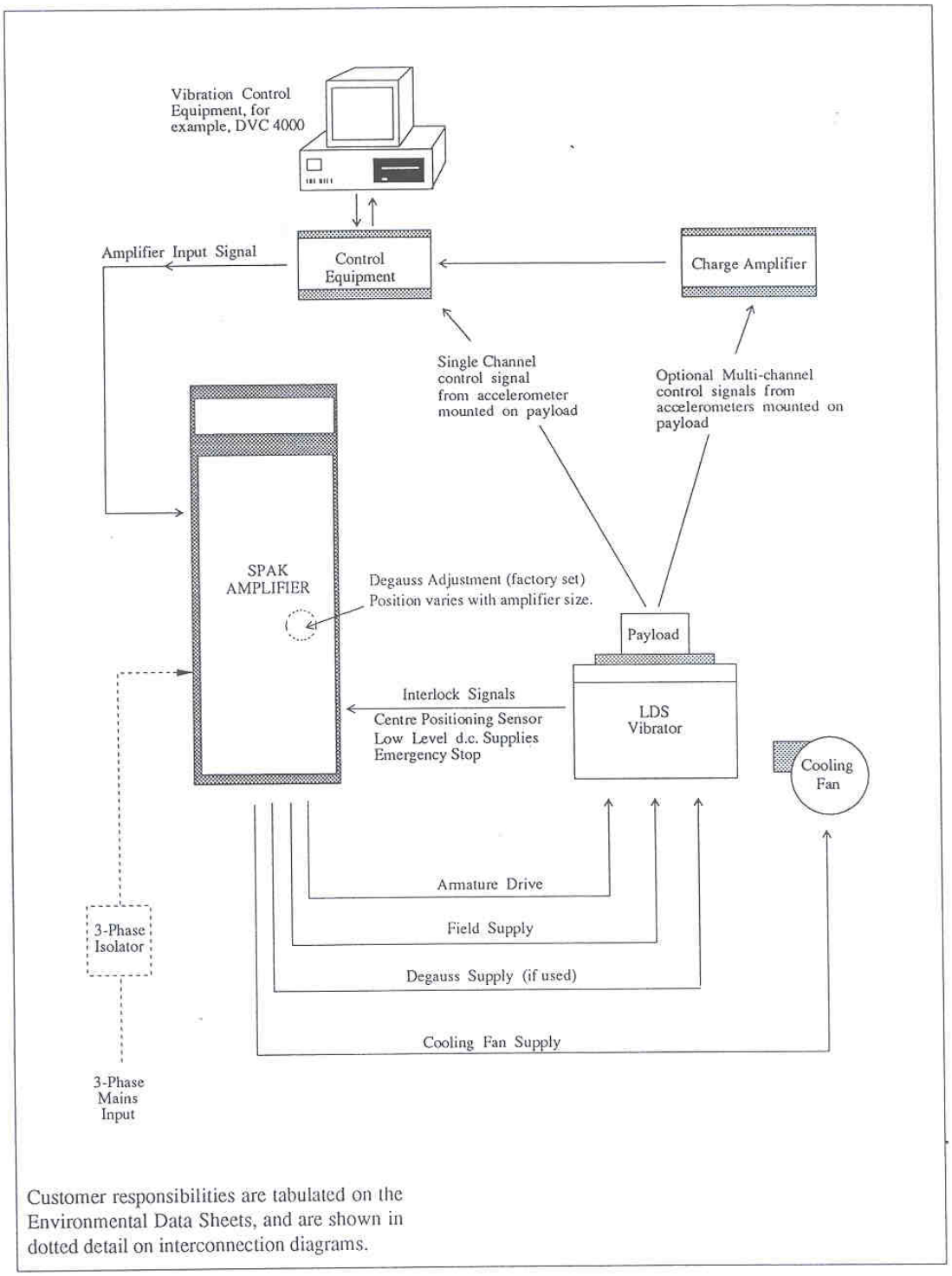

Figure 3-6 LDS vibration test system

Figure 3-7 LDS 350 vibration shaker

Figure 3-8 DACTRON vibration control system and SPAK amplifier

3.2.3 Experimental Setup

The experimental setup is shown in Figure 3-9. The connector consists of a 16 pin connector system for both the male and female terminals. These 16 wire leads were attached at each end of the connector and the other ends were clamped in the fixture. The connector was clamped at the fixture by the male terminal housing. A supplementary mass was clamped to the wire leads close to the connector housing, with a 2 mm gap between the connector housing and the mass. This inertial mass consisted of three plates, with one plate positioned between the two rows of wire leads and the remaining two plates on the outside of each row, with the resulting assembly clamped together with bolts. The entire assembly was bolted to a horizontal slip table, which was driven by a vibratory shaker.

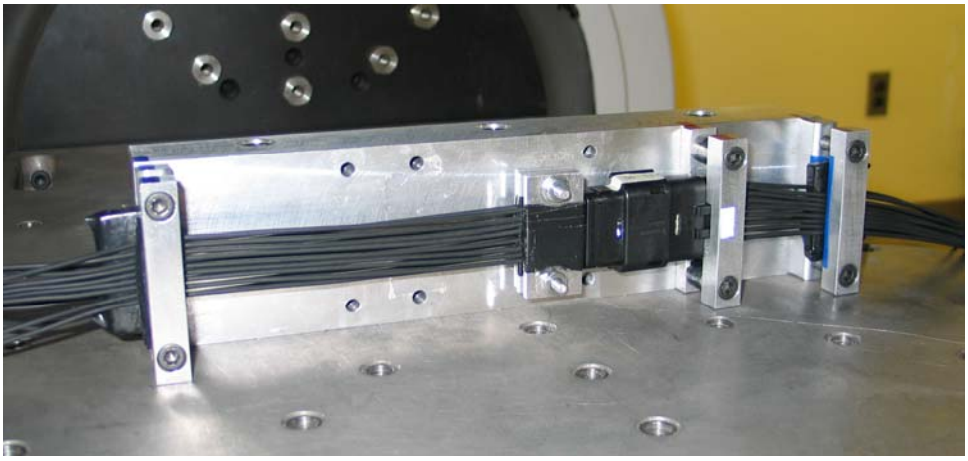

Figure 3-9 Photograph of the experimental setup

Figure 3-10 shows a typical transfer function measured by the system. This is very similar to the transfer functions measurement in the study reported in Chapter 2, with the measuring direction horizontal. Figure 3-11 shows the transfer functions with and without the supplementary mass for this experimental setup. For the transfer function

without supplementary mass, the first resonant frequency for the connector attached to the shaker table was 600 Hz. Preliminary testing indicated that this frequency was much too high to allow excitation amplitudes sufficient to produce fretting in the sample connector. In order to ensure consistent fretting degradation in the frequency and amplitude ranges provided by the available laboratory shaker system, the supplementary mass described above was therefore added in this system. The addition of the supplementary mass lowered the first resonant frequency to less than 200 Hz, which was within the acceptable range for the shaker system.

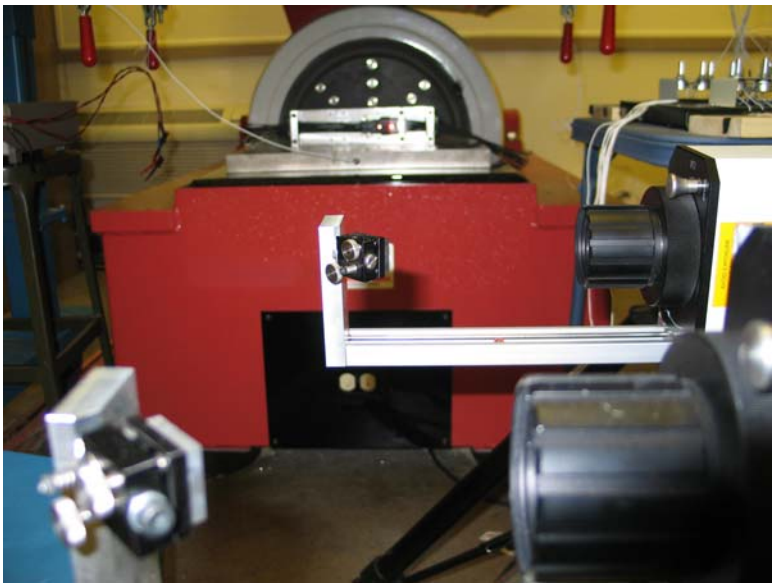

Figure 3-10 Measurement of the transfer function

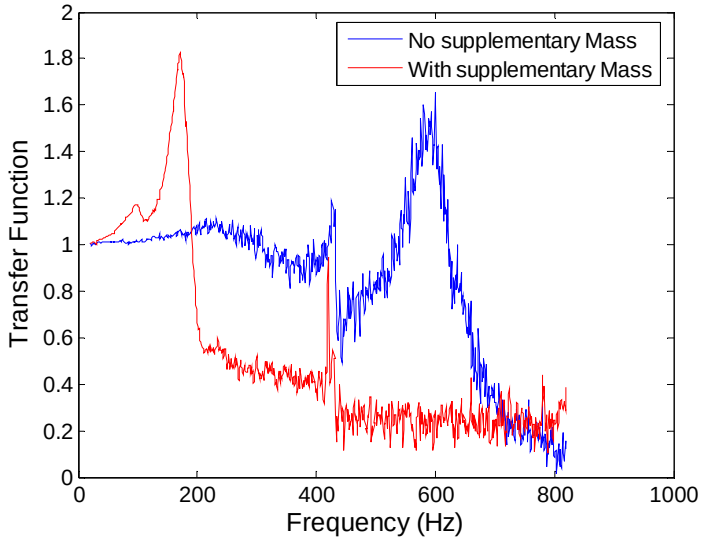

Figure 3-11 Transfer functions with or without supplementary mass

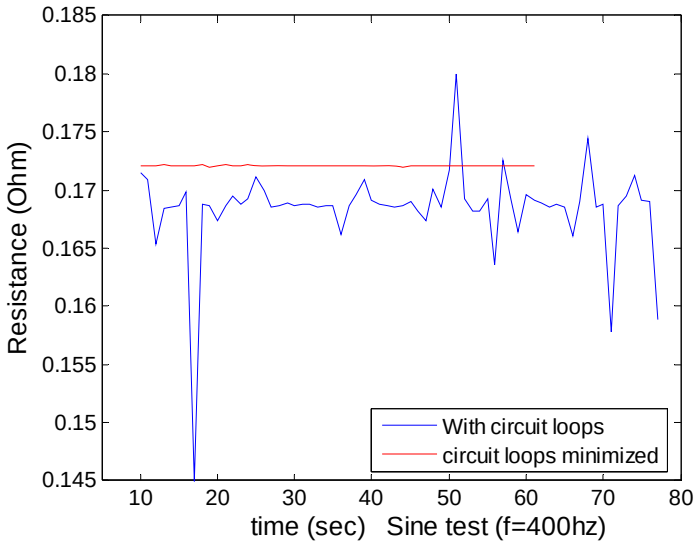

Figure 3-12 Ohmmeter reading with and without circuit loops in cable

Other investigators working on the vibration testing of electrical systems have reported some difficulty in measuring resistance values during vibration due to electromagnetic interference from the shaker [47]. As shown in Figure 3-12, the testing performed for the current study indicated that this phenomenon can definitely be a

problem. However, if looping of the wire leads and ohmmeter cables was minimized, as shown in Figure 3-13, the effect on the measured resistance values appeared to be negligible, as demonstrated by the steady value obtained at about 173 mOhms.

Figure 3-13 Connector resistance measurement with circuit loops minimized

The contact resistance value reported in this work was a composite measure of the resistance value across all of the terminals. This was accomplished by linking the terminals in a series circuit with the wire leads connected together such that they switched back and forth, thus minimizing the looping effects.

Because the experimental objective for the alternative commercial connector is to compare the fretting corrosion performance between the automotive connector and the alternative commercial connector, the setup of this experiment needed to utilize unmodified samples, with no supplementary masses added. Figure 3-14 and Figure 3-15 show the experimental setup for the comparison of fretting performance.

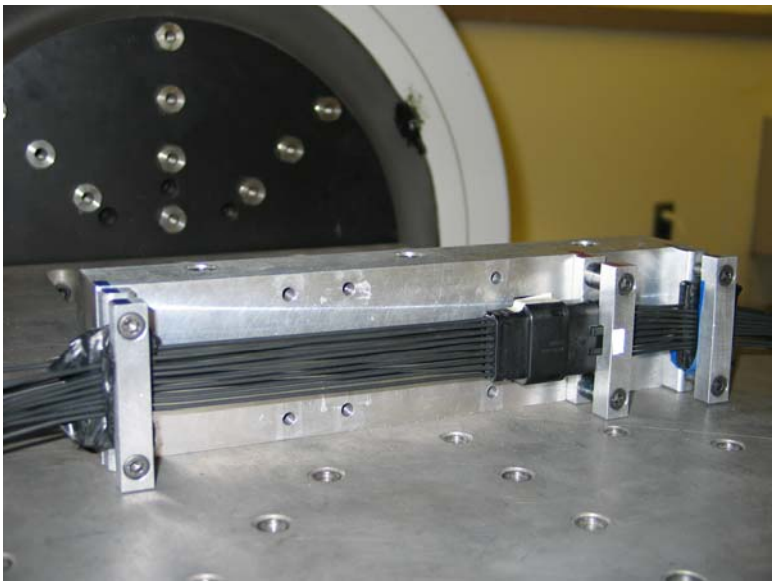

Figure 3-14 Setup for the unmodified Auto connector in the comparison experiment

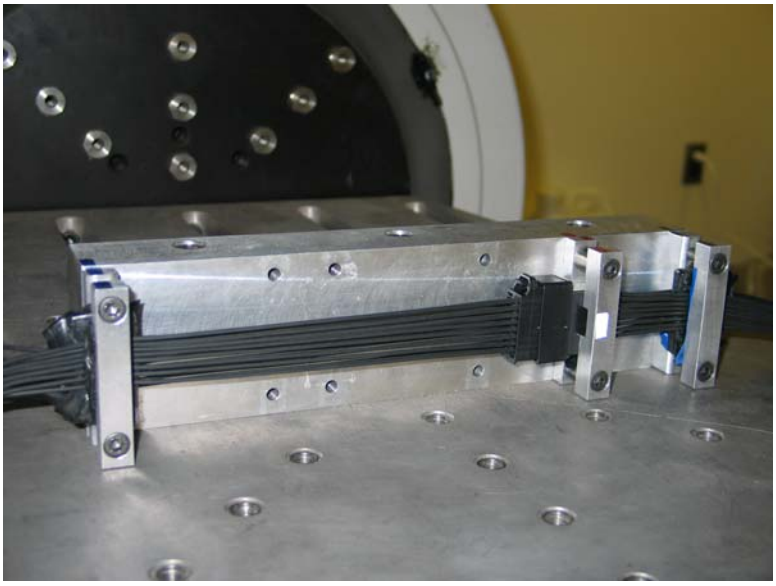

Figure 3-15 Setup for the unmodified alternative connector in the comparison experiment

3.3 Experimental Result and Analysis

In order to evaluate the effectiveness of the dynamic analysis and the relative motion transfer function techniques developed in earlier investigations and their applicability to multi-row connector designs, the two types of connector samples

described earlier were experimentally evaluated using the same procedures as those described in Chapter 2. First, the transfer functions were determined for each specimen. Then combining the phase and magnitude of the transfer functions, the relative motion of the contact members can be calculated using equation 3 from the previous chapter:

$$Z_F = \sqrt{[1 - M\cos(\phi)]^2 + [M\sin(\phi)]^2} \tag{3}$$

The transfer functions and relative motion functions for type 1 and type 2 specimens are shown in Figure 3-16 through Figure 3-19. There are generally two primary peaks for each of the sample types. As confirmed by testing several terminal pairs external to any connector housings, the lower peak (at around 110 Hz) represents a rocking mode at the connector interface. The higher peak (at around 170 Hz) represents a translational or bounce-type mode at the contact interface. As the normal force is increased, the bounce-type mode tends to be suppressed in favor of the rocking-type mode.

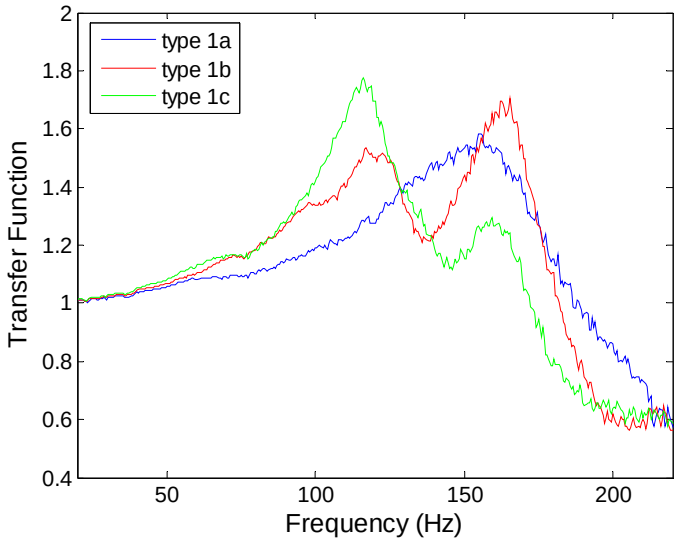

Figure 3-16 Transfer function for type 1 specimens

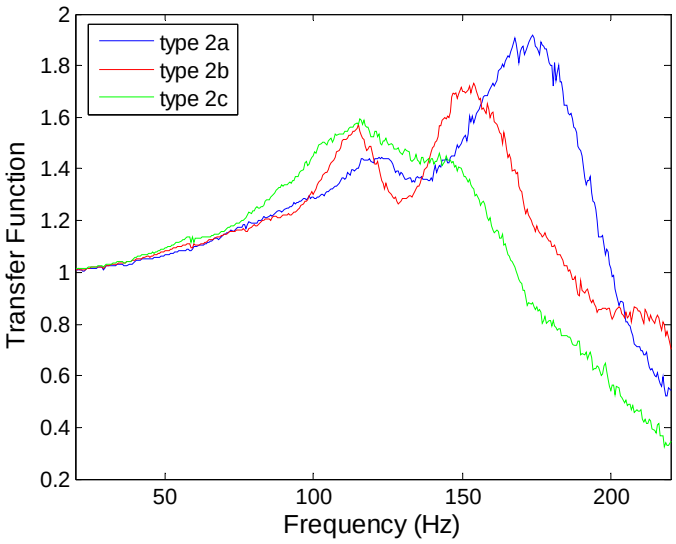

Figure 3-17 Transfer function for type 2 specimens

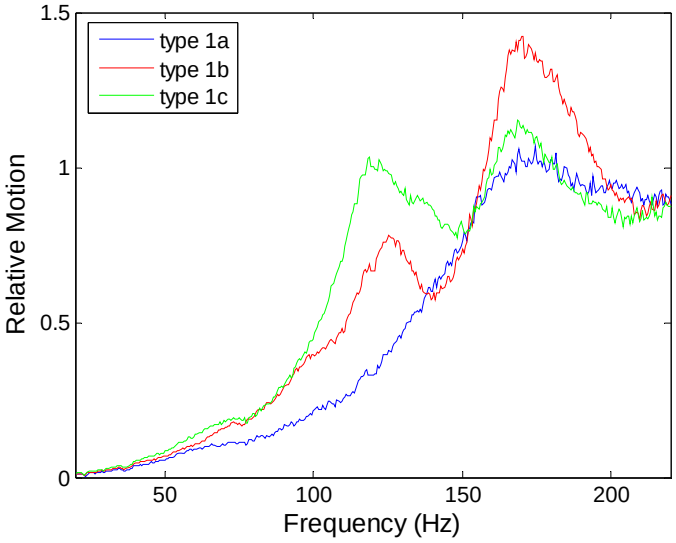

Figure 3-18 Relative motion function for type 1 specimens

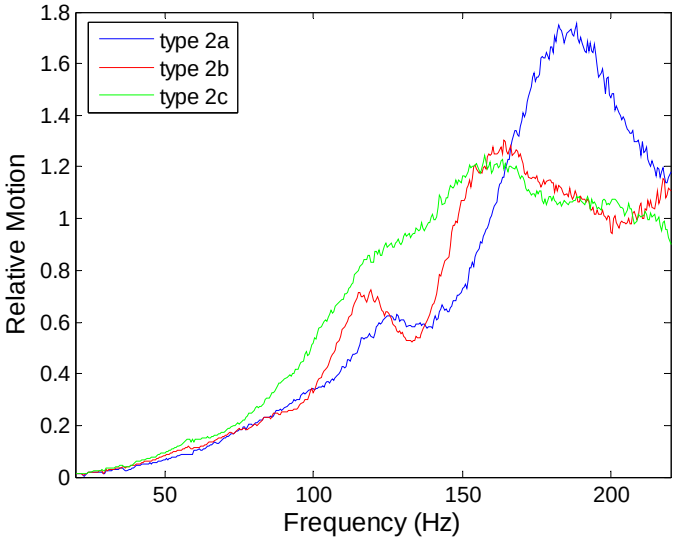

Figure 3-19 Relative motion function for type 2 specimens

It was observed that the relative motion was quite consistent from one sample to another of the same finish / base metal type and normal force. Nevertheless, there were significant differences between the type 1 and type 2 samples, as highlighted by cases where the normal force levels were similar (e.g. 4.7 N for type 1a and 4.3 N for type 2a). As one would intuitively expect, the resonant frequency and the associated amplitude peak for the lower friction finish (type 2) were somewhat higher. Thus, it appears that differences in contact dynamics can be observed by comparing the characteristics of the transfer functions. Fretting tests were also performed for each type of sample. This testing was done at 90 Hz, which was selected based upon the amplitude/frequency capability of the available shaker system. At this frequency, the relative motions among type 1 were c>b>a, among type 2 were c>a>b.

First, the threshold vibration level was determined for each sample type, as shown in Figure 3-20 and Figure 3-21. This was done by monitoring the composite resistance of the connector sample and wire leads using a 4-wire measurement system. If no change in

resistance was observed after 200 seconds of exposure to a given vibration amplitude, then the shaker g-level was incremented and the observations repeated. The lowest g-level for which a sustained resistance change was observed was recorded as the threshold level for that sample. A total of three samples were tested for each sample type. The average result for each sample type is tabulated in Table 3-2.

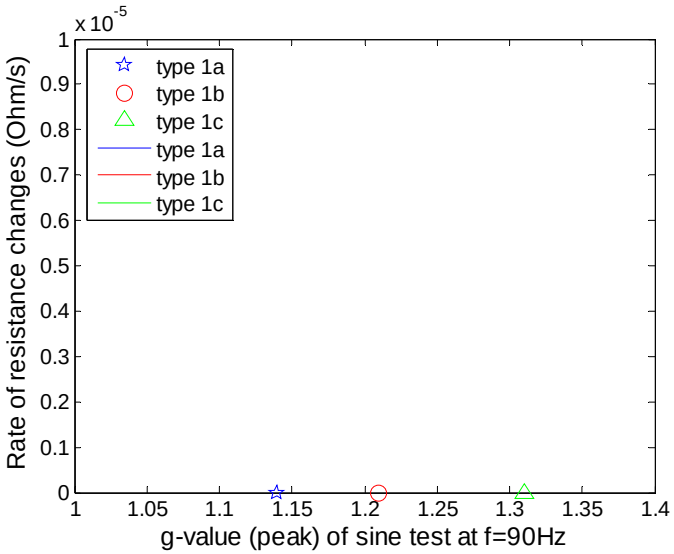

Figure 3-20 Threshold g-level for type 1 samples

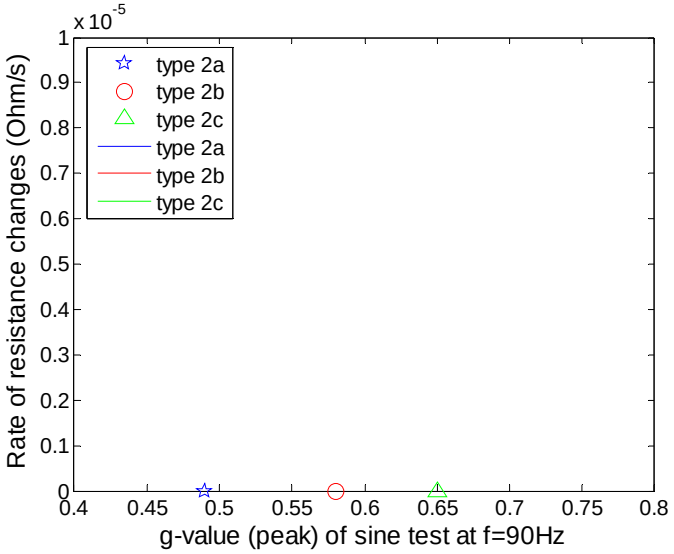

Figure 3-21 Threshold g-level for type 2 samples

Table 3-2 Summary of fretting test results

Type	Threshold G-Level Shaker Head (g - peak)	Threshold G-Level Between Contact Members (g - peak)	Fretting rate at 90Hz, 4.6g (10^{-5} Ohm/ second)	Fretting rate at 90Hz, 6.5g (10^{-5} Ohm/ second)
1a	1.14	0.19	5.2297	7.4259
1b	1.21	0.36	5.0156	8.074
1c	1.31	0.39	5.9668	8.7887
2a	0.49	0.14	3.3081	5.7267
2b	0.58	0.15	2.8067	4.1339
2c	0.65	0.26	3.5697	5.9891

As expected, increasing the normal force resulted in a higher threshold g-level, corresponding to a higher tolerance for vibration without the onset of fretting, for both finish types. Comparing the results for the two finish types showed significant differences between the threshold values, with the lower friction finish having a markedly lower threshold vibration level.

After the threshold vibration level was determined for each sample, the fretting behavior at two specific g-levels above the threshold, 4.6 g and 6.5 g, was measured. The change in resistance was recorded for 100 seconds. As described in earlier investigations, the initial fretting rate was determined in terms of the rate of resistance change at the onset of observable fretting during this initial 100 seconds of degradation [44]. Again a total of three samples were tested for each sample type. The average results are tabulated in Table 3-2. The overall results shown in Table 3-2 are also presented graphically in Figure 3-22 and Figure 3-23. It is observed that the fretting rates for type 1 finish generally are larger than that of type 2 finish. Among type 1, the fretting rates are c>b>a, which is consistent with their relative motions c>b>a at 90 Hz. Among type 2, the fretting rates are c>a>b and it is consistent with type 2 relative motions c>a>b at 90 Hz.

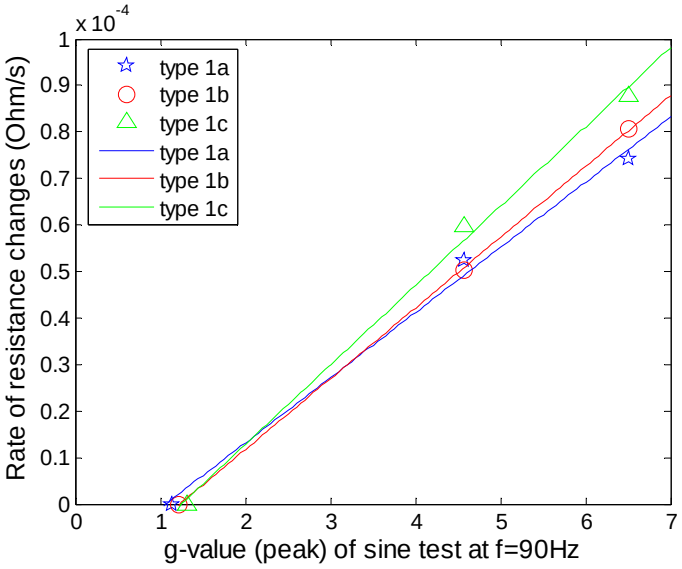

Figure 3-22 Fretting rate for type 1 samples

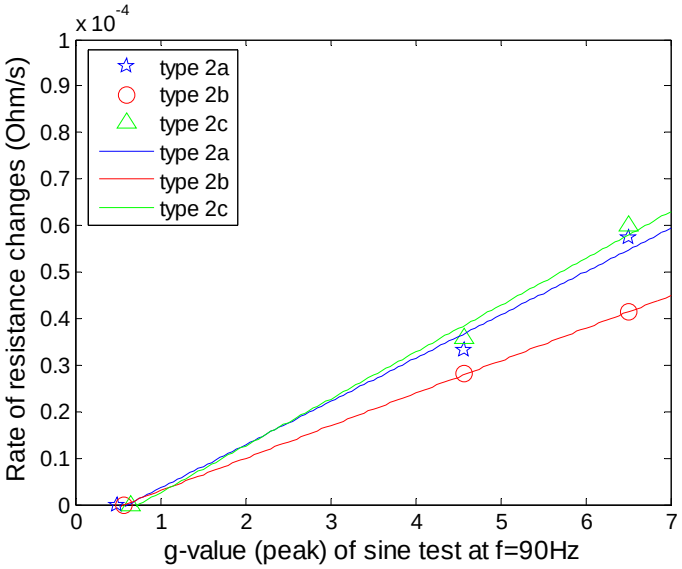

Figure 3-23 Fretting rate for type 2 samples

The overall results tend to support the basic theory that was developed as part of the earlier work on this topic. In the previous work, it was observed that the fretting degradation rate satisfied the relationship:

$$\frac{d\Delta R}{dt} = E\frac{Z_F}{f^2}(G_f - G_{f,threshhold})f \qquad (11)$$

where Z_F is the magnitude of the transfer function describing the relative motion between mating terminals (nominally equivalent to the motion of the "output" terminal relative to the "input" shaker head), G_f is the G-level acceleration of the shaker head, $G_{threshold}$ is the threshold vibration of the shaker head before the onset of fretting, f is the frequency of vibration, and E is a scaling factor.

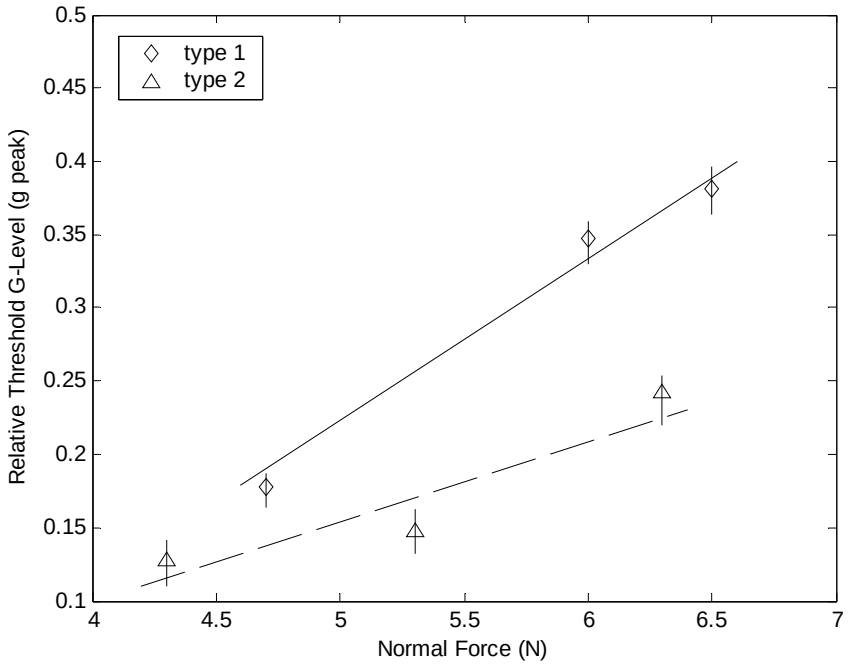

Figure 3-24 Relative threshold g-level as a function of normal force

Figure 3-24 provides a graphical comparison of the measured threshold values for each finish type and normal force in terms of the nominal normal force, with the range of data represented by vertical error bars for each data point. Again, there is a marked difference between the threshold values for the different finish types. In addition, it can be observed that the threshold values increase with increases in the normal force, as one might intuitively expect. The slopes of the linear regression lines for the type 1 and type 2

samples are approximately 0.12 and 0.06, respectively, resulting in a 2:1 ratio that correlates with the 2:1 ratio of the friction coefficients for each finish type.

In order to determine the extent of the degradation exhibited within the contact interface for the plating finish experiencing the more significant contact resistance changes (Sample type 1), a more detailed examination was carried out via scanning electron microscopy (SEM), with the result shown as Figure 3-25 and Figure 3-26. Using backscattered electron imaging to highlight the elemental contrast within the analysis zone, the distinction between tin (light features) and base metal (dark features) was readily discernable. Fretting wear was evidenced by the exposure of significant amounts of base metal and by the displacement of metallic fretting debris to the periphery of the contact zone.

Figure 3-25 SEM examination of the fretting degradation zone for type 1 receptacle

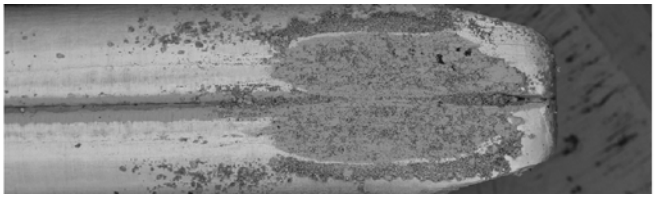

Figure 3-26 SEM examination of the fretting degradation zone for type 1 blade

As an application of the study, an experiment was also done to compare the fretting performance for the automotive connector and an alternative commercial connector, which has the same wire leads, but different housing structures. The resulting

different transfer functions and relative motions between the two contact pairs for these two types of connectors are shown as Figure 3-27 and Figure 3-28.

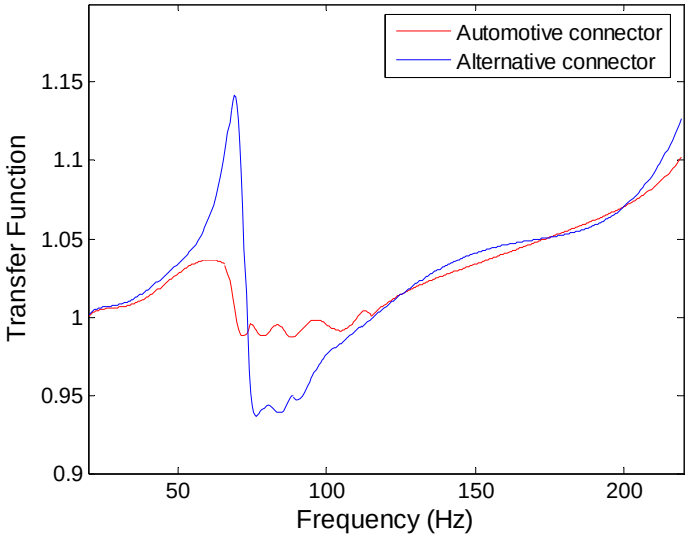

Figure 3-27 Transfer functions for the automotive connector and the alternative connector

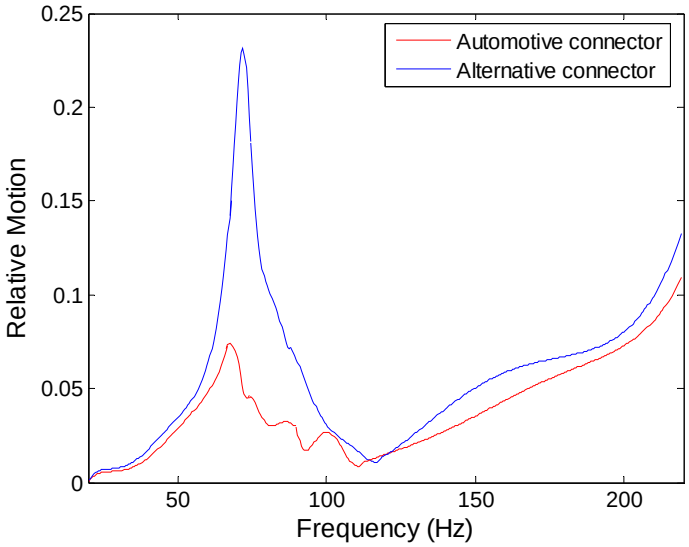

Figure 3-28 Relative motions for the automotive connector and the alternative connector

Figure 3-29 shows the fretting curves for the automotive connector and the alternative connector. The fretting performance for the automotive connector is much better than that of the alternative commercial connector because the relative motion of the alternative connector is much larger than that of the automotive connector at 70 Hz. From this experiment and the results of the fretting study, it can be seen how important structure design is and how different structural designs can significantly affect the fretting performance of connectors.

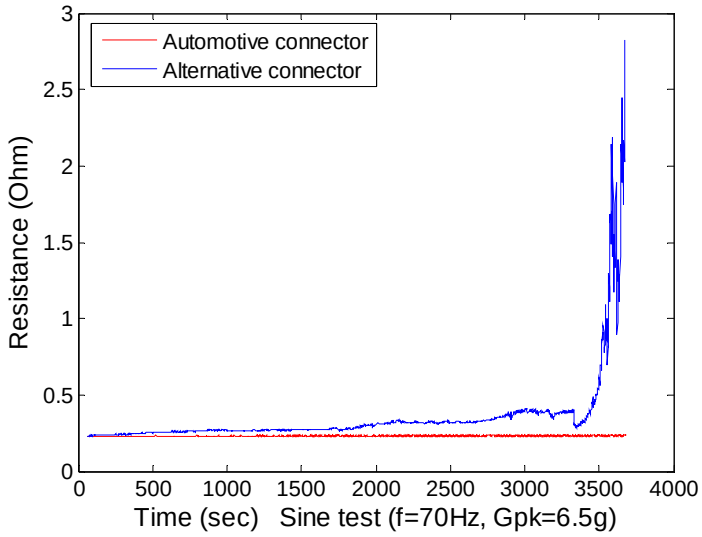

Figure 3-29 Fretting for the automotive connector and the alternative connector

3.4 Summary and Conclusions

This chapter presents a study of the influence of normal force and finish characteristics for vibration-induced fretting degradation of a specific connector design. Two variations of finish type were considered, with each finish type having three variations of normal force level. When tested in a typical application configuration, no fretting of the connector systems could be induced. However, as demonstrated by the

response of the relative motion transfer functions, the systems could be made susceptible to fretting by introducing artificial loading conditions on the wire bundle. When tested in this revised configuration, all samples showed a definite threshold vibration level, below which fretting degradation was not observed. Once this threshold level was exceeded, the rate of initial resistance change increased in an approximately linear fashion with increased g-level, as was observed in earlier investigations. The relative motion transfer function was shown to provide a good measure of the tendency of such systems to fret once the threshold vibration level had been exceeded. A comparison of the fretting performance between two commercial connectors was done as an application of this fretting study. This study can be concluded as follows:

- The fretting rates for type 1 finish were larger than that for type 2 finish for the automotive connector used in this study.
- The threshold g-level tended to increase as the normal force increased.
- The existence of threshold vibration level and the linear fashion resistance change of fretting were found to be consistent with the previous study.
- The relative motion function was also shown to provide a good measure of the tendency of such systems to fret.
- The technique was successfully applied to compare the performance of two similar commercial products.

CHAPTER 4 THE APPLICATION OF FEA SIMULATION TECHNIQUES TO THE PREDICTION OF VIBRATION-INDUCED FRETTING DEGRADATION: ANALYSIS OF A BLADE/RECEPTACLE PAIR

4.1 Introduction to This Study

Fretting degradation has long been recognized as a major failure mechanism, having been first identified as such over 65 years ago [41] and continuing as a topic of considerable research interest over the years. The importance, necessity and current status for the study of fretting degradation have been introduced in previous chapters. The author's previous investigations on the topic of vibration-induced fretting degradation have already demonstrated some interesting behaviors, specifically a threshold vibration level for the onset of fretting and a strong relationship between vibration amplitude (beyond the threshold level) and the rate of resistance change [18][25][34][44].

At present, most evaluations of the fretting propensity of particular connector designs and the influence of variations in those designs on fretting performance are conducted through exhaustive experimental testing, requiring a major commitment of time and resources. A simulation-based method would therefore be of great value to those working on connector design and applications.

Accordingly, the long-range objective of this work is to develop and validate a procedure for using modeling and simulation to predict the influence of various design factors on vibration-induced fretting propensity in electrical connectors. This research seeks to develop detailed finite element models for connector systems that will relate the observed relative motion at the contact interface to the threshold vibration levels for the onset of fretting.

The present investigation is the first step in this effort. An initial study is presented here in which a detailed finite element model was developed for a blade/receptacle pair. Using this model, a series of simulations were performed in order to evaluate the threshold vibration levels as a function of excitation frequency, wire tie-off length, wire mass, interface friction coefficient, and normal force. A series of experiments were also conducted to validate and test the simulation. The results showed that for this limited system, finite element modeling and analysis have great potential for the evaluation of the influence of design variation on fretting behavior.

This study is divided into two parts covering the experimental and FEA modeling aspects of the problem. The experimental section introduces the details of the experiment, including the blade/receptacle samples and the experimental setup, and presents the test results. The FEA modeling section covers the generation of the FEA model. Because the setup, geometric dimensions, material properties and boundary conditions of the FEA model were based on values derived experimentally, the experimental procedure and results are described first in this chapter, followed by a detailed description of the FEA modeling. Finally, the results from the simulation are introduced and compared with the results from the experiment.

4.2 Experimental Description

4.2.1 Experimental Samples

This study was limited to blade/receptacle pairs, such as those shown as Figure 4-1 and Figure 4-2. These blade/receptacle pairs are the same as those used for the automotive connectors in the previous study (Chapter 3). There is a spring component inside the receptacle and a gap exists between the end of this spring and the inner layer in the bottom of the receptacle. The height of this gap is less than that of the blade. When the blade is inserted into the receptacle, the end of the spring is forced to bend up by the blade because of this small gap height, thus forming the contact pair. The samples had two different plating finishes (type 1 and type 2) and three sizes of gaps in the receptacles, namely 0.53mm, 0.48mm and 0.43mm.

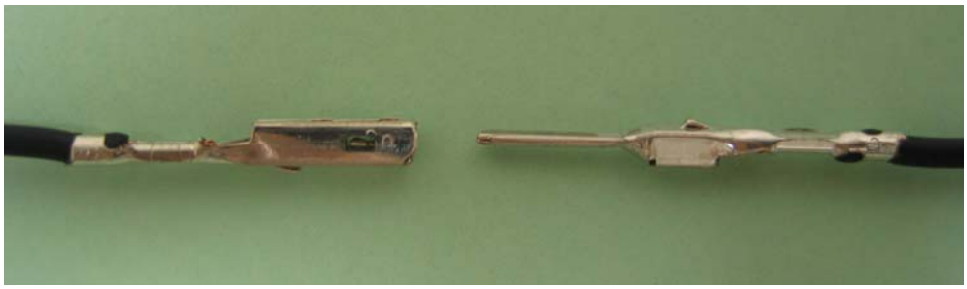

Figure 4-1 photograph of the blade and receptacle

Figure 4-2 mated blade/receptacle pair

4.2.2 Experimental Equipment

The experimental equipment used in this study was the same as that used in the previous studies and included a Keithley Model 2010 multimeter, HP 35665A Dynamic Signal Analyzer, POLYTEC laser vibrometer, DACTRON Vibration Control System, PA500L Amplifier and V408 Shaker. All of these instruments were introduced in detail in the Chapters 2 and 3.

4.2.3 Electromagnetic Interference During Resistance Measurements

For the setup of the experiment, a particular issue that must be addressed concerns electromagnetic interference from the shaker during the resistance measurement. This electromagnetic interference is likely to contaminate the measured resistance values when the shaker system is in operation. This effect was observed in the author's previous study when a big shaker was used, and was described in the previous chapter. Even though a small shaker was used in this study, because the nominal resistance level was expected to be very low for a single blade/receptacle pair, this electromagnetic interference was still a cause for concern.

Only electrical wires (not contact pairs) were used in this interference testing. Figure 4-3 and Figure 4-4 show the first method used to set up the samples and measure the resistance. Here, the wire was clamped between the fixtures and the two ends of the electrical wire separated at opposite sides of the shaker. However, using this setup, one end of the wire had to be close to the shaker head. Consequently, the four gator connectors for the 4-wire resistance measurement also had to be separated at the two

sides of the shaker and the four measuring wires could not be plaited together, as was done in the earlier study.

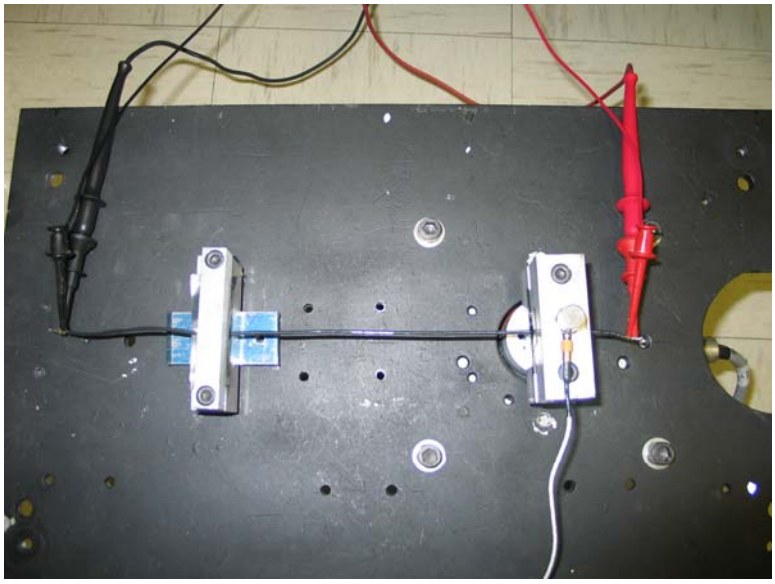

Figure 4-3 Method 1: sample setup for the electromagnetic interference test

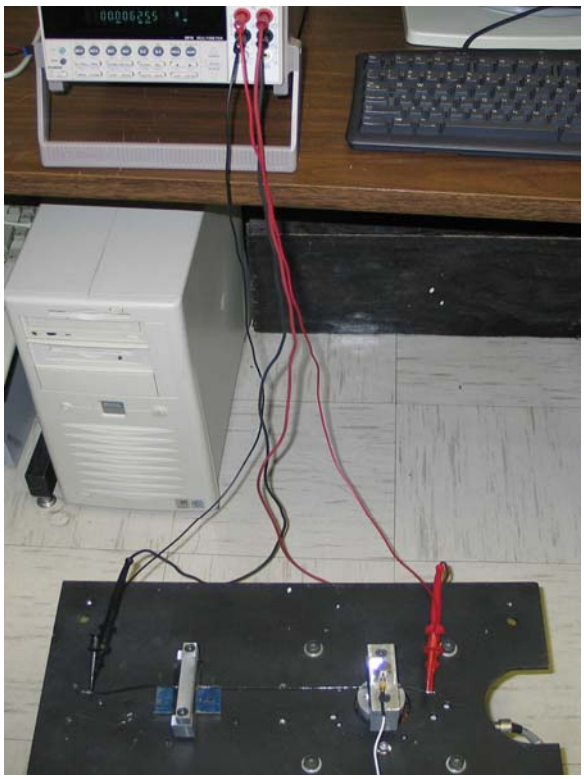

Figure 4-4 Method 1: resistance measurement in the electromagnetic interference test

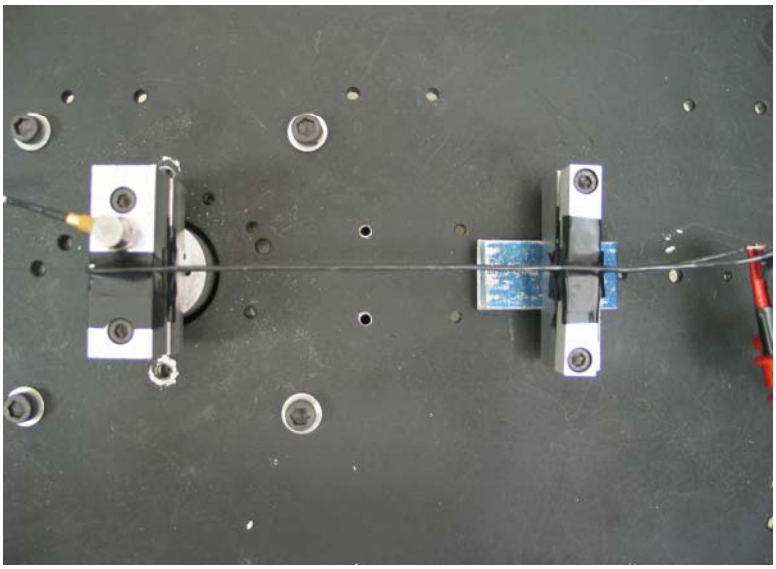

Figure 4-5 Method 2: sample setup for the electromagnetic interference test

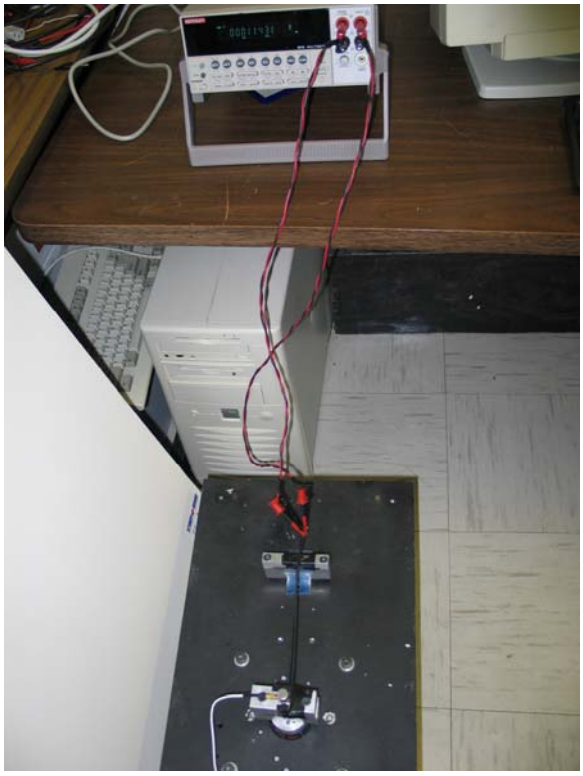

Figure 4-6 Method 2: resistance measurement in the electromagnetic interference test

Figure 4-5 and Figure 4-6 show the second method used to set up the samples and measure the resistance. Here, one end of an electrical wire was clamped in the fixture

while the other end was bent and secured to the top of the fixture so that both ends of the wire could be placed together at the same side of the shaker. Because the two ends of the electrical wire were close together, the four gator connectors of the multimeter were also close together and the four measuring wires could be plaited together to minimize the circuit loops.

Both methods placed the wire samples along the center line of the shaker to minimize electromagnetic interference during the resistance measurements. Using the same vibration conditions, the measured resistances were compared, as shown in Figure 4-7 (there were a resistance shift because two different wires were used in method 1 and method 2). For the first method, the amplitude of the sinusoidal noise component during the resistance measurement was 2.2 milliohms, which dropped to about 0.6 milliohms for the second method. 0.6 milliohms was considered adequate for the purposes of the present study. Therefore, the second method was adopted for the resistance measurements of the blade/receptacle pairs.

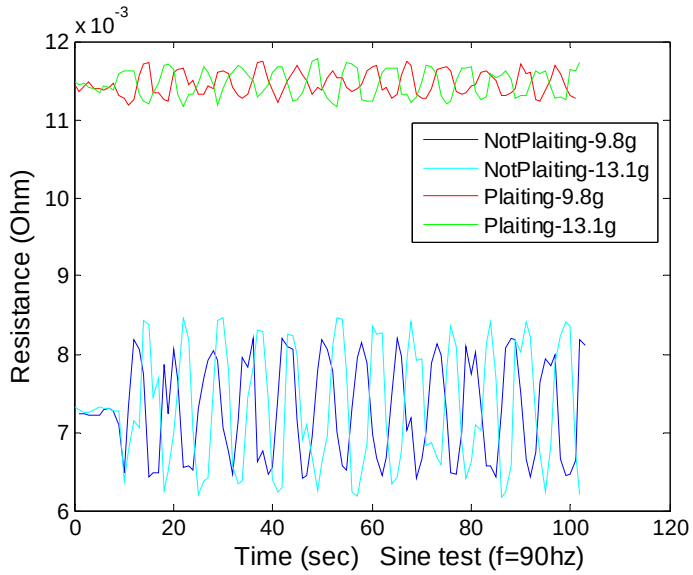

Figure 4-7 Comparison of the measured resistances for the two experimental setup

4.2.4 Experimental Setup

Based on the results of the electromagnetic interference testing, the experimental setup for this study was selected to be method 2, as shown in Figure 4-8. A wire lead 6.0 inches in length was attached to the receptacle sample and a group of three steel balls was attached to the wire lead to serve as a supplementary mass to lower the natural frequency and increase the fretting propensity of the system. Without the addition of the supplementary mass, it was very difficult to impart sufficient energy to the system to produce fretting. These small diameter (0.1 inch diameter) steel balls were attached to the wiring lead ½ inch from the junction with the receptacle. This receptacle was mated to the blade, with the other end of the wire lead clamped to a fixed (non-vibrating) table. The blade to be tested was firmly attached to the shaker head with a clamp and a part of its wire lead was bent and secured to the top of the fixture, as shown. The two ends of the wire leads were thus at the same side, far away from the shaker head, and gripped by the four gator connectors used to measure the resistance of the contact pair.

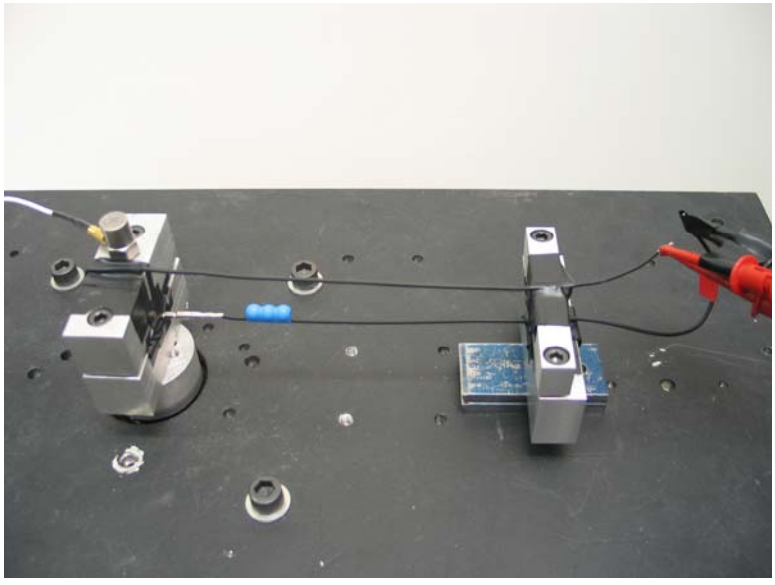

Figure 4-8 Photograph of the experimental setup for the blade/receptacle pair

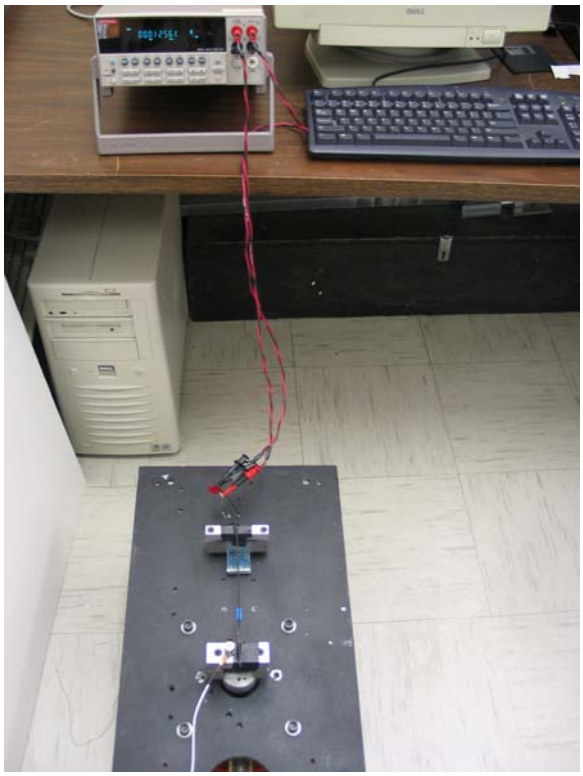

Figure 4-9 Resistance measurement for the blade/receptacle pair

Figure 4-10 Transfer function measurement for the blade/receptacle pair

Figure 4-9 shows the resistance measurement for the blade/receptacle pair, with the circuit loops minimized. Figure 4-10 shows the measurement of the transfer function for the blade/receptacle pair. This measurement used the same method as that used in the previous studies. The displacements of the blade and receptacle were measured using a non-contacting laser displacement measurement system.

A matter of critical interest in this setup was the determination of the significance of any horizontal (side-to-side) motion that may be induced by coupling effects with the vertical (driven) motion. In order to address this issue, transfer functions were measured where the input was the vertical input excitation and the output was the side-to-side motion, using the setup, shown in Figure 4-11. A typical result is shown in Figure 4-12. Inspection of this transfer function shows that the side-to-side motion is relatively small, being less than 2% of the excitation amplitude for vibration frequencies below 50 Hz.

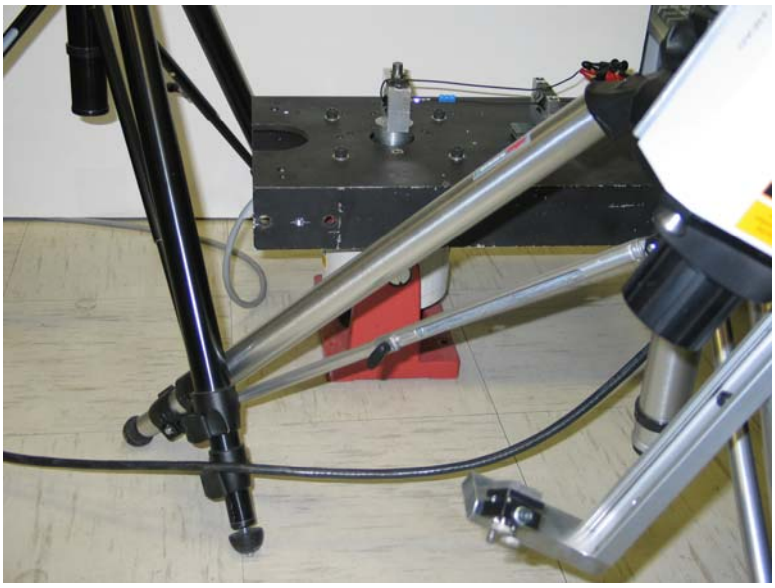

Figure 4-11 Measurement of the side-motion transfer function

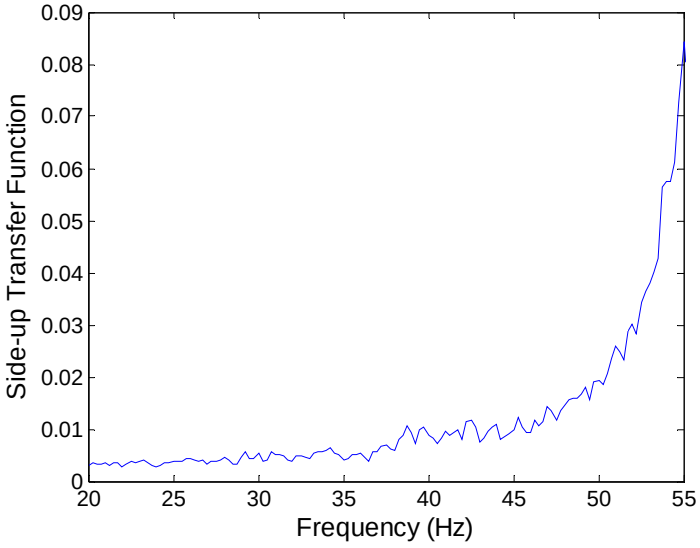

Figure 4-12 Side-motion transfer function below 50Hz for the setup

4.3 Experimental Results

As shown in Figure 4-7, the resistance trace for the wire (not contact pair) using the modified setup for the electromagnetic interference testing had an amplitude 0.6-milliohm, but the trend of the trace was flat. Hence the electromagnetic noise level can be assumed to be 0.6 milliohms, with no change in the overall resistance value.

For the fretting threshold study of the blade/receptacle samples, we focused on the trend of the resistance change curve rather than the amplitude of the trace, which was again approximately 0.6 milliohms. When the vibration g-level was very low, the trend of the curve was flat, but once the vibration displacement (or g-level) on the shaker head reached a certain value, the trend of this curve rose. After this point, the larger the g-level, the larger the resistance change. This value of the vibration displacement (or g-level) was then designated the threshold fretting displacement (or g-level).

A series of experiments were performed to measure the threshold displacements for type 1 and type 2 contact pairs with a 0.53mm gap at frequencies of 30Hz, 35Hz, 40Hz, 45Hz and 50Hz. Figure 4-13 shows an example of how the threshold displacement value was determined using the change in resistance curves.

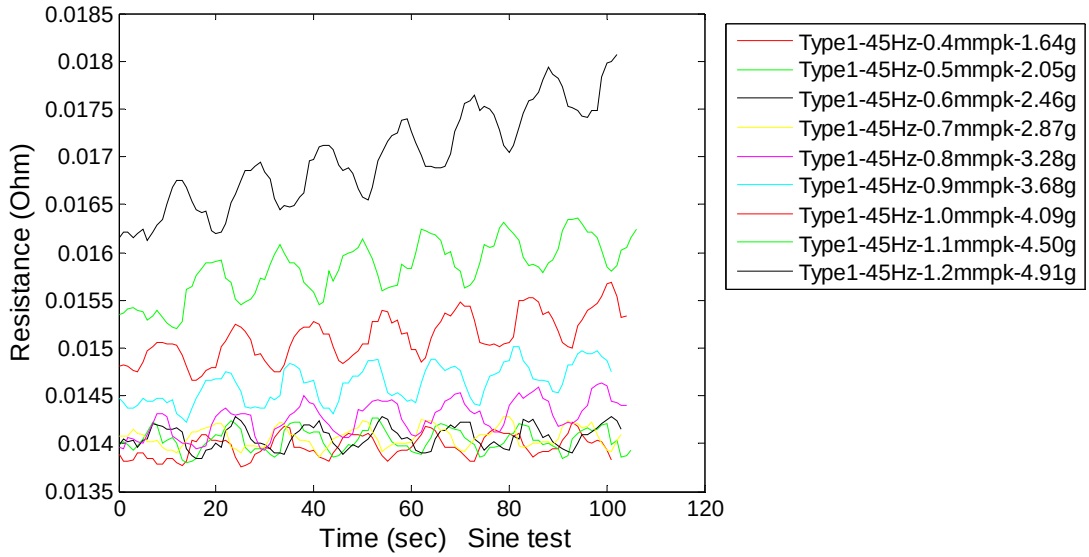

Figure 4-13 Identification of the threshold displacement (or g-level)

In this example (for a type1 connector at 45Hz), below 0.8mmpk, which signifies a vibration displacement of 0.8 mm peak-to-peak at the shaker head, the trends of the resistance change curves are flat. Once the displacement reached 0.8mmpk, however, the trend began to rise and after 0.8mmpk, the trends continued to increase. Consequently, 0.8mmpk was determined to be the threshold displacement at the shaker head for the type1 connector with a 0.53mm gap at 45Hz. The other contact pairs were also characterized in the same way. Table 4-1 lists the measured threshold displacements for the type1 and type2 blade/receptacle pairs with a 0.53mm gap.

Table 4-1 Threshold displacements for type1 and type2 (0.53mm gap) contact pair

Frequency	Threshold displacement at shaker head (peak): Type1	Threshold displacement at shaker head (peak): Type2
30Hz	3.0mm	2.9mm
35Hz	1.4mm	1.2mm
40Hz	0.6mm	0.6mm
45Hz	0.8mm	1.0mm
50Hz	0.9mm	1.45mm

The transfer functions for type1 and type 2 blade/receptacle pairs for the 0.43mm, 0.48mm and 0.53mm gaps were measured and compared with each other. Figure 4-14 through Figure 4-16 show the transfer functions for these three gap sizes and Figure 4-17 shows the relative motion function for the 0.53mm gap.

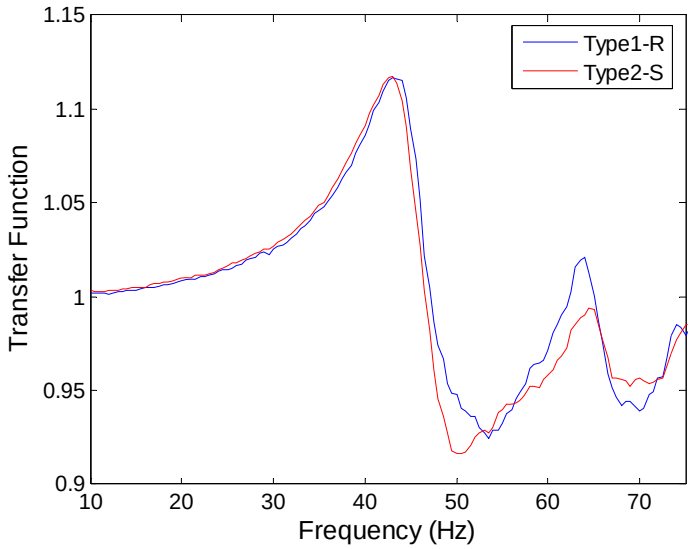

Figure 4-14 Transfer function of type 1 and type 2 contact pairs with a 0.43mm gap

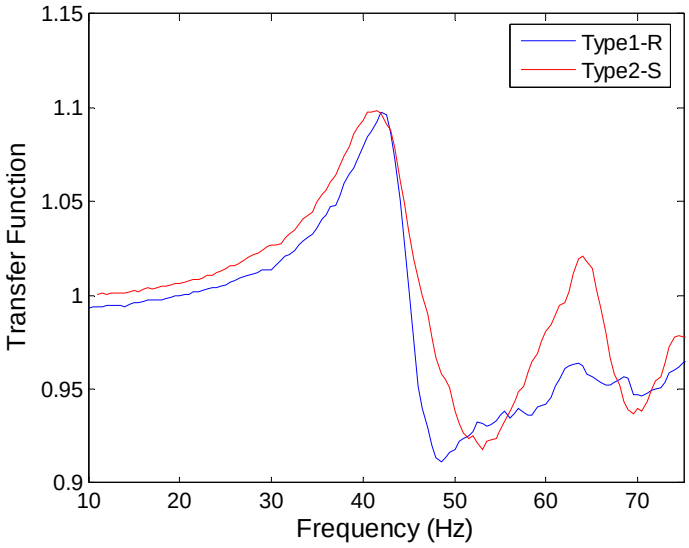

Figure 4-15 Transfer function of type 1 and type 2 contact pairs with a 0.48mm gap

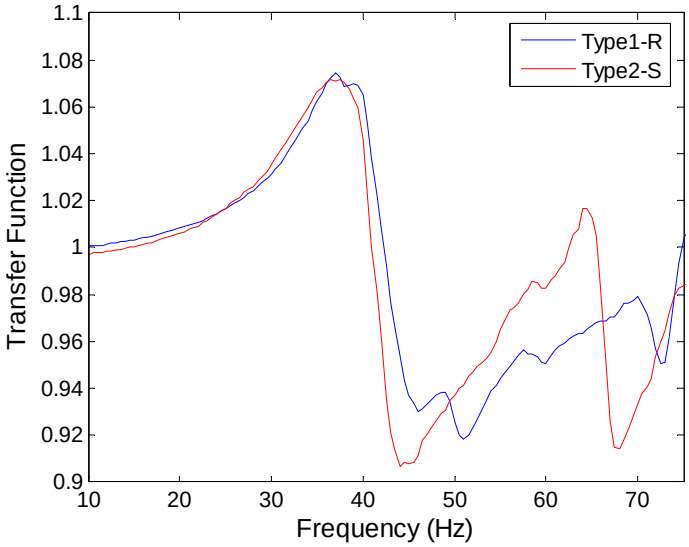

Figure 4-16 Transfer function of type 1 and type 2 contact pairs with a 0.53mm gap

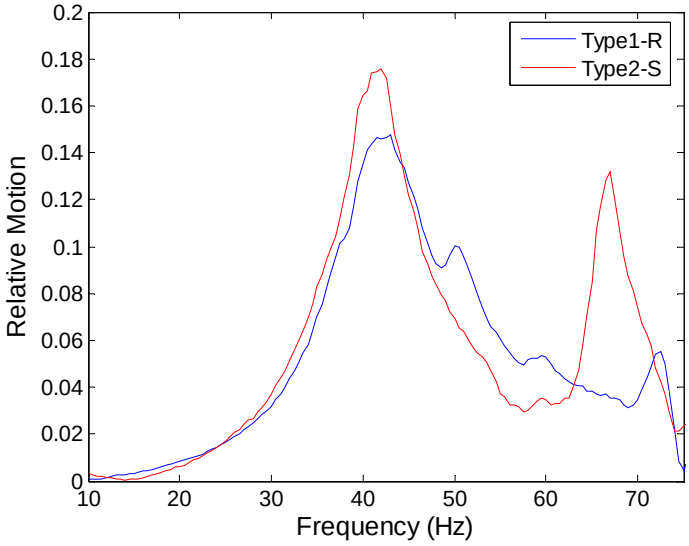

Figure 4-17 Relative motion of type 1 and type 2 contact pairs with a 0.53mm gap

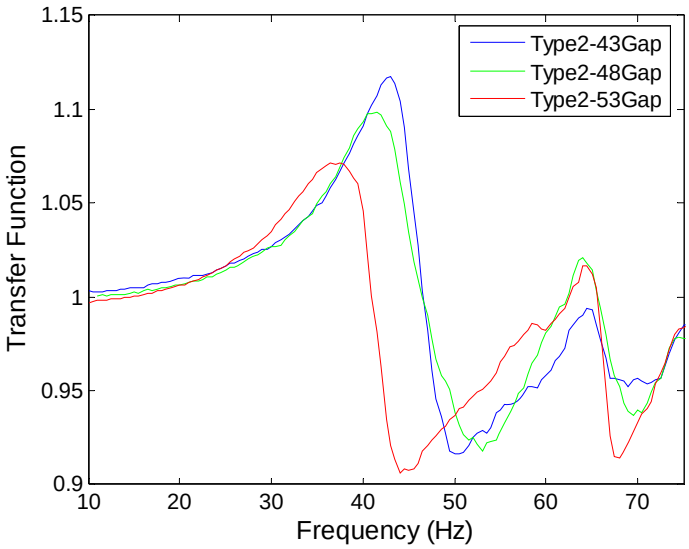

Figure 4-18 Comparison of type 2 transfer functions for three gap widths

Connectors with each gap width were found to have very similar transfer functions for the type 1 and type 2 contact pairs. However, for the same type 2 contact pair, the transfer functions for different gap widths (0.43mm, 0.48mm and 0.53mm) were slightly different, as shown in Figure 4-18. The amplitude of the transfer function

increased as the gap became smaller and the peak frequencies of the transfer functions underwent a small shift to higher frequencies.

The same method as that reported in the previous two chapters was again used here to analyze the relationship between the threshold displacement at the shaker head and the corresponding relative motion function for type 1 and type 2 contact pairs with a 0.53mm gap. The excitation frequencies, amplitudes of the relative motion, threshold displacement at the shaker head, and their product values are listed in Table 4-2 and Table 4-3 for type 1 and type 2 connectors, respectively.

Table 4-2 Relationship analysis for 0.53mm gap type 1 contact pair

Frequency	Relative Motion (RM)	Threshold displacement at shaker head (peak)	Product of RM and Displacement
30Hz	0.0321	3.0mm	0.0963mm
35Hz	0.0696	1.4mm	0.0974mm
40Hz	0.1355	0.6mm	0.0813mm
45Hz	0.1273	0.8mm	0.1019mm
50Hz	0.1004	0.9mm	0.0904mm

Table 4-3 Relationship analysis for 0.53mm gap type 2 contact pair

Frequency	Relative Motion (RM)	Threshold displacement at shaker head (peak)	Product of RM and Displacement
30Hz	0.0371	2.9mm	0.1076mm
35Hz	0.0826	1.2mm	0.0991mm
40Hz	0.1645	0.6mm	0.0987mm
45Hz	0.1221	1.0mm	0.1221mm
50Hz	0.0696	1.45mm	0.1009mm

Again, it was found that the products of the threshold displacement at the shaker head and the relative motion for each of the type 1 and type 2 0.53mm gap contact pairs remained approximately constant. This result is consistent with the results reported in the

last two chapters. Figure 4-19 shows that these threshold displacements match the corresponding scaled reversed relative motion functions for the type 1 and type 2 contact pairs very well.

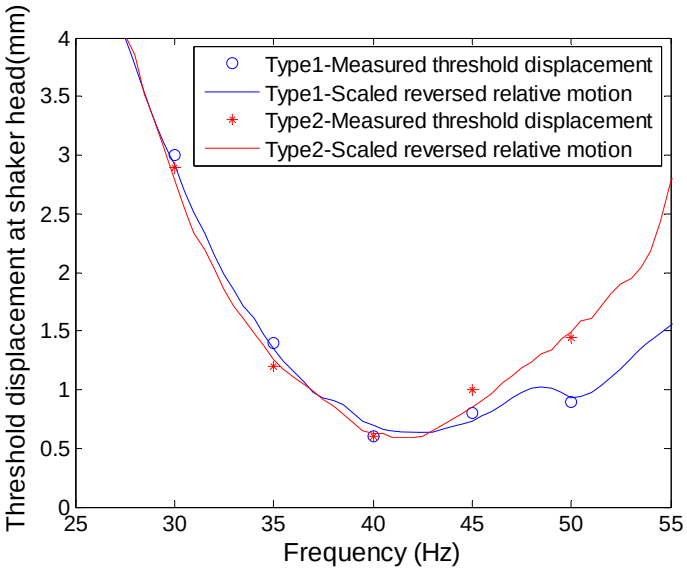

Figure 4-19 Relationship between the threshold displacement and the relative motion

4.4 Generation of the FEA Model

A 2D finite element simulation model was developed consisting of a single blade/ receptacle pair with attached wiring. The model was developed using ANSYS [48] and based on the same samples, setup and testing conditions as those used in the experiment introduced in the first part of this chapter.

There were two reasons to use a 2D, rather than a 3D model in this research. First, although the Molex engineers provided an original 3D meshed model for the blade and receptacle, the element number of this meshed model was very large, with about 65,000 elements, and this was the only model they could provide. This would make the model very hard to converge when it was solved using the computers available in our lab, which

normally provided good results for models with less than 15,000 elements. The large number of elements would also make the computation time very long for each run, at around four to six hours, and could even extend to a day. This study needed to run many cases, so it was not practical to use a long-run model. Second, because their model had been meshed, only elements and nodes existed in this model, with no surfaces. When a contact pair is created in ANSYS, thousands of nodes must be selected one by one to define the target surface and the contact surface. Consequently, it would be very complicated, at best to create the contact pair using ANSYS. Therefore, the provided 3D model was not adopted in this study, but instead a 2D model was used. A 2D model with thicknesses can dramatically reduce the number of elements and can still provide a good simulation of the experiment.

4.4.1 Geometric model

The dimensions of the geometric model followed those of the real blade/receptacle sample, wire and balls used in the experiment, except for the thickness. Figure 4-20 and Figure 4-21 show the full geometric model and a zoom view of the blade/receptacle section of the model, respectively.

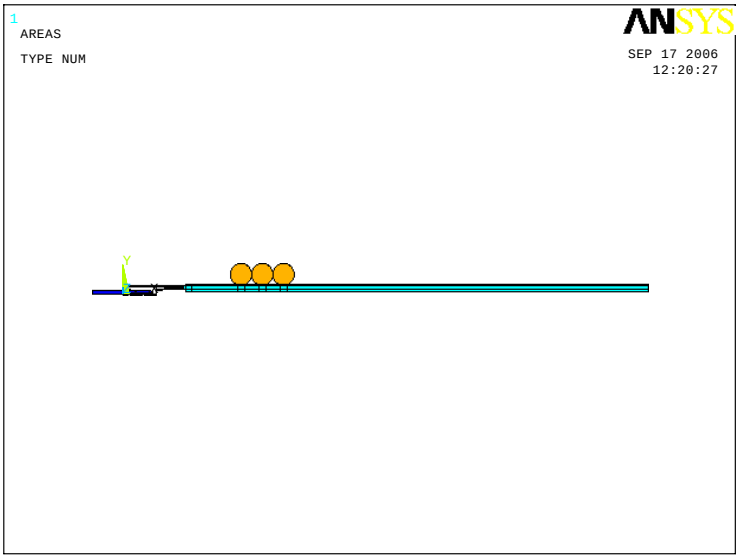

Figure 4-20 Full geometric model

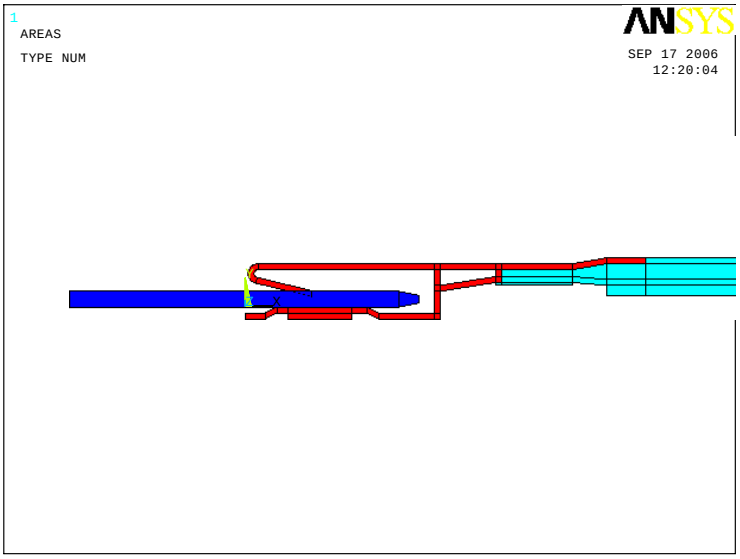

Figure 4-21 Blade/receptacle section of the geometric model

In the above figures, the blue part represents the blade, the red part the receptacle, the yellow part the supplementary balls and the cyan part the wire. Compared with the real components, only the outer structure of the receptacle was changed and the annulus and the spring inside the receptacle remained the same. The real outer structure of the 3D receptacle was composed of four metal pieces that formed a frame. This held the annulus

and the spring component inside the receptacle, and its upper and bottom surface was fixed. For the 2D model, a U-shape structure with thickness was used for the outer structure of the receptacle. The function of this outer structure remained the same when it became very stiff, which was achieved by changing the Young's modulus of the outer structure to a very large value, as explained in the next section. The thicknesses for each part of the components are listed in Table 4-4.

Table 4-4 Thicknesses of the components in the geometry model

Components	Thickness
Blade (front-part: the part inside the receptacle)	1.5mm
Blade (rear-part: the part outside the receptacle)	1.5mm
Annulus in the receptacle	1.9mm
Spring in receptacle	1.5mm
Receptacle and a part of wire (under the receptacle)	2.55mm
Wire (the rest part on the right side of the receptacle)	1.12mm
Balls	2.55mm

Here, 1.5mm was the real thickness of the blade and spring component, 1.9mm was the real thickness of the annulus and 2.55mm was the real thickness of the receptacle. However, 1.12mm was not the real thickness of the wire because when the 2D model was used for the 3D real wire, it was necessary to ensure that the $I_{equivalent} * E_{equivalent}$ for the 2D wire model was equal to the $I_{real} * E_{real}$ for the 3D real wire, where I is the wire's inertia moment, which is a function of its dimensions, and E is its Young's modulus. This requirement resulted in the 2D wire being assigned a thickness of 1.12mm.

4.4.2 Material Properties

To ensure the correct functioning of the model, the material properties of each component utilized the corresponding values from the real 3D samples. The weights of

the blade, receptacle, balls and wire using for the 2D model were exactly the same as the weights of their real world counterparts. Because some of the components, particularly the outer structure of the receptacle and the wire, had their dimensions or thicknesses adjusted, the volume of these components had also changed. Hence, their densities also had to be adjusted to match the weights of the original 3D samples.

As mentioned before, the Young's modulus for the outer structure of the receptacle was also increased to ensure that the whole outer structure (excluding the annulus and spring inside the receptacle) did not deform when the blade was inserted into the receptacle. A simulation revealed that this Young's modulus needed to be 1000 times bigger to obtain this result, while the Young's moduli of the other components retained their original values. The main material properties of each component in the FEA model are listed in Table 4-5.

Table 4-5 Material properties of the components in the FEA model

Components	Density	Young's Modulus
Blade (front-part: the part inside the receptacle)	8910 kg/m^3	129,742Mpa
Blade (rear-part: the part outside the receptacle)	6974 kg/m^3	129,742Mpa
Annulus in the receptacle	8910 kg/m^3	129,742Mpa
Spring in receptacle	8910 kg/m^3	129,742Mpa
Receptacle and a part of wire (under the receptacle)	8794 kg/m^3	129742,000Mpa
Wire (other parts on the right side of the receptacle)	4564 kg/m^3	96,534Mpa
Balls	12876kg/m^3	195,000Mpa

4.4.3 Meshing

The geometric model needed to be meshed in order to perform the finite element analysis for the sample. In general, a mapped mesh was used for this model except for the balls, where a free mesh was applied. The mapped mesh ensured the elements had regular patterns and solutions [48]. As key components, the annulus and the spring in the

receptacle were meshed with an even finer pitch. Figure 4-22 shows the meshed blade and receptacle.

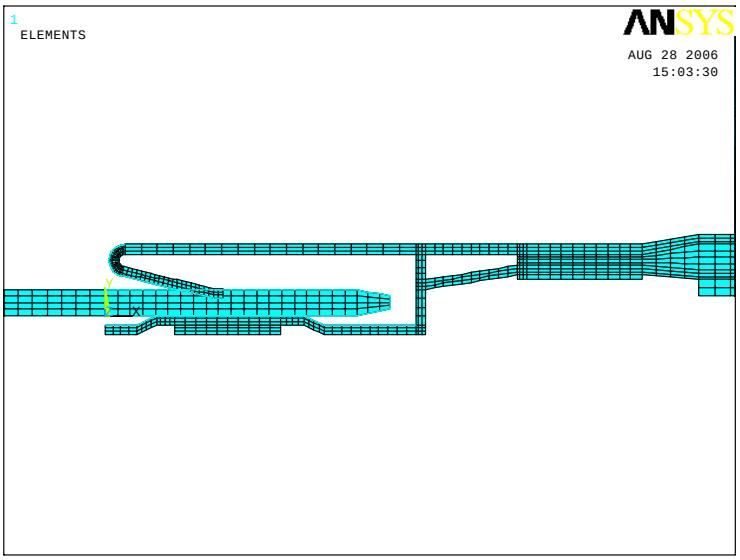

Figure 4-22 Meshed blade/receptacle model

4.4.4 Creating the Contact Pair

All the models of the contacts and connectors needed to create a contact pair, which was composed of the target surface and contact surface. In this model, the target surface consisted of the surface of the part of the blade located inside the receptacle and was likely to touch the annulus, spring and the bottom inner surface of the receptacle. The contact surface consisted of the surface of the annulus, spring, and the bottom inner surface of the receptacle and would touch some parts of the blade. Figure 4-23 shows the contact pair of this model.

Figure 4-23 Creating the contact pair

4.4.5 Boundary Conditions

It was important to ensure the boundary conditions of the model match the real conditions with respect to the experimental setup and vibration. For the experimental setup, the blade was clamped on the shaker head and the end of the wire (which was attached with the receptacle) was also clamped onto the fixture, as shown in Figure 4-8. For the vibration in the experiment, the blade and the shaker head moved up and down (only along the y-axis) as a sinusoidal vibration. Consequently, for the boundary conditions of this model the end of the wire was fixed in all DOF (degree of freedom) and the end of the blade was constrained to vibrate only in the y-axis. This was achieved by defining its x-axis displacement as zero and its y-axis displacement as a sinusoidal function. Neither the experiment nor the simulation included any restraint on the receptacle.

For the sinusoidal vibration, each cycle was evenly divided into forty substeps. These small substep intervals made it easier to perform the solving convergence and the analysis of the results. Figure 4-24 and Figure 4-25 show the boundary conditions of the model and the sinusoidal vibration excitation with the load substeps.

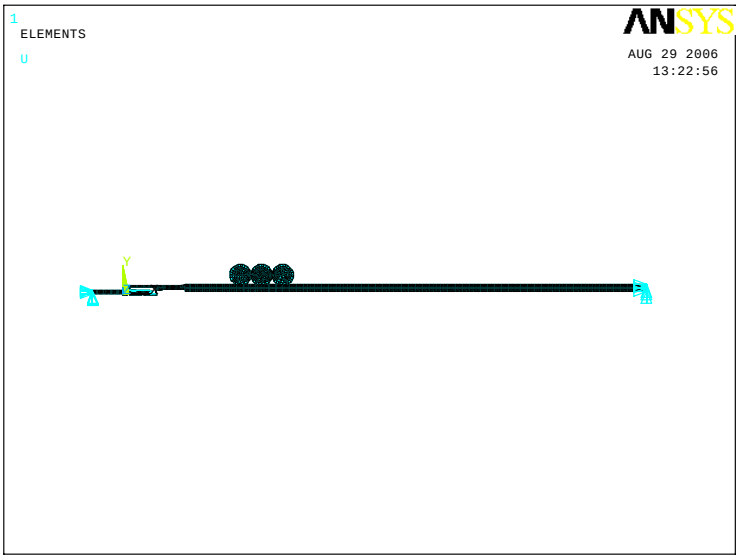

Figure 4-24 Boundary conditions for the model

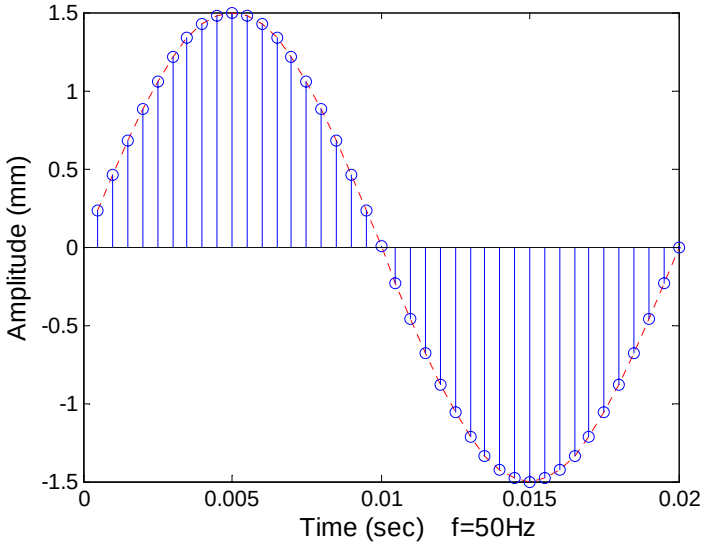

Figure 4-25 Sinusoidal vibration excitation with the load substeps

4.5 Vibration Process Simulation

In the previous and current studies, several questions were addressed. How and which kind of motion does the receptacle undergo when the system is vibrated. Is the receptacle rotating or simply sliding along with the blade? The results of this vibration process simulation answered these questions.

As shown in Figure 4-26 and Figure 4-27, the excitation of the sinusoidal vibration at the blade produced motion in the wiring and the supplementary mass (balls). In turn, that motion caused motion of the receptacle and at the connector interface. Figure 4-28 and Figure 4-29 show the motion of the receptacle, which clearly indicates that the receptacle rocks (rotates), rather than simply sliding along with the blade. Rocking was found to be the main mode for the receptacle's motion.

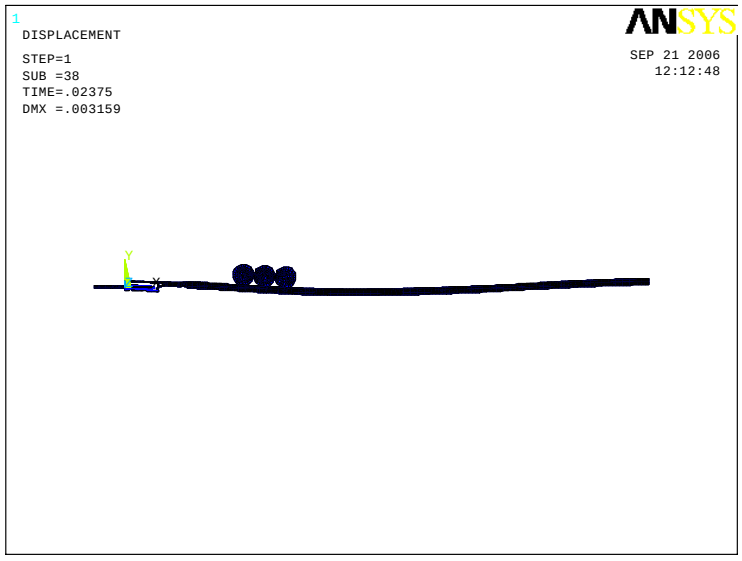

Figure 4-26 Full model motion at time 1 during vibration

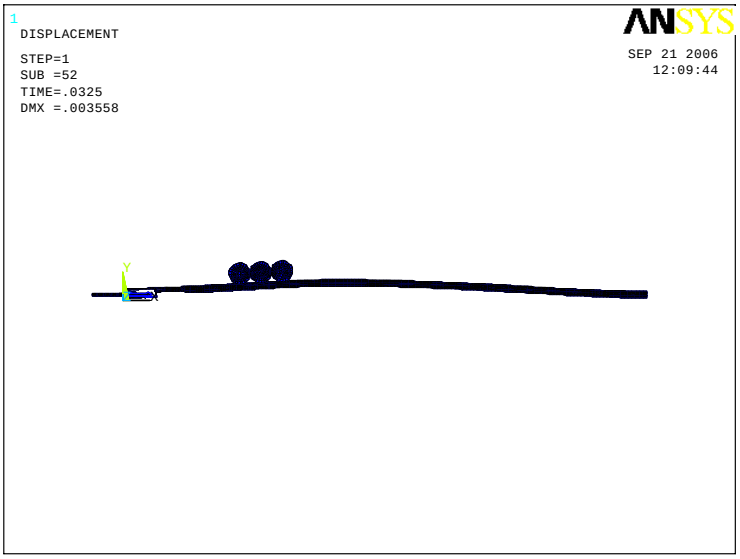

Figure 4-27 Full model motion at time 2 during vibration

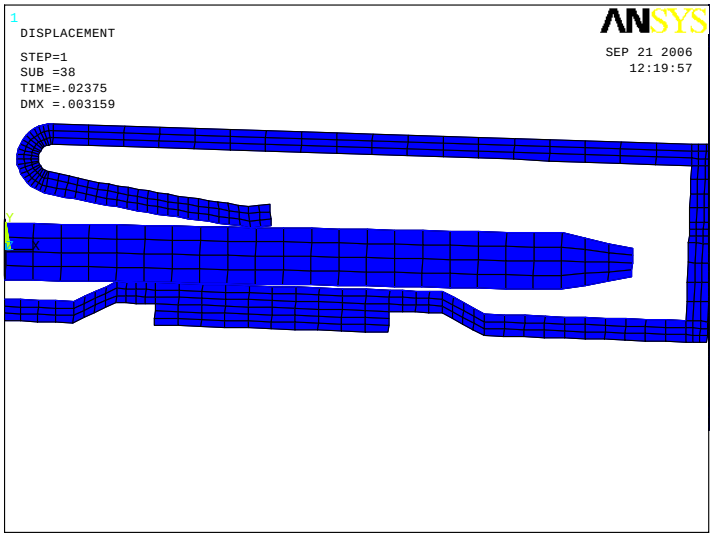

Figure 4-28 Motion of the blade and the receptacle at time 1

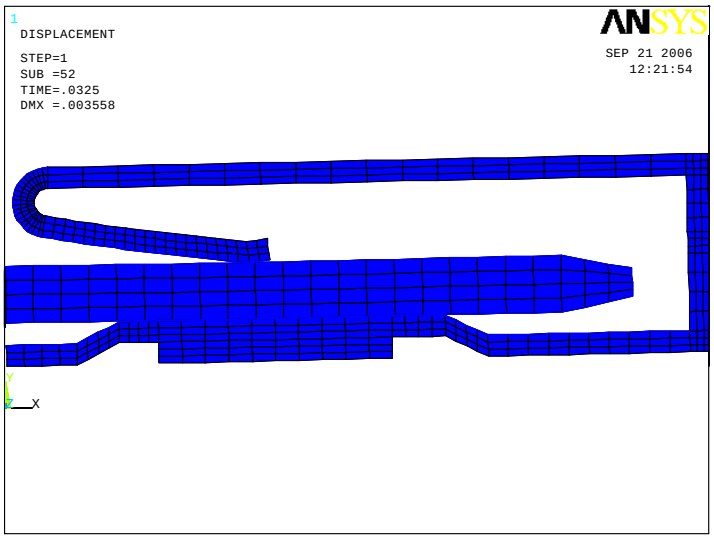

Figure 4-29 Motion of the blade and the receptacle at time 2

4.6 FEA Simulation Results and Comparison with the Experimental Results

A series of simulation studies were performed using this model. The primary objective of these tests was to evaluate the transfer functions and the threshold vibration levels for a variety of parametric configurations (different coating finishes and gap widths) and compare them with the experimental results described in the previous section.

For the transfer function simulation, the input and output measurement locations remained the same as the locations for the transfer function measurements in the experiment. In this model, the input location was therefore on node 124 and the output location was on node 743, as shown in Figure 4-30, which corresponded to the two locations at which the laser spots measured the transfer function in the experiment.

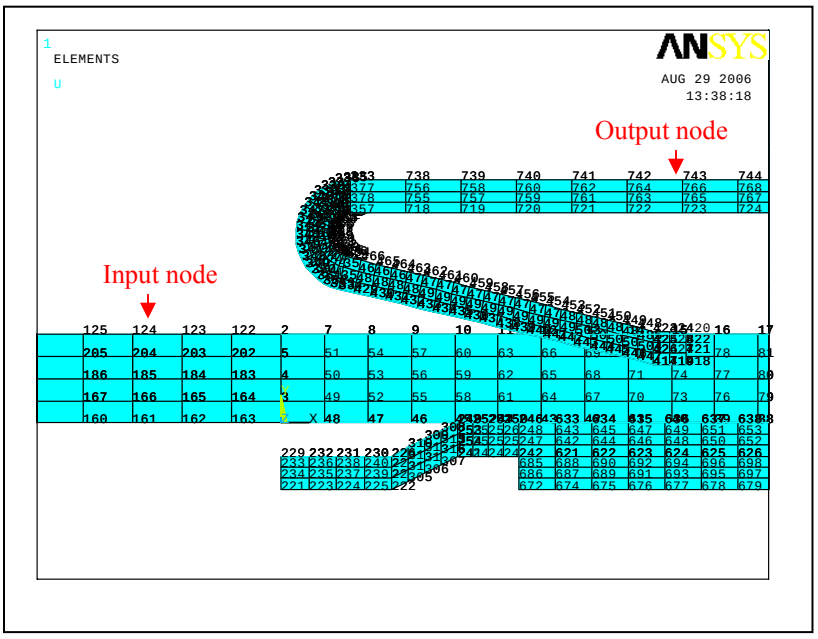

Figure 4-30 Node locations for the transfer function simulation

The transfer functions for the type 1 and type 2 finish connector (both for 0.53mm gap) from the simulation are shown in Figure 4-31 and the comparison of transfer functions from the simulation and the experiment is shown in Figure 4-32. The transfer functions for the type 1 and type 2 finish connector generated by the model were very similar, and they also matched the experimental measured values very well.

The reason why these two types of finish contact pairs had a similar transfer function was because the main motion mode of the receptacle was the rocking mode. This rocking motion mode minimized the effect of change in the friction coefficient between the blade and receptacle due to the different surface finish on the connector. Thus, the change in the finish type also had little effect on the transfer functions.

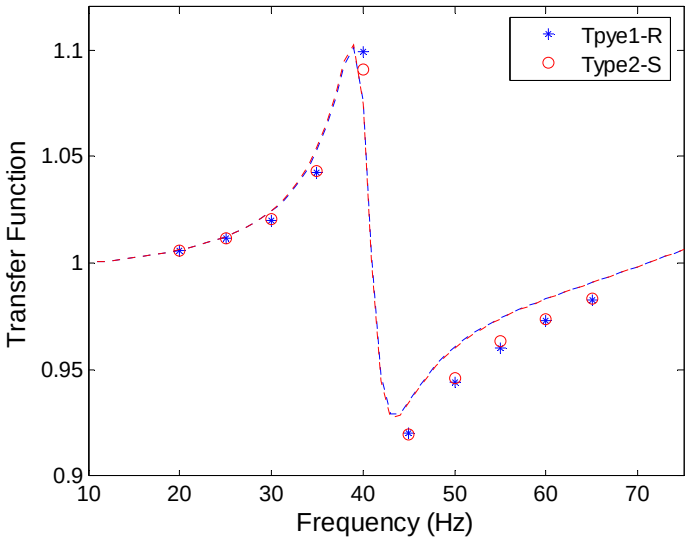

Figure 4-31 Transfer functions for the 0.53mm gap contact pair from the simulation

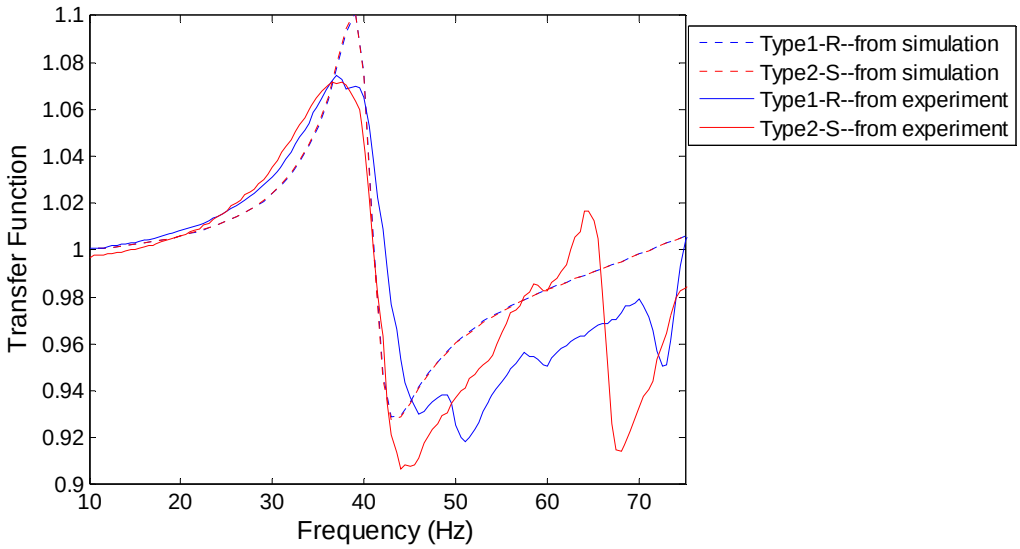

Figure 4-32 Comparison of the transfer functions from the simulation and experiment

The threshold relative motion displacements (or g-levels) at the contact interface for the type 2 0.53mm gap blade/receptacle pair was also simulated. Because of the rocking motion mode of the receptacle, three points of contact were of particular interest, as shown in Figure 4-33. Position 1 was the point of contact between the blade and the

end of the spring during the vibration, Position 2 was the point of contact between the blade and the left inner bottom surface of the receptacle during the rocking motion, and Position 3 was the point of contact between the blade and the right inner bottom surface of the receptacle during the rocking motion.

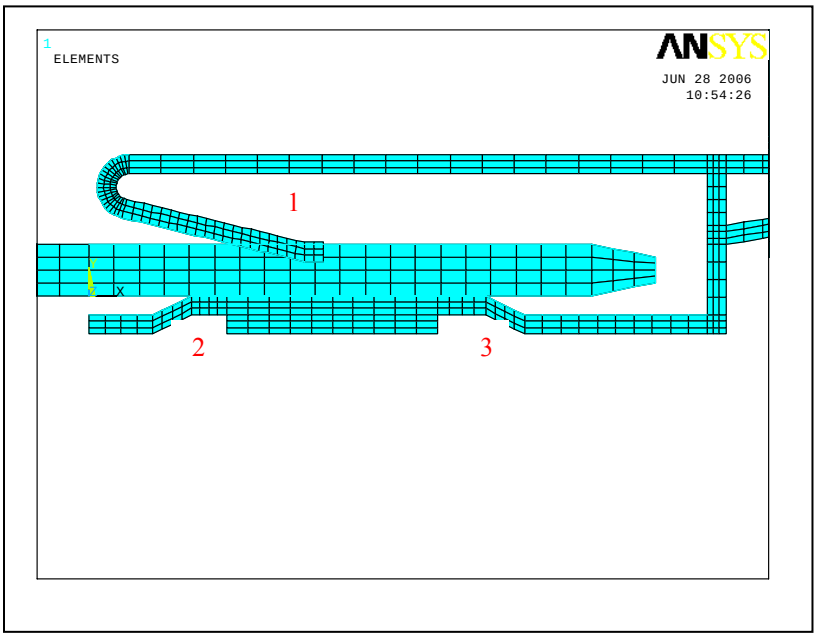

Figure 4-33 Simulated relative motion locations between the blade and the receptacle

Initially, the threshold displacements at the shaker head for different frequencies obtained from the experiment were used as the input excitation displacement for the vibration simulation. It was found that at each position, the x-axis relative motions for these different frequencies were very similar but the y-axis relative motions were quite different. This indicates that the fretting was only related to the x-axis (not y-axis) relative motion between the contact interfaces, as expected. It was also found that position 2 had the largest x-axis relative motion compared to position 1 and position 3 (about 4 times larger), which meant that the x-axis relative motion at position 2 made the

largest contribution to the fretting. After adjusting the input excitation displacement slightly for some frequencies, exactly the same x-axis relative motions at position 2 for these frequencies were obtained. Figure 4-34 through Figure 4-39 show the x-axis and y-axis relative motions for these input excitation levels and the frequencies of 30Hz, 35Hz, 40Hz, and 50Hz. For 45Hz, it was hard to achieve similar simulated results because this frequency was located at the concave point of the transfer function and consequently the phase shift made it hard to simulate.

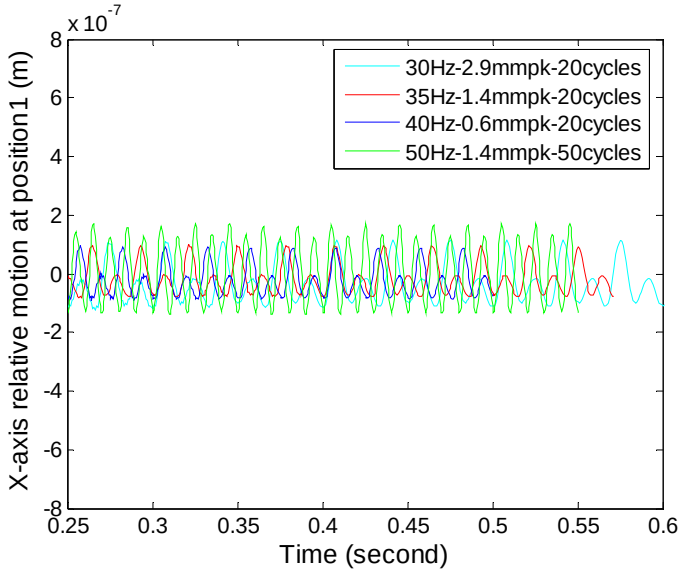

Figure 4-34 Simulated X-axis relative motion at position 1

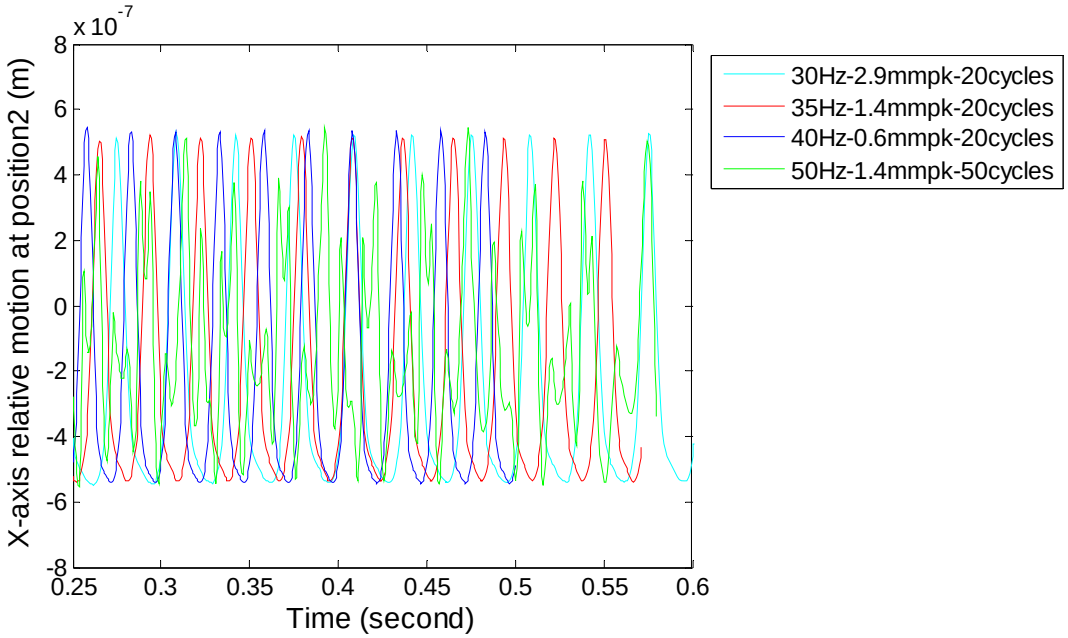

Figure 4-35 Simulated X-axis relative motion at position 2

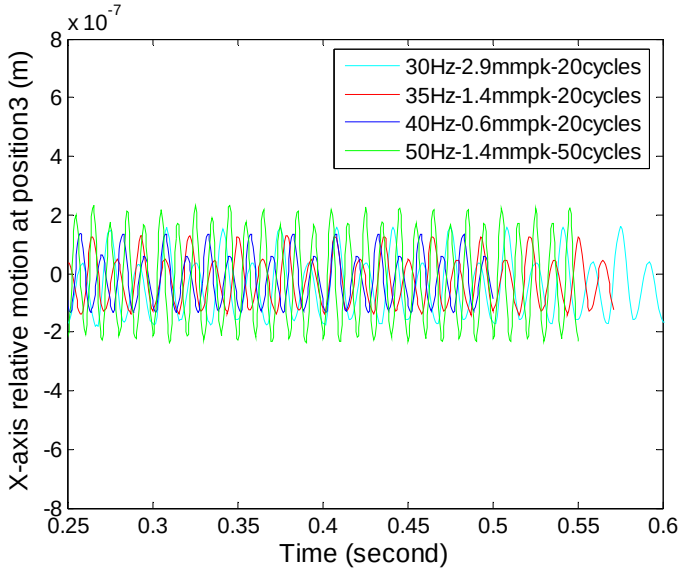

Figure 4-36 Simulated X-axis relative motion at position 3

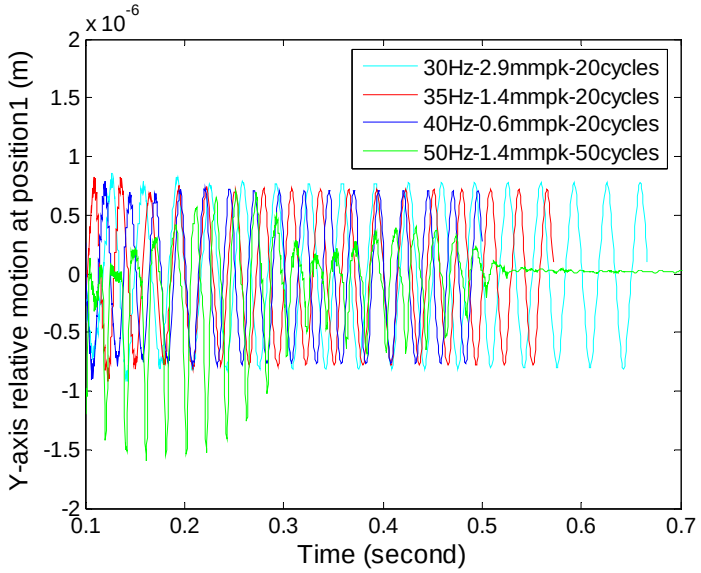

Figure 4-37 Simulated Y-axis relative motion at position 1

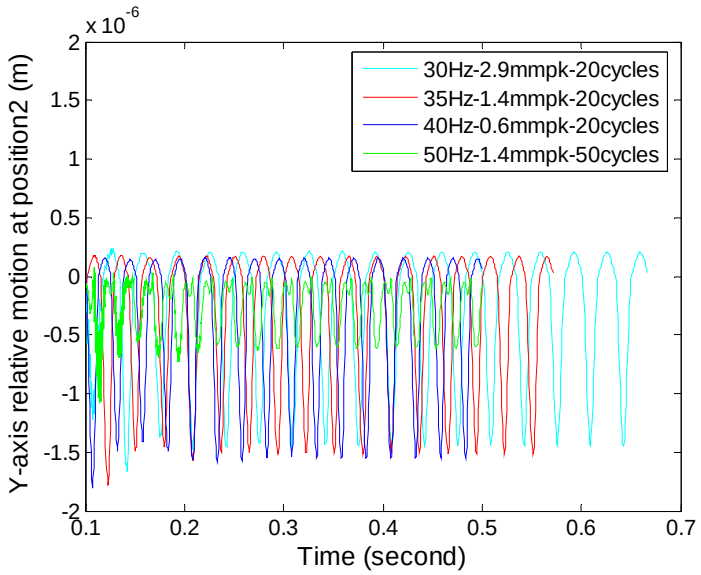

Figure 4-38 Simulated Y-axis relative motion at position 2

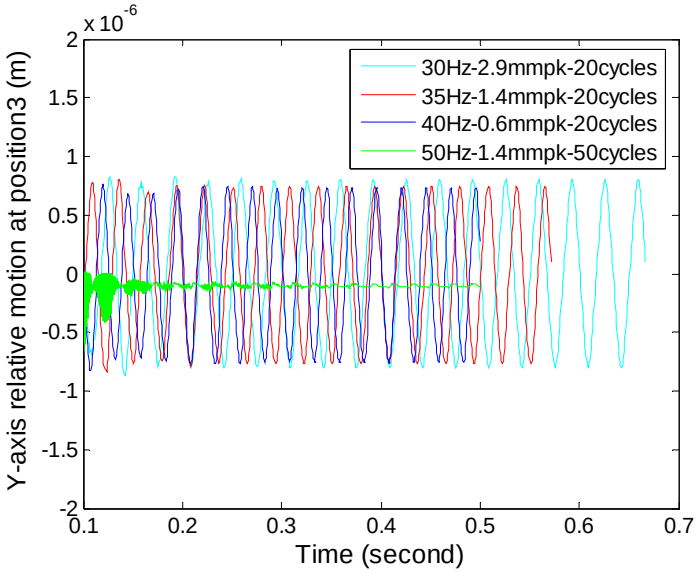

Figure 4-39 Simulated Y-axis relative motion at position 3

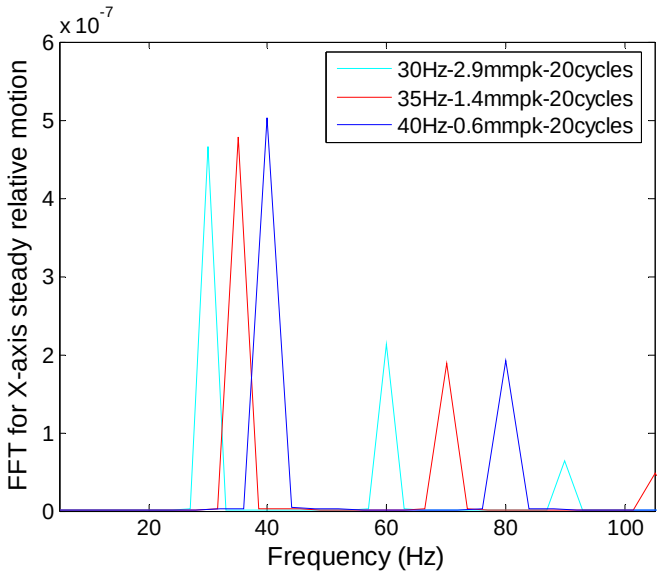

Figure 4-40 FFT analysis for the simulated X-axis relative motion at position2

The x-axis relative motions at the three positions were analyzed by FFT, which indicated that the frequency of the relative motion between the contact interfaces was the same frequency as that of the input excitation, implying that the relative motion at the

contact interfaces was caused solely by the input excitation. Figure 4-40 shows the FFT analysis for three relative motions at position 2.

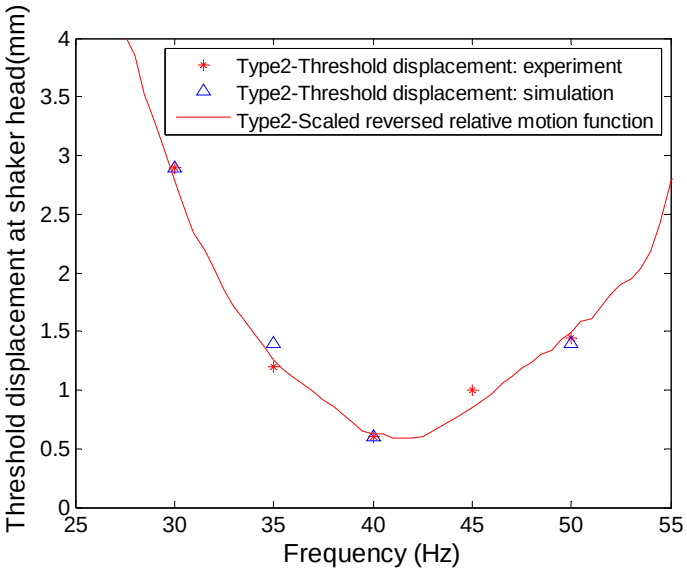

Figure 4-41 Threshold displacement comparison between the simulation and experiment

Figure 4-41 shows a comparison between the simulation and the experimentally obtained values for the threshold displacement at the shaker head, which resulted in the same relative motions at the contact interfaces. It was found that these threshold displacements from the experiment and the simulation matched very well, indicating that the relationship between the threshold displacement at the shaker head and the relative motion function (note that their product is constant regardless of the excitation frequencies) was also valid in this simulation.

Finally, the transfer functions for the same type 2 contact pair but with the three different gap widths (0.43mm, 0.48mm and 0.53mm) were simulated. Figure 4-42 shows the main part of these transfer functions. Compared with the transfer functions obtained experimentally, shown in Figure 4-18, the change trend of the peak amplitude was the

same and once again the amplitude of the transfer function increased as the gap became smaller. However, in this simulation the peak frequencies of the transfer functions did not shift as the gap widths changed, as observed in the experiment. This inconsistency may be ascribed to a lack of information, as the connector manufacturer did not provide any information on how the other 2 kinds of gaps (0.43mm and 0.48mm) were made and how the annulus and the spring inside the receptacle were modified to accommodate them. This issue became a concern after this inconsistency in the peak frequency shifts appeared. Before this, it was assumed that there were no changes in the annulus and the spring for the different gap widths in the model. Determining the differences in the annulus and spring between the three gaps of contact pairs is therefore recommended for future studies.

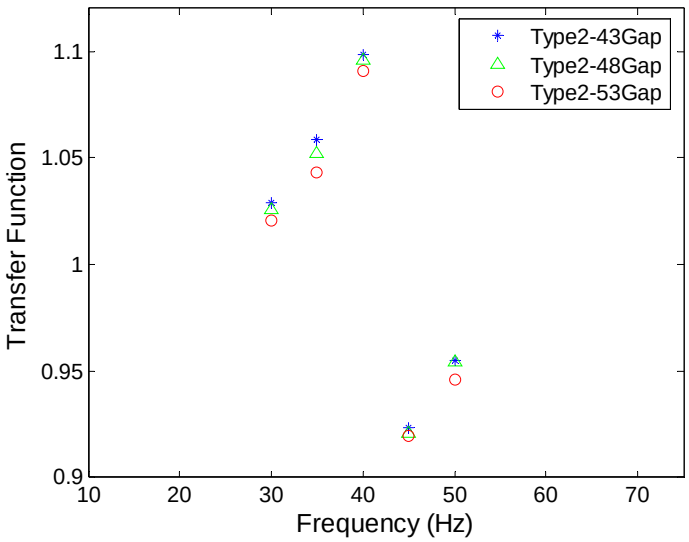

Figure 4-42 Transfer function simulation for three kinds of gaps for type 2 contact pair

4.7 Summary and Conclusions

This chapter presented a study of the application of FEA simulation techniques to the prediction of vibration-induced fretting degradation. A single blade/receptacle contact pair was analyzed both experimentally and with an FEA model. Two variations of finish type were considered, with each finish type having three gap widths. Three supplementary steel balls served as an artificial loading condition and were attached to the wires of the contact samples to make the system susceptible to fretting. The transfer functions and the fretting threshold displacement for a series of frequencies were measured in the experiment. The relative motion function was once again shown to be a good measure of the tendency of such systems to fret. The geometric dimensions, material properties and boundary conditions of the FEA model were generated based on the experimental values. The x-axis and y-axis relative motions for the contact interfaces and the transfer functions of two types of finishes and three gap widths were simulated using this model. The same x-axis relative motion at the contact interfaces was observed when the experimental threshold displacements were used as the input vibration levels for this single blade/receptacle pair system. Finally, the results from the simulation were compared with the results from the experiment and generally found to be in good agreement. It was demonstrated that, for this limited system, finite element modeling and analysis are potentially valuable tools for the evaluation of the influence of design variations on the fretting behavior of connector. This study's findings can be summarized and concluded as follows:

- Threshold fretting displacement at the shaker head at different frequencies for the single blade/receptacle pair was observed in the experiment.

- The relationship between the relative motion function and the threshold fretting displacement at the shaker head for this contact pair system was consistent with previous studies.
- The x-axis relative motion at the contact interface was indicated to be the main source of fretting for this contact pair.
- The results from the simulation generally matched that from the experiment very well.
- Finite element modeling and analysis have great potential for evaluating the influence of design variations on fretting behavior.

CHAPTER 5 CONCLUSIONS AND FUTURE WORK

Four studies concerned with fretting corrosion in electrical connectors have been presented in this dissertation. The first two examined the physical characteristics of vibration-induced fretting corrosion and focused on PC-type connectors and automotive-type connectors, respectively. The influence of connector design, wire tie-off length, vibration profile, and lubrication were considered. After modifications, both connector designs exhibited self-consistent relative displacement thresholds for the onset of fretting corrosion and a general linear dependency upon the g-level with regard to fretting rates for single frequency excitations. Regardless of the excitation frequency applied to the overall system, the existence of a relative displacement threshold that caused fretting at the connector interface was observed. Based on the findings of this work, a mathematical model was developed that related the early stage fretting corrosion rate to the threshold vibration levels for the connector, the dynamic characteristics of the connector / wiring configuration, and the vibration frequency. A high degree of consistency between this mathematical model and the experimental data was demonstrated. Additionally, a connector lubricant was observed to inhibit fretting over the amplitude and frequency ranges tested, as expected.

The third study examined the influence of normal force and finish characteristics for vibration-induced fretting degradation of a specific connector design.

Two variations of finish type were considered, with each finish type having three variations of normal force level. By introducing artificial loading conditions on the wire bundle, the connector system was made susceptible to fretting. It was observed that the fretting rates for the type 1 finish were larger than that for type 2 finish, and the threshold g-level tended to increase as the normal force increased for the connectors used in this study. The existence of threshold vibration level and the linear resistance change of the fretting were found to be consistent with the findings of the previous study. The relative motion transfer function was shown to provide a good measure of the tendency of such systems to fret once the threshold vibration level had been exceeded. As an application of this study, this technique was successfully applied to compare the fretting performance of two similar commercial products.

The fourth study presented an application of FEA simulation techniques to the prediction of vibration-induced fretting degradation. A single blade/receptacle contact pair was analyzed both experimentally and with an FEA model. Three supplementary steel balls attached on the wires made this contact system susceptible to fretting. The transfer functions and the fretting threshold displacement of this system for a series of frequencies were measured in the experiment. The results indicated that the relationship between the relative motion function and the threshold fretting displacement at the shaker head for this contact pair system was also consistent with that observed in the previous studies. An FEA model was constructed and a simulation performed based on the characteristics of the experimental setup. The same transfer functions for one type of contact pair were obtained from both simulation and experiment, and the same x-axis relative motions were observed in the simulation when the threshold fretting

displacements from the experiment were used. Generally, the results from the simulation matched those from the experiment very well. It was demonstrated that, for this limited system, finite element modeling and analysis offer great potential for the evaluation of the influence of design variation on the fretting behavior of connector. Future research work is recommended to include:

- Investigation of the effect of the annulus and spring for the different gaps in the blade/receptacle pair.
- Refining the FEA model for different gaps, if needed.
- More detailed study of the threshold relative motion at the contact interfaces through the simulation.
- Simulations of the fretting rates at larger vibration levels.
- 3D model simulation, if possible.

REFERENCES

[1] I-Ming Feng and H. Uhlig, *J. Appl. Mech.,* 21, 395 (1954)

[2] K. Wright, *Proc. Inst. Mech. Engrs. (B),* 1B (11), 556 (1952-1953)

[3] E.M. Bock and J.H. Whitley, "Fretting Corrosion in Electric Contacts", *Electric Contacts -1974*, Chicago, 1974, p.128

[4] S. Krumbein, "Contact Properties of Tin Plates", *Electric Contacts -1974*, Chicago, 1974, p.38

[5] M. Antler, W.F. Graddick and H.G. Tompkins, "Base Metal Contacts: An Exploratory Study of Separable Connection To Tin-Lead", *Electric Contacts - 1975*, Chicago, 1975, p.25

[6] J.H. Whitley, "Investigation of Fretting Corrosion Phenomena in Electric Contacts", *Proc. 8Th Int. Conf. Electrical Contact Phenomena*, Tokyo, 1976, pp.659-665

[7] M. Antler, and E.S. Sproles, "Effect of Fretting on the Contact Resistance of Palladium", *IEEE Trans. CHMT*, V.5, N.1, 1982, p.158

[8] J.M. Hooyer and K. Peekstok, "The Influence of Practical Contact Parameters on Fretting Corrosion of Tin-Base Low-Level Connector Contacts", *Electric Contacts -1987, IEEE - HOLM*, Chicago, 1987, p.43

[9] M. Antler, “Survey of Contact Fretting in Electrical Contacts”, *Proceedings of the Twenty Ninth IEEE Holm Conference on Electrical Contacts*, 1984, pp.3-22

[10] A. Lee and M.S. Mamrick, “Fretting Corrosion of Tin with Electrical Load”, *Proc. 13 International Conference On Electric Contacts*, Lausanne, Switzerland, 1986, p.476

[11] A. Lee and M.S. Mamrick, “Fretting Corrosion of Tin-Plated Copper Alloy”, *IEEE Trans. CHMT – 10*, 1987, p.63

[12] A.Lee and M.S.Mamrick “Fretting Corrosion of Tin at Elevated Temperatures” *Proceedings of the Thirty Fourth IEEE Holm Conference on Electrical Contacts*, 1988, p. 87-91

[13] M. Braunovic, “ Fretting Damage in Tin-Plated Aluminum and Copper Connections”, *Electric Contacts -1988*, IEEE-HOLM, San Francisco, 1988, p.179

[14] J.J. Motine and B.T. Reagor, “Investigation of Fretting Corrosion at Dissimilar Metal Interfaces on Socketed IC Device Applications”, *IEEE Trans. CHMT-7*, V.7, N.1, 1984, p.61-68

[15] M.D. Bryant, “Resistance Buildup in Electrical Connectors Due To Fretting Corrosion of Rough Surfaces”, *IEEE Transactions on Components, Packaging, and Manufacturing Technology*, V.17, N.1, March 1994, pp.86-95

[16] R. D. Malucci, “Multispot Model of Contacts Based on Surface Features”, *Electric Contacts -1990, IEEE - HOLM*, Montreal, 1990, p.625

[17] R. D. Malucci, “Impact of Fretting Parameters on Contact Degradation”, *Proceedings of the 42nd IEEE Holm Conference on Electrical Contacts*, 1996, pp.395-403

[18] G. T. Flowers, F. Xie, M. Bozack, and R.D. Malucci, "Vibration Thresholds for Fretting Corrosion in Electrical Connectors," *Proceedings of the 48th IEEE Holm Conference on Electrical Connectors*, October 21-23, 2002, pp.133-139

[19] L. Lam, J. W. McBride, C. Maul, and J. K. Atkinson, **"**Displacement Measurements at the Connector Contact Interface Employing a Novel Thick Film Sensor", *Electrical Contacts, 2005. Proceedings of the Fifty-First IEEE Holm Conference on* 26-28 Sept. 2005 Page(s): 89 – 96

[20] G. Villeneuve, D. Kulkarni, P. Bastnagel, and D. Berry, "Dynamic Finite Element Analysis Simulation of the Terminal Crimping Process", *Electrical Contacts, 1996., Proceedings of the Forty-Second IEEE Holm Conference Joint with the 18th International Conference on Electrical Contacts,* Sept. 1996 Page(s):156 – 172

[21] A. Monnier, B. Froidurot, C. Jarrige, R. Meyer, and P. Teste, "A Mechanical, Electrical, Thermal Coupled-field Simulation of a Sphere-plane Electrical Contact", *Electrical Contacts, 2005. Proceedings of the Fifty-First IEEE Holm Conference on* 26-28 Sept. 2005 Page(s):224 – 231

[22] C. Leung, E. Streicher, D. Fitzgerald, and J. Cook, "Contact Erosion of $Ag/SnO_2/In_2O_3$ Made by Internal Oxidation and Powder Metallurgy", *Electrical Contacts, 2005. Proceedings of the Fifty-First IEEE Holm Conference on* 26-28 Sept. 2005 Page(s):22 – 27

[23] E. D. Taylor; "Cathode Spot Behavior on Tungsten-Copper Contacts in Vacuum and the Effect on Erosion", *Electrical Contacts, 2005. Proceedings of the Fifty-First IEEE Holm Conference on* 26-28 Sept. 2005 Page(s):135 – 138

[24] A. Gunatilake, S. Rowland, Z. Wang, and N. Allen, "Modeling and Management of Microshocks under High Voltage Transmission Lines", *Electrical Contacts, 2005. Proceedings of the Fifty-First IEEE Holm Conference on* 26-28 Sept. 2005 Page(s):63 – 68

[25] G. Flowers, F. Xie, M. Bozack, B. Rickett, and R. Malucci, "The Influence of Contact Interface Characteristics on Vibration-Induced Fretting Degradation", *Electrical Contacts, 2005. Proceedings of the Fifty-First IEEE Holm Conference on* 26-28 Sept. 2005 Page(s):82 – 88

[26] M. Braunovic, V. Izmailov, and M. Novoselova, "A Model for Life Time Evaluation of Closed Electrical Contacts", *Electrical Contacts, 2005. Proceedings of the Fifty-First IEEE Holm Conference on* 26-28 Sept. 2005 Page(s):217 – 223

[27] D. J. Dickrell; M. T. Dugger, "The Effects of Surface Contamination on Resistance Degradation of Hot-Switched Low-Force MEMS Electrical Contacts", *Electrical Contacts, 2005. Proceedings of the Fifty-First IEEE Holm Conference on* 26-28 Sept. 2005 Page(s):255 – 258

[28] E. Takano, "Equivalent Constriction Resistance Measured with the Low Dc Voltage Method under the Influence of Fretting Phenomena", *Electrical Contacts, 2005. Proceedings of the Fifty-First IEEE Holm Conference on* 26-28 Sept. 2005 Page(s):284 – 290

[29] T. Ueno, and N. Morita, "Influence of Surface Roughness on Contact Voltage Drop of Sliding Contacts", *Electrical Contacts, 2005. Proceedings of the Fifty-First IEEE Holm Conference on* 26-28 Sept. 2005 Page(s):324 – 328

[30] D. Sallais, N. Jemaa, E. Carou, C. Bourda, and D. Jeannot, "An Arc Study at High DC Current Levels in Automotive Applications", *Electrical Contacts, 2005. Proceedings of the Fifty-First IEEE Holm Conference* on 26-28 Sept. 2005 Page(s):329 – 334

[31] J. Aronstein, "Performance Classification for Electrical Connection Using ASTM B868", *Electrical Contacts, 2005. Proceedings of the Fifty-First IEEE Holm Conference on* 26-28 Sept. 2005 Page(s):162 – 166

[32] P. Castel, A. Menet, and A. Carballeira, "Fretting Corrosion in Low Level Electrical Contacts: A Quantitative Analysis of the Significant Variables", *Proceedings of the Twelfth International Conference on Electrical Contact Phenomena & Thirtieth Holm Conference on Electrical Contacts*, 1984, page(s): 75-81.

[33] R. Malucci, "Fretting Corrosion Degradation, Threshold Behavior and Contact Instability", Ragnar Holm Scientific Achievement Award Address, *Proceedings of the Forty-Ninth IEEE Holm Conference on Electrical Contacts*, pp. 1-15, Washington, D.C., 2003, pp. 1-15.

[34] G. T. Flowers, F. Xie, M. Bozack, R. Horvath, R. D. Malucci,, and B. Rickett., "Vibration Testing of Fretting Corrosion in Electrical Connectors Subjected to Multi-Frequency and Random Spectral Profiles," *Proceedings of the Forty-Ninth IEEE Holm Conference on Electrical Contacts*," pp. 45-50, Washington, DC, 2003, pp. 45-50.

[35] *Model 2010 Multimeter User's Manual*, Keithley Instruments, Inc., USA, 1999

[36] *HP 35665A Dynamic Signal Analyzer Installation and Verification Guide,* Hewlett-Packard Company, USA, 1991

[37] *Laser Vibrometer User Manual, Controller OFV-2610/2620, Sensor Head OFV-353*, POLYTEC Co., Germany

[38] *Installation and Operating Manual PA 500/1000L-CE Amplifiers*, LDS Company, USA

[39] *Installation and Operating Manual V400 Series Vibrators*, LDS Company, USA

[40] F. Xie, *Thesis "A Study of Electrical Connector Performance In Fretting",* Auburn University, 2003

[41] G. A. Tomlinson, P. L. Thorpe, and H. J. Gough. "An Investigation of the Fretting Corrosion of Closely Fitting Surfaces," *Proceeding of the Institution of Mechanical Engineers*, Vol. 141,1939

[42] M. Braunovic, N. S.S. Mcintyre, W. J. Chauvin, and I. Aitchison, "Surface Analysis of Fretting Damage in Electrical Contact of Aluminum with Different Contact Materials," *IEEE Transactions on Components, Hybrids, and Manufacturing Technology*, Vol. CHMT-7, No.1, March 1984, pp. 96-106.

[43] J. Swingler and J. W. McBride, "Fretting Corrosion and the Reliability of Multicontact Connector Terminals," *IEEE Transactions on Components and Packaging Technologies*, Vol. 25, No. 4, December 2002, pp. 670-676.

[44] G. T. Flowers, F. Xie, M. Bozack, X. Hai, B. Rickett, and R. D. Malucci, "A Study of the Physical Characteristics of Vibration Induced Fretting Corrosion," Proceedings of the *Fiftieth IEEE Holm Conference on Electrical Contacts*," pp. 312-319, Washington, DC, September 20-23, 2004.

[45] *V850 Vibration Testing Systems Manual*, LDS Company, USA

[46] *LASER Shaker Control System Guide*, Dactron Incorporated, Milpitas, CA95035

[47] F. Hubner-Obenland and J. Minuth, "A New Test Equipment for High Dynamic Real-Time Measuring of Contact Resistances," *Proceedings of the Forty-Fifth IEEE Holm Conference,* pp. 193-202, Oct. 4-6, 1999

[48] *ANSYS Release 9.0 Documentation*, ANSYS, Inc. 2004

APPENDIX A MATLAB CODE EXAMPLE FOR REGRESSING THE EARLY-STAGE FRETTING CURVES

Regress_PC_normal_short_20.m

```
clear;

load H:\Ford_connector\PC_normal_short_20hz\pc_short_20hz_1p5grms.dat;
load H:\Ford_connector\PC_normal_short_20hz\pc_short_20hz_2p0grms.dat;
load H:\Ford_connector\PC_normal_short_20hz\pc_short_20hz_2p5grms.dat;
load H:\Ford_connector\PC_normal_short_20hz\pc_short_20hz_3p0grms.dat;
load H:\Ford_connector\PC_normal_short_20hz\pc_short_20hz_3p5grms.dat;
load H:\Ford_connector\PC_normal_short_20hz\pc_short_20hz_4p0grms.dat;

%Processing for Sine testing

Y_Sine_1p5 = pc_short_20hz_1p5grms(:,2);
X_Sine_1p5 = round(pc_short_20hz_1p5grms(:,1)-25);

Y_Sine_2p0 = pc_short_20hz_2p0grms(:,2);
X_Sine_2p0 = round(pc_short_20hz_2p0grms(:,1)-20);

Y_Sine_2p5 = pc_short_20hz_2p5grms(:,2);
X_Sine_2p5 = round(pc_short_20hz_2p5grms(:,1)-28);

Y_Sine_3p0 = pc_short_20hz_3p0grms(:,2);
X_Sine_3p0 = round(pc_short_20hz_3p0grms(:,1)-18);

Y_Sine_3p5 = pc_short_20hz_3p5grms(:,2);
X_Sine_3p5 = round(pc_short_20hz_3p5grms(:,1)-53);

Y_Sine_4p0 = pc_short_20hz_4p0grms(:,2);
X_Sine_4p0 = round(pc_short_20hz_4p0grms(:,1)-22);

figure(1);
hold on;
plot(X_Sine_1p5,Y_Sine_1p5,'k');
```

```
plot(X_Sine_2p0,Y_Sine_2p0,'m');
plot(X_Sine_2p5,Y_Sine_2p5,'c');
plot(X_Sine_3p0,Y_Sine_3p0,'r');
plot(X_Sine_3p5,Y_Sine_3p5,'g');
plot(X_Sine_4p0,Y_Sine_4p0,'b');
hold off;

xlabel('          time (sec)   Sine test (f=20hz) for PC short cable');
ylabel('Resistance (Ohm)');
legend('1.5grms','2.0grms','2.5grms','3.0grms','3.5grms','4.0grms',2);

for i=1:40
   y_sine_1p5(i) = Y_Sine_1p5(i+16) - Y_Sine_1p5(1+16);
   x_sine_1p5(i) = X_Sine_1p5(i+16);
   y_sine_2p0(i) = Y_Sine_2p0(i+13) - Y_Sine_2p0(1+13);
   x_sine_2p0(i) = X_Sine_2p0(i+13);
   y_sine_2p5(i) = Y_Sine_2p5(i+20) - Y_Sine_2p5(1+20);
   x_sine_2p5(i) = X_Sine_2p5(i+20);
   y_sine_3p0(i) = Y_Sine_3p0(i+10) - Y_Sine_3p0(1+10);
   x_sine_3p0(i) = X_Sine_3p0(i+10);
   y_sine_3p5(i) = Y_Sine_3p5(i+8) - Y_Sine_3p5(1+8);
   x_sine_3p5(i) = X_Sine_3p5(i+8);
   y_sine_4p0(i) = Y_Sine_4p0(i+9) - Y_Sine_4p0(1+9);
   x_sine_4p0(i) = X_Sine_4p0(i+9);
end

figure(4);
set(gcf,'Color','w');
plot(x_sine_1p5,y_sine_1p5,'k');
hold on;
plot(x_sine_2p0,y_sine_2p0,'m');
plot(x_sine_2p5,y_sine_2p5,'c');
plot(x_sine_3p0,y_sine_3p0,'r');
plot(x_sine_3p5,y_sine_3p5,'g');
plot(x_sine_4p0,y_sine_4p0,'b');

xlabel('Time (second)   Sine test (f=20hz) for PC short cable','FontSize',14);
ylabel('Resistance Change (Ohm)','FontSize',14);
legend('1.5grms','2.0grms','2.5grms','3.0grms','3.5grms','4.0grms',2);

slope_1p5=regress(y_sine_1p5',x_sine_1p5');
slope_2p0=regress(y_sine_2p0',x_sine_2p0');
slope_2p5=regress(y_sine_2p5',x_sine_2p5');
slope_3p0=regress(y_sine_3p0',x_sine_3p0');
slope_3p5=regress(y_sine_3p5',x_sine_3p5');
```

```
slope_4p0=regress(y_sine_4p0',x_sine_4p0');

y_s_1p5=slope_1p5*x_sine_1p5;
y_s_2p0=slope_2p0*x_sine_2p0;
y_s_2p5=slope_2p5*x_sine_2p5;
y_s_3p0=slope_3p0*x_sine_3p0;
y_s_3p5=slope_3p5*x_sine_3p5;
y_s_4p0=slope_4p0*x_sine_4p0;
plot(x_sine_1p5,y_s_1p5,'k:');
plot(x_sine_2p0,y_s_2p0,'m:');
plot(x_sine_2p5,y_s_2p5,'c:');
plot(x_sine_3p0,y_s_3p0,'r:');
plot(x_sine_3p5,y_s_3p5,'g:');
plot(x_sine_4p0,y_s_4p0,'b:');
hold off;

figure(3);
plot(1.5, slope_1p5,'ro');
hold on;
plot(2.0, slope_2p0,'rx');
plot(2.5, slope_2p5,'r+');
plot(3.0, slope_3p0,'r*');
plot(3.5, slope_3p5,'rs');
plot(4.0, slope_4p0,'rd');

%xlabel('g-value (rms) of sine test for short cable (PC samples)');
%xlabel('g-value (rms) of sine test--20hz for short cable (PC samples)');
%ylabel('Rate of resistance changes (Ohm/s)');
%legend('1.5grms','2.0grms','2.5grms','3.0grms','3.5grms','4.0grms',2);

x_sine=[1.5 2.0 2.5 3.0 3.5 4.0];
y_slope=[slope_1p5 slope_2p0 slope_2p5 slope_3p0 slope_3p5 slope_4p0];

p=polyfit(x_sine,y_slope,1);
x_s=1.5:0.05:4.5;
y_s=polyval(p,x_s);
plot(x_s,y_s,'r');

x_s0=0:0.05:1.5;
y_s0=polyval(p,x_s0);
plot(x_s0,y_s0,'r:');

%axis([0 18  -0.00002 0.00055]);
hold off;
```

APPENDIX B MATLAB CODE EXAMPLE FOR CALCULATING THE TRANSFER FUNCTIONS AND RELATIVE MOTIONS

TransFunc_Type1_Type2_3mass_53gap.m

```
clear all;

type2a= textread('R53TF1.txt');
type2b= textread('S53TF1.txt');

TF_type2a_freq = type2a(:,1);
for i=1:length(type2a)
   TF_type2a(i)=sqrt(type2a(i,2)^2 + type2a(i,3)^2);
   Phase_type2a(i)=atand(type2a(i,3)/type2a(i,2));
   RM_type2a(i)=sqrt((1-type2a(i,2))^2+type2a(i,3)^2);
   RM_W_type2a(i)=RM_type2a(i)/(TF_type2a_freq(i)^2);
   Reversed_RM_type2a(i) = 1/RM_type2a(i);

end

TF_type2b_freq = type2b(:,1);
for i=1:length(type2b)
   TF_type2b(i)=sqrt(type2b(i,2)^2 + type2b(i,3)^2);
   Phase_type2b(i)=atand(type2b(i,3)/type2b(i,2));
   RM_type2b(i)=sqrt((1-type2b(i,2))^2+type2b(i,3)^2);
   RM_W_type2b(i)=RM_type2b(i)/(TF_type2b_freq(i)^2);
   Reversed_RM_type2b(i) = 1/RM_type2b(i);
end

figure(1);
set(gcf,'Color','w');
plot(TF_type2a_freq,TF_type2a,'b');
hold on;
plot(TF_type2b_freq,TF_type2b,'r');

xlabel('Frequency (Hz)','FontSize',14);
ylabel('Transfer Function','FontSize',14);
```

```
%legend('Reflow','Star',1);
legend('Type1-R','Type2-S',1);
axis([10 75 0.9 1.1]);
hold off;

figure(2);
set(gcf,'Color','w');
plot(TF_type2a_freq,Phase_type2a,'b');
hold on;
plot(TF_type2b_freq,Phase_type2b,'r');

xlabel('Frequency (Hz)','FontSize',14);
ylabel('Phase (degree)','FontSize',14);
%title('Type 1 and 2 connector--Pining/Pining','FontSize',14);
legend('Type1-R','Type2-S',1);
%legend('Reflow','Star',1);
axis([10 75 -12 2]);
hold off;

figure(3);
set(gcf,'Color','w');
plot(TF_type2a_freq,RM_type2a,'b');
hold on;
plot(TF_type2b_freq,RM_type2b,'r');

xlabel('Frequency (Hz)','FontSize',14);
ylabel('Relative Motion','FontSize',14);
legend('Type1-R','Type2-s',1);
%legend('Reflow','Star',1);
axis([10 75 0 0.25]);
hold off;

figure(4);
set(gcf,'Color','w');
plot(TF_type2a_freq,RM_W_type2a,'b');
hold on;
plot(TF_type2b_freq,RM_W_type2b,'r');

xlabel('Frequency (Hz)','FontSize',14);
ylabel('Relative Motion/f^2','FontSize',14);
legend('Type1-R','Type2-S',1);
%legend('Reflow','Star',1);
axis([10 75 0 1.2e-4]);
hold off;
 Reflow_threshold_freq=[30 35 40 45 50];
```

```
Reflow_threshold_displacement=[3.0 1.4 0.6 0.8 0.9];
Reflow_k_constant=0.6/6.4;
figure(5);
set(gcf,'Color','w');
plot(Reflow_threshold_freq,Reflow_threshold_displacement,'bo');
hold on;
plot(TF_type2a_freq,Reversed_RM_type2a*Reflow_k_constant,'b');

Star_threshold_freq=[30 35 40 45 50];
Star_threshold_displacement=[2.9 1.2 0.6 1.0 1.45];
Star_k_constant=0.6/5.8;
plot(Star_threshold_freq,Star_threshold_displacement,'r*');
hold on;
plot(TF_type2b_freq,Reversed_RM_type2b*Star_k_constant,'r');

xlabel('Frequency (Hz)','FontSize',14);
ylabel('Threshold displacement at shaker head(mm)','FontSize',14);
legend('Type1-Measured threshold displacement','Type1-Scaled reversed relative motion function','Type2-Measured threshold displacement','Type2-Scaled reversed relative motion function',1);
axis([25 55 0 4]);
hold off;
Star_threshold_displacement_simu=[2.9 1.4 0.6 -1.0 1.4];
figure(6);
set(gcf,'Color','w');
plot(Star_threshold_freq,Star_threshold_displacement,'r*');
hold on;
plot(Star_threshold_freq,Star_threshold_displacement_simu,'b^');
plot(TF_type2b_freq,Reversed_RM_type2b*Star_k_constant,'r');
xlabel('Frequency (Hz)','FontSize',14);
ylabel('Threshold displacement at shaker head(mm)','FontSize',14);
legend('Type2-Threshold displacement: experiment','Type2-Threshold displacement: simulation','Type2-Scaled reversed relative motion function',1);
axis([25 55 0 4]);
hold off;

figure(7);
set(gcf,'Color','w');
plot(TF_type2b_freq,TF_type2b,'r');
%hold on;
xlabel('Frequency (Hz)','FontSize',14);
ylabel('Transfer Function','FontSize',14);
legend('Type2-43Gap','Type2-48Gap','Type2-53Gap',1);
axis([10 75 0.9 1.15]);
hold off;
```

APPENDIX C ANSYS LOG FILE FOR GENERATING THE FEA MODEL OF THE BLADE/RECEPTACLE PAIR

```
/PREP7
!*
!*set element type as plane42 with thickness*!
ET,1,PLANE42
!*
KEYOPT,1,1,0
KEYOPT,1,2,0
KEYOPT,1,3,3
KEYOPT,1,5,0
KEYOPT,1,6,0
!*
!*thickness set1=2.55e-3 for receptacle*!
R,1,2.55e-3,
!*
!*thickness set2=1.90e-3 for partial annulus*!
R,2,0.0019,
!*
!*thickness set3=1.50e-3 for blade and spring*!
R,3,0.0015,
!* thickness set3=1.12e-3 for wire*!
R,4,0.00112,

!*set material properties*!

!*type1-C19025-Star: blade,annulus*!
MPTEMP,,,,,,,,
MPTEMP,1,0
MPDATA,EX,1,,1.29742e11
MPDATA,PRXY,1,,0.3
MPTEMP,,,,,,,,
MPTEMP,1,0
MPDATA,DENS,1,,8910
MPTEMP,,,,,,,,
MPTEMP,1,0
```

```
MPDATA,MU,1,,0.33

!*type2-star: spring*!
MPTEMP,,,,,,,,
MPTEMP,1,0
MPDATA,EX,2,,1.29742e11
MPDATA,PRXY,2,,0.3
MPTEMP,,,,,,,,
MPTEMP,1,0
MPDATA,DENS,2,,8910
MPTEMP,,,,,,,,
MPTEMP,1,0
MPDATA,MU,2,,0.33
MPTEMP,,,,,,,,
MPTEMP,1,0
MPDATA,DAMP,2,,0.005

!*type3: wire for 2D model*!
MPTEMP,,,,,,,,
MPTEMP,1,0
MPDATA,EX,3,,1.35e9
!!MPDATA,EX,3,,0.96534e9
MPDATA,PRXY,3,,0.3
!!TB,MELA,3,1,8,
!!TBTEMP,0
!!TBPT,,0.001475,1.49e6
!!TBPT,,0.002475,1.99e6
!!TBPT,,0.003475,2.39e6
!!TBPT,,0.004475,2.73e6
!!TBPT,,0.005475,3.04e6
!!TBPT,,0.006475,3.32e6
!!TBPT,,0.007475,3.55e6
!!TBPT,,0.008475,3.70e6
MPTEMP,,,,,,,,
MPTEMP,1,0
MPDATA,DENS,3,,4564
MPTEMP,,,,,,,,
MPTEMP,1,0
MPDATA,DAMP,3,,0.0005

!*type4: Balls for 2D model*!
MPTEMP,,,,,,,,
MPTEMP,1,0
MPDATA,EX,4,,1.95e11
MPDATA,PRXY,4,,0.3
```

```
MPTEMP,,,,,,,,
MPTEMP,1,0
MPDATA,DENS,4,,12876.3

!*original type4 material property for balls. Used for 3D model*!
!!MPTEMP,,,,,,,,
!!MPTEMP,1,0
!!MPDATA,EX,4,,1.95e11
!!MPDATA,PRXY,4,,0.3
!!MPTEMP,,,,,,,,
!!MPTEMP,1,0
!!MPDATA,DENS,4,,7793
!*Can not be used in 2D model*!

!*type5-C19025-Star-equivalent: receptacle*!
MPTEMP,,,,,,,,
MPTEMP,1,0
MPDATA,EX,5,,1.29742e14
MPDATA,PRXY,5,,0.3
MPTEMP,,,,,,,,
MPTEMP,1,0
MPDATA,DENS,5,,8794
MPTEMP,,,,,,,,
MPTEMP,1,0
MPDATA,MU,5,,0.33

!*type6-klf5-Reflow-equivqlent*!
MPTEMP,,,,,,,,
MPTEMP,1,0
MPDATA,EX,6,,1.20622e14
MPDATA,PRXY,6,,0.3
MPTEMP,,,,,,,,
MPTEMP,1,0
MPDATA,DENS,6,,3210
MPTEMP,,,,,,,,
MPTEMP,1,0
MPDATA,MU,6,,0.44

!*type7: blade rear_part*!
MPTEMP,,,,,,,,
MPTEMP,1,0
MPDATA,EX,7,,1.29742e11
MPDATA,PRXY,7,,0.3
MPTEMP,,,,,,,,
MPTEMP,1,0
```

```
MPDATA,DENS,7,,6974.3
MPTEMP,,,,,,,,
MPTEMP,1,0
MPDATA,MU,7,,0.33
!!MPTEMP,,,,,,,,
!!MPTEMP,1,0
!!MPDATA,DAMP,7,,0.001

!*type8:  end rectangle of spring*!
MPTEMP,,,,,,,,
MPTEMP,1,0
MPDATA,EX,8,,1.29742e11
MPDATA,PRXY,8,,0.3
MPTEMP,,,,,,,,
MPTEMP,1,0
MPDATA,DENS,8,,8910
MPTEMP,,,,,,,,
MPTEMP,1,0
MPDATA,MU,8,,0.33

!*generate blade*!
K,1,0,0,,
K,2,0,0.8e-3,,
K,3,7.85e-3,0.8e-3,,
K,4,7.85e-3,0,,
K,5,8.85e-3,0.2e-3,,
K,6,8.85e-3,0.6e-3,,
K,7,-9.0e-3,0,,
K,8,-9.0e-3,0.8e-3,,

FLST,2,4,3
FITEM,2,1
FITEM,2,2
FITEM,2,3
FITEM,2,4
A,P51X

FLST,2,4,3
FITEM,2,3
FITEM,2,4
FITEM,2,5
FITEM,2,6
A,P51X

FLST,2,4,3
```

```
FITEM,2,1
FITEM,2,2
FITEM,2,8
FITEM,2,7
A,P51X
!*generate receptacle--front part*!
RECTNG,0,1.0e-3,-0.6e-3,-0.3e-3,

RECTNG,1.6e-3,2.15e-3,-0.3e-3,0,
RECTNG,2.15e-3,5.45e-3,-0.3e-3,0,
RECTNG,5.45e-3,6.2e-3,-0.3e-3,0,

RECTNG,2.15e-3,5.45e-3,-0.6e-3,-0.3e-3,

RECTNG,6.80e-3,9.65e-3,-0.6e-3,-0.3e-3,
RECTNG,9.65e-3,9.95e-3,-0.6e-3,-0.3e-3,

FLST,2,4,3
FITEM,2,11
FITEM,2,10
FITEM,2,13
FITEM,2,16
A,P51X
FLST,2,4,3
FITEM,2,22
FITEM,2,29
FITEM,2,32
FITEM,2,23
A,P51X

CYL4,0.63e-3,1.70e-3,0.2e-3,90,0.5e-3,257
RECTNG,3.37e-3,3.67e-3,0.53e-3,0.83e-3,

FLST,2,4,3
FITEM,2,39
FITEM,2,38
FITEM,2,41
FITEM,2,44
A,P51X

RECTNG,0.63e-3,9.65e-3,1.90e-3,2.20e-3,
RECTNG,9.65e-3,9.95e-3,1.90e-3,2.20e-3,

RECTNG,9.65e-3,9.95e-3,-0.30e-3,0.8e-3,
RECTNG,9.65e-3,9.95e-3,0.80e-3,1.10e-3,
```

```
RECTNG,9.65e-3,9.95e-3,1.10e-3,1.90e-3,

!*generate receptacle--rear part*!
RECTNG,9.95e-3,12.80e-3,1.90e-3,2.20e-3,
RECTNG,12.80e-3,13.10e-3,1.90e-3,2.20e-3,
RECTNG,12.80e-3,13.10e-3,1.55e-3,1.90e-3,
RECTNG,12.80e-3,13.10e-3,1.25e-3,1.55e-3,
RECTNG,12.80e-3,13.10e-3,1.10e-3,1.25e-3,

FLST,2,4,3
FITEM,2,59
FITEM,2,55
FITEM,2,77
FITEM,2,73
A,P51X

RECTNG,13.10e-3,16.70e-3,1.90e-3,2.20e-3,
RECTNG,13.10e-3,16.70e-3,1.55e-3,1.90e-3,
RECTNG,13.10e-3,16.70e-3,1.25e-3,1.55e-3,
RECTNG,13.10e-3,16.70e-3,1.10e-3,1.25e-3,

RECTNG,18.45e-3,20.45e-3,2.20e-3,2.50e-3,
RECTNG,18.45e-3,20.45e-3,1.40e-3,2.20e-3,
RECTNG,18.45e-3,20.45e-3,1.10e-3,1.40e-3,
RECTNG,18.45e-3,20.45e-3,0.60e-3,1.10e-3,

FLST,2,4,3
FITEM,2,87
FITEM,2,86
FITEM,2,101
FITEM,2,104
A,P51X
FLST,2,4,3
FITEM,2,86
FITEM,2,90
FITEM,2,105
FITEM,2,101
A,P51X
FLST,2,4,3
FITEM,2,90
FITEM,2,94
FITEM,2,109
FITEM,2,105
A,P51X
```

```
!*generate wire and balls*!
RECTNG,20.45e-3,34.00e-3,2.20e-3,2.50e-3,
RECTNG,20.45e-3,34.00e-3,1.40e-3,2.20e-3,
RECTNG,20.45e-3,34.00e-3,1.10e-3,1.40e-3,
RECTNG,20.45e-3,34.00e-3,0.60e-3,1.10e-3,
!*three balls*!
CYL4,35.00e-3,5.5e-3,3.16e-3
CYL4,41.32e-3,5.5e-3,3.16e-3
CYL4,47.64e-3,5.5e-3,3.16e-3

RECTNG,34.00e-3,36.00e-3,2.20e-3,2.50e-3,
RECTNG,34.00e-3,36.00e-3,1.40e-3,2.20e-3,
RECTNG,34.00e-3,36.00e-3,1.10e-3,1.40e-3,
RECTNG,34.00e-3,36.00e-3,0.60e-3,1.10e-3,

RECTNG,36.00e-3,40.32e-3,2.20e-3,2.50e-3,
RECTNG,36.00e-3,40.32e-3,1.40e-3,2.20e-3,
RECTNG,36.00e-3,40.32e-3,1.10e-3,1.40e-3,
RECTNG,36.00e-3,40.32e-3,0.60e-3,1.10e-3,

RECTNG,40.32e-3,42.32e-3,2.20e-3,2.50e-3,
RECTNG,40.32e-3,42.32e-3,1.40e-3,2.20e-3,
RECTNG,40.32e-3,42.32e-3,1.10e-3,1.40e-3,
RECTNG,40.32e-3,42.32e-3,0.60e-3,1.10e-3,

RECTNG,42.32e-3,46.64e-3,2.20e-3,2.50e-3,
RECTNG,42.32e-3,46.64e-3,1.40e-3,2.20e-3,
RECTNG,42.32e-3,46.64e-3,1.10e-3,1.40e-3,
RECTNG,42.32e-3,46.64e-3,0.60e-3,1.10e-3,

RECTNG,46.64e-3,48.64e-3,2.20e-3,2.50e-3,
RECTNG,46.64e-3,48.64e-3,1.40e-3,2.20e-3,
RECTNG,46.64e-3,48.64e-3,1.10e-3,1.40e-3,
RECTNG,46.64e-3,48.64e-3,0.60e-3,1.10e-3,

RECTNG,48.64e-3,156.00e-3,2.20e-3,2.50e-3,
RECTNG,48.64e-3,156.00e-3,1.40e-3,2.20e-3,
RECTNG,48.64e-3,156.00e-3,1.10e-3,1.40e-3,
RECTNG,48.64e-3,156.00e-3,0.60e-3,1.10e-3,

!*substract three rectangles from three balls*!
RECTNG,34.00e-3,36.00e-3,2.20e-3,2.50e-3,
RECTNG,40.32e-3,42.32e-3,2.20e-3,2.50e-3,
RECTNG,46.64e-3,48.64e-3,2.20e-3,2.50e-3,
```

```
!*firstly, change the booleans tolerance to 0.3e-3*!
BOPTN,KEEP,0
BOPTN,NWARN,0
BOPTN,VERS,RV52
BTOL,3e-004,
!*
ASBA,     44,     71
ASBA,     43,     70
ASBA,     42,     69

!*change the booleans tolerance back to 1e-5*!
BOPTN,KEEP,0
BOPTN,NWARN,0
BOPTN,VERS,RV52
BTOL,1e-005,
!*

!*glue*!
FLST,2,3,5,ORDE,2
FITEM,2,1
FITEM,2,-3
AGLUE,P51X

FLST,2,65,5,ORDE,5
FITEM,2,4
FITEM,2,-41
FITEM,2,43
FITEM,2,-68
FITEM,2,72
AGLUE,P51X

!*compress number for areas*!
NUMCMP,AREA
NUMMRG,KP, , , ,LOW
APLOT

SAVE,'model_LongBlade_static_LowE_step1','db','C:\Ansys_program\Molex_Auto_Mo
del\Model2D_formal2\'

!*named blade*!
ALLSEL,ALL
FLST,5,3,5,ORDE,2
FITEM,5,1
FITEM,5,-3
ASEL,R, , ,P51X
```

```
CM,blade,AREA

!*named receptacle*!
ALLSEL,ALL
FLST,5,25,5,ORDE,4
FITEM,5,4
FITEM,5,-14
FITEM,5,17
FITEM,5,-30
ASEL,R, , ,P51X
/MREP,EPLOT
CM,receptacle,AREA

!*named balls*!
ALLSEL,ALL
FLST,5,3,5,ORDE,2
FITEM,5,66
FITEM,5,-68
ASEL,R, , ,P51X
CM,balls,AREA

!*named wire*!
ALLSEL,ALL
FLST,5,37,5,ORDE,4
FITEM,5,15
FITEM,5,-16
FITEM,5,31
FITEM,5,-65
ASEL,R, , ,P51X
CM,wire,AREA

!*color the blade, receptacle, balls and wire*!
ALLSEL,ALL
APLOT
/COLOR,CM,ORAN,BALLS
/REPLOT
!*
/COLOR,CM,BLUE,BLADE
/REPLOT
!*
/COLOR,CM,RED,RECEPTACLE
/REPLOT
!*
/COLOR,CM,CYAN,WIRE
/REPLOT
```

```
!*define material property, real constant, element type*!
!*blade_front part: MP=1, RC=3 thickness(1.5mm), ET=1*!
FLST,5,2,5,ORDE,2
FITEM,5,1
FITEM,5,-2
CM,_Y,AREA
ASEL, , , ,P51X
CM,_Y1,AREA
CMSEL,S,_Y
!*
CMSEL,S,_Y1
AATT,      1,      3,   1,      0,
CMSEL,S,_Y
CMDELE,_Y
CMDELE,_Y1
!*

!*blade_rear part: MP=7, RC=1 thickness(2.55mm), ET=1*!
CM,_Y,AREA
ASEL, , , ,      3
CM,_Y1,AREA
CMSEL,S,_Y
!*
CMSEL,S,_Y1
AATT,      7,      1,   1,      0,
CMSEL,S,_Y
CMDELE,_Y
CMDELE,_Y1
!*

!*spring: MP=2, RC=3 thickness(1.5mm), ET=1*!
CM,_Y,AREA
ASEL, , , ,      11
CM,_Y1,AREA
CMSEL,S,_Y
!*
CMSEL,S,_Y1
AATT,      2,      3,   1,      0,
CMSEL,S,_Y
CMDELE,_Y
CMDELE,_Y1
!*

!*end of the spring: MP=8, RC=2 thickness(1.9mm), ET=1*!
CM,_Y,AREA
```

```
ASEL, , , ,      10
CM,_Y1,AREA
CMSEL,S,_Y
!*
CMSEL,S,_Y1
AATT,     8,     2,   1,      0,
CMSEL,S,_Y
CMDELE,_Y
CMDELE,_Y1
!*

!*annulus: MP=1, RC=2 thickness(1.9mm), ET=1*!
CM,_Y,AREA
ASEL, , , ,      9
CM,_Y1,AREA
CMSEL,S,_Y
!*
CMSEL,S,_Y1
AATT,     1,     2,   1,      0,
CMSEL,S,_Y
CMDELE,_Y
CMDELE,_Y1
!*

!*receptacle: MP=5(equivalent MP), RC=1 thickness(2.55mm), ET=1*!
FLST,5,31,5,ORDE,7
FITEM,5,4
FITEM,5,-8
FITEM,5,12
FITEM,5,-32
FITEM,5,34
FITEM,5,-37
FITEM,5,43
CM,_Y,AREA
ASEL, , , ,P51X
CM,_Y1,AREA
CMSEL,S,_Y
!*
CMSEL,S,_Y1
AATT,     5,     1,   1,      0,
CMSEL,S,_Y
CMDELE,_Y
CMDELE,_Y1
!*
```

```
!*balls: MP=4, RC=1 thickness(2.55mm), ET=1*!
FLST,5,3,5,ORDE,2
FITEM,5,66
FITEM,5,-68
CM,_Y,AREA
ASEL, , , ,P51X
CM,_Y1,AREA
CMSEL,S,_Y
!*
CMSEL,S,_Y1
AATT,      4,      1,   1,      0,
CMSEL,S,_Y
CMDELE,_Y
CMDELE,_Y1
!*

!*wire: MP=3, RC=4 thickness(1.12mm), ET=1*!
FLST,5,28,5,ORDE,5
FITEM,5,33
FITEM,5,38
FITEM,5,-42
FITEM,5,44
FITEM,5,-65
CM,_Y,AREA
ASEL, , , ,P51X
CM,_Y1,AREA
CMSEL,S,_Y
!*
CMSEL,S,_Y1
AATT,      3,      4,   1,      0,
CMSEL,S,_Y
CMDELE,_Y
CMDELE,_Y1
!*

!*mesh size control*!

!*manual mesh size for blade*!
!*thickness of blade into 4 divisions*!
FLST,5,4,4,ORDE,4
FITEM,5,1
FITEM,5,3
FITEM,5,6
FITEM,5,9
CM,_Y,LINE
```

```
LSEL, , , ,P51X
CM,_Y1,LINE
CMSEL,,_Y
!*
LESIZE,_Y1, , ,4, , , , ,1
!*

!*length of bladehead into 3 divisions*!
FLST,5,2,4,ORDE,2
FITEM,5,5
FITEM,5,7
CM,_Y,LINE
LSEL, , , ,P51X
CM,_Y1,LINE
CMSEL,,_Y
!*
LESIZE,_Y1, , ,3, , , , ,1
!*

!*length of bladebody into 20 divisions*!
FLST,5,2,4,ORDE,2
FITEM,5,2
FITEM,5,4
CM,_Y,LINE
LSEL, , , ,P51X
CM,_Y1,LINE
CMSEL,,_Y
!*
LESIZE,_Y1, , ,20, , , , ,1
!*

!*length of blade back part into 20 divisions*!
FLST,5,2,4,ORDE,2
FITEM,5,8
FITEM,5,10
CM,_Y,LINE
LSEL, , , ,P51X
CM,_Y1,LINE
CMSEL,,_Y
!*
LESIZE,_Y1, , ,20, , , , ,1
!*

!*manual mesh size for receptacle*!
!*thickness into 3 divisions*!
```

```
FLST,5,36,4,ORDE,35
FITEM,5,12
FITEM,5,14
FITEM,5,16
FITEM,5,18
FITEM,5,20
FITEM,5,24
FITEM,5,32
FITEM,5,34
FITEM,5,36
FITEM,5,44
FITEM,5,46
FITEM,5,48
FITEM,5,50
FITEM,5,54
FITEM,5,58
FITEM,5,63
FITEM,5,67
FITEM,5,74
FITEM,5,78
FITEM,5,81
FITEM,5,85
FITEM,5,93
FITEM,5,95
FITEM,5,98
FITEM,5,114
FITEM,5,116
FITEM,5,264
FITEM,5,-266
FITEM,5,268
FITEM,5,272
FITEM,5,275
FITEM,5,278
FITEM,5,283
FITEM,5,-284
FITEM,5,287
CM,_Y,LINE
LSEL, , , ,P51X
CM,_Y1,LINE
CMSEL,,_Y
!*
LESIZE,_Y1, , ,3, , , , ,1
!*

!*length of samll rectangles into 4 divisions*!
```

```
FLST,5,14,4,ORDE,10
FITEM,5,11
FITEM,5,13
FITEM,5,15
FITEM,5,17
FITEM,5,39
FITEM,5,-42
FITEM,5,261
FITEM,5,-262
FITEM,5,279
FITEM,5,-282
CM,_Y,LINE
LSEL, , , ,P51X
CM,_Y1,LINE
CMSEL,,_Y
!*
LESIZE,_Y1, , ,4, , , , ,1
!*

!*length of springend rectangle into 2 divisions*!
FLST,5,2,4,ORDE,2
FITEM,5,47
FITEM,5,49
CM,_Y,LINE
LSEL, , , ,P51X
CM,_Y1,LINE
CMSEL,,_Y
!*
LESIZE,_Y1, , ,2, , , , ,1
!*

!*length of median rectangles into 10 divisions*!
FLST,5,11,4,ORDE,11
FITEM,5,27
FITEM,5,31
FITEM,5,33
FITEM,5,94
FITEM,5,96
FITEM,5,155
FITEM,5,-156
FITEM,5,276
FITEM,5,-277
FITEM,5,285
FITEM,5,-286
CM,_Y,LINE
```

```
LSEL, , , ,P51X
CM,_Y1,LINE
CMSEL,,_Y
!*
LESIZE,_Y1, , ,10, , , , ,1
!*

!*length of spring into 20 divisions*!
FLST,5,2,4,ORDE,2
FITEM,5,51
FITEM,5,-52
CM,_Y,LINE
LSEL, , , ,P51X
CM,_Y1,LINE
CMSEL,,_Y
!*
LESIZE,_Y1, , ,20, , , , ,1
!*

!*curves of partial circle into 20 divisions*!
FLST,5,2,4,ORDE,2
FITEM,5,43
FITEM,5,45
CM,_Y,LINE
LSEL, , , ,P51X
CM,_Y1,LINE
CMSEL,,_Y
!*
LESIZE,_Y1, , ,20, , , , ,1
!*

!*length of large rectangle into 18 divisions*!
FLST,5,2,4,ORDE,2
FITEM,5,269
FITEM,5,-270
CM,_Y,LINE
LSEL, , , ,P51X
CM,_Y1,LINE
CMSEL,,_Y
!*
LESIZE,_Y1, , ,18, , , , ,1
!*

!*length of rectangle-rear part into 4 divisions*!
FLST,5,4,4,ORDE,4
```

```
FITEM,5,113
FITEM,5,115
FITEM,5,129
FITEM,5,-130
CM,_Y,LINE
LSEL, , , ,P51X
CM,_Y1,LINE
CMSEL,,_Y
!*
LESIZE,_Y1, , ,4, , , , ,1
!*

!*manual mesh size control for cable*!
!*tiny thickness into 1 division*!
FLST,5,3,4,ORDE,3
FITEM,5,290
FITEM,5,-291
FITEM,5,313
CM,_Y,LINE
LSEL, , , ,P51X
CM,_Y1,LINE
CMSEL,,_Y
!*
LESIZE,_Y1, , ,1, , , , ,1
!*

!*continue the previous: thickness into 3*!
FLST,5,3,4,ORDE,3
FITEM,5,134
FITEM,5,136
FITEM,5,295
CM,_Y,LINE
LSEL, , , ,P51X
CM,_Y1,LINE
CMSEL,,_Y
!*
LESIZE,_Y1, , ,3, , , , ,1
!*

!*continue the previous: length of median rectangle into 10*!
FLST,5,3,4,ORDE,3
FITEM,5,298
FITEM,5,-299
FITEM,5,312
CM,_Y,LINE
```

```
LSEL, , , ,P51X
CM,_Y1,LINE
CMSEL,,_Y
!*
LESIZE,_Y1, , ,10, , , , ,1
!*

!*continue the previous: length of small rectangle into 4*!
FLST,5,5,4,ORDE,5
FITEM,5,117
FITEM,5,121
FITEM,5,125
FITEM,5,132
FITEM,5,135
CM,_Y,LINE
LSEL, , , ,P51X
CM,_Y1,LINE
CMSEL,,_Y
!*
LESIZE,_Y1, , ,4, , , , ,1
!*

!*thickness of median rectangle into 4*!
FLST,5,5,4,ORDE,5
FITEM,5,131
FITEM,5,133
FITEM,5,288
FITEM,5,-289
FITEM,5,292
CM,_Y,LINE
LSEL, , , ,P51X
CM,_Y1,LINE
CMSEL,,_Y
!*
LESIZE,_Y1, , ,4, , , , ,1
!*

FLST,5,2,4,ORDE,2
FITEM,5,296
FITEM,5,-297
CM,_Y,LINE
LSEL, , , ,P51X
CM,_Y1,LINE
CMSEL,,_Y
!*
```

```
LESIZE,_Y1, , ,2, , , , ,1
!*

!*continue the previous: thickness into 3*!
FLST,5,14,4,ORDE,14
FITEM,5,138
FITEM,5,214
FITEM,5,230
FITEM,5,246
FITEM,5,302
FITEM,5,306
FITEM,5,311
FITEM,5,317
FITEM,5,323
FITEM,5,331
FITEM,5,337
FITEM,5,343
FITEM,5,349
FITEM,5,355
CM,_Y,LINE
LSEL, , , ,P51X
CM,_Y1,LINE
CMSEL,,_Y
!*
LESIZE,_Y1, , ,3, , , , ,1
!*

!*continue the previous: thickness of median rectangle into 4*!
FLST,5,7,4,ORDE,7
FITEM,5,315
FITEM,5,321
FITEM,5,328
FITEM,5,335
FITEM,5,341
FITEM,5,347
FITEM,5,353
CM,_Y,LINE
LSEL, , , ,P51X
CM,_Y1,LINE
CMSEL,,_Y
!*
LESIZE,_Y1, , ,4, , , , ,1
!*

!*continue the previous: thickness of median rectangle into 2*!
```

```
FLST,5,7,4,ORDE,7
FITEM,5,319
FITEM,5,325
FITEM,5,333
FITEM,5,339
FITEM,5,345
FITEM,5,351
FITEM,5,357
CM,_Y,LINE
LSEL, , , ,P51X
CM,_Y1,LINE
CMSEL,,_Y
!*
LESIZE,_Y1, , ,2, , , , ,1
!*

!*length of median rectangles into 20 divisions*!
FLST,5,5,4,ORDE,5
FITEM,5,293
FITEM,5,-294
FITEM,5,314
FITEM,5,316
FITEM,5,318
CM,_Y,LINE
LSEL, , , ,P51X
CM,_Y1,LINE
CMSEL,,_Y
!*
LESIZE,_Y1, , ,20, , , , ,1
!*

!*joint lines between cable and balls into 2 divisions*!
FLST,5,15,4,ORDE,15
FITEM,5,267
FITEM,5,300
FITEM,5,-301
FITEM,5,303
FITEM,5,-304
FITEM,5,310
FITEM,5,320
FITEM,5,322
FITEM,5,324
FITEM,5,334
FITEM,5,336
FITEM,5,338
```

```
FITEM,5,346
FITEM,5,348
FITEM,5,350
CM,_Y,LINE
LSEL, , , ,P51X
CM,_Y1,LINE
CMSEL,,_Y
!*
LESIZE,_Y1, , ,2, , , , ,1
!*

!*lines between balls into 8 divisions*!
FLST,5,10,4,ORDE,10
FITEM,5,305
FITEM,5,307
FITEM,5,326
FITEM,5,-327
FITEM,5,329
FITEM,5,-330
FITEM,5,332
FITEM,5,340
FITEM,5,342
FITEM,5,344
CM,_Y,LINE
LSEL, , , ,P51X
CM,_Y1,LINE
CMSEL,,_Y
!*
LESIZE,_Y1, , ,8, , , , ,1
!*

!*longest length of cable into 100 divisions*!
FLST,5,5,4,ORDE,5
FITEM,5,308
FITEM,5,-309
FITEM,5,352
FITEM,5,354
FITEM,5,356
CM,_Y,LINE
LSEL, , , ,P51X
CM,_Y1,LINE
CMSEL,,_Y
!*
LESIZE,_Y1, , ,100, , , , ,1
!*
```

```
!*mesh blade, receptacle, and cable*!
FLST,5,65,5,ORDE,2
FITEM,5,1
FITEM,5,-65
CM,_Y,AREA
ASEL, , , ,P51X
CM,_Y1,AREA
CHKMSH,'AREA'
CMSEL,S,_Y
!*
MSHKEY,1
AMESH,_Y1
MSHKEY,0
!*
CMDELE,_Y
CMDELE,_Y1
CMDELE,_Y2
!*mesh balls*!
SMRTSIZE,6

MSHKEY,0
FLST,5,3,5,ORDE,2
FITEM,5,66
FITEM,5,-68
CM,_Y,AREA
ASEL, , , ,P51X
CM,_Y1,AREA
CHKMSH,'AREA'
CMSEL,S,_Y
!*
AMESH,_Y1
!*
CMDELE,_Y
CMDELE,_Y1
CMDELE,_Y2
!*

SAVE,'model_LongBlade_static_LowE_step2','db','C:\Ansys_program\Molex_Auto_Mo
del\Model2D_formal2\'

!*generate contact pair*!
!*
/COM, CONTACT PAIR CREATION - START
CM,_NODECM,NODE
CM,_ELEMCM,ELEM
```

```
CM,_KPCM,KP
CM,_LINECM,LINE
CM,_AREACM,AREA
CM,_VOLUCM,VOLU
/GSAV,cwz,gsav,,temp
MP,MU,1,0.33
MAT,1
MP,EMIS,1,7.88860905221e-031
R,5
REAL,5
ET,2,169
ET,3,172
R,5,,,0.01,0.1,0,
RMORE,,,1.0E20,0.0,1.0,
RMORE,0.0,0,1.0,,1.0,0.5
RMORE,0,1.0,1.0,0.0,,1.0
KEYOPT,3,3,0
KEYOPT,3,4,0
KEYOPT,3,5,0
KEYOPT,3,7,0
KEYOPT,3,8,0
KEYOPT,3,9,0
KEYOPT,3,10,1
KEYOPT,3,11,0
KEYOPT,3,12,0
KEYOPT,3,2,0
! Generate the target surface
LSEL,S,,,2
LSEL,A,,,4
LSEL,A,,,5
LSEL,A,,,6
LSEL,A,,,7
CM,_TARGET,LINE
TYPE,2
NSLL,S,1
ESLN,S,0
ESURF
CMSEL,S,_ELEMCM
! Generate the contact surface
LSEL,S,,,13
LSEL,A,,,17
LSEL,A,,,33
LSEL,A,,,40
LSEL,A,,,42
LSEL,A,,,43
```

```
LSEL,A,,,47
LSEL,A,,,51
LSEL,A,,,156
LSEL,A,,,262
CM,_CONTACT,LINE
TYPE,3
NSLL,S,1
ESLN,S,0
ESURF
ALLSEL
ESEL,ALL
ESEL,S,TYPE,,2
ESEL,A,TYPE,,3
ESEL,R,REAL,,5
/PSYMB,ESYS,1
/PNUM,TYPE,1
/NUM,1
EPLOT
ESEL,ALL
ESEL,S,TYPE,,2
ESEL,A,TYPE,,3
ESEL,R,REAL,,5
CMSEL,A,_NODECM
CMDEL,_NODECM
CMSEL,A,_ELEMCM
CMDEL,_ELEMCM
CMSEL,S,_KPCM
CMDEL,_KPCM
CMSEL,S,_LINECM
CMDEL,_LINECM
CMSEL,S,_AREACM
CMDEL,_AREACM
CMSEL,S,_VOLUCM
CMDEL,_VOLUCM
/GRES,cwz,gsav
CMDEL,_TARGET
CMDEL,_CONTACT
/COM, CONTACT PAIR CREATION - END
/MREP,EPLOT

EPLOT

SAVE,'model_LongBlade_static_LowE_step3','db','C:\Ansys_program\Molex_Auto_Mo
del\Model2D_formal2\'
```

APPENDIX D ANSYS LOG FILE FOR THE TRANSIENT ANALYSIS OF THE FEA MODEL

```
/CWD,'C:\Ansys_program\Molex_Auto_Model\Model2D_formal2'
RESUME,'model_LongBlade_static_LowE_step3','db','C:\Ansys_program\Molex_Auto_
Model\Model2D_formal2\',0,0

EPLOT
!*
FINISH
/SOL
!*define loads*!
!*The end of wire is fixed*!
FLST,2,3,1,ORDE,3
FITEM,2,1286
FITEM,2,2112
FITEM,2,2710
!*
/GO
D,P51X, ,0, , , ,ALL, , , , ,

!*read sine_static_xxHz_0p3mm function*!
*DEL,_FNCNAME
*DEL,_FNCMTID
*DEL,_FNCCSYS
*SET,_FNCNAME,'SS0p3_40'
*SET,_FNCCSYS,0
! /INPUT,sine_static_40Hz_0p3mm.func
*DIM,%_FNCNAME%,TABLE,6,6,1,,,,%_FNCCSYS%
!
! Begin of equation: 0.0006*sin(251.2*{TIME})
*SET,%_FNCNAME%(0,0,1), 0.0, -999
*SET,%_FNCNAME%(2,0,1), 0.0
*SET,%_FNCNAME%(3,0,1), 0.0
*SET,%_FNCNAME%(4,0,1),0.0
*SET,%_FNCNAME%(5,0,1), 0.0
*SET,%_FNCNAME%(6,0,1), 0.0
```

```
*SET,%_FNCNAME%(0,1,1), 1.0, -1, 0, 251.2, 0, 0, 1
*SET,%_FNCNAME%(0,2,1), 0.0, -2, 0, 1, -1, 3, 1
*SET,%_FNCNAME%(0,3,1),   0, -1, 9, 1, -2, 0, 0
*SET,%_FNCNAME%(0,4,1), 0.0, -2, 0, 0.0006, 0, 0, -1
*SET,%_FNCNAME%(0,5,1), 0.0, -3, 0, 1, -2, 3, -1
*SET,%_FNCNAME%(0,6,1), 0.0, 99, 0, 1, -3, 0, 0
! End of equation: 0.0006*sin(251.2*{TIME})
!-->

!*define displacement of blade at x-axis as 0*!
FLST,2,3,1,ORDE,3
FITEM,2,121
FITEM,2,141
FITEM,2,143
!*
/GO
D,P51X, ,0, , , ,UX, , , , ,

!*define displacement of blade at y-axis as sine_static_xxHz_0p3mm function*!
FLST,2,3,1,ORDE,3
FITEM,2,121
FITEM,2,141
FITEM,2,143
!*
/GO
D,P51X, , %SS0p3_40% , , , ,UY, , , , ,

!*solution control*!
!*analysis type: transient*!
ANTYPE,4
TRNOPT,FULL
LUMPM,0
!*
ANTYPE,4
NLGEOM,1
NSUBST,800,800,800
OUTRES,ERASE
OUTRES,ALL,ALL
TIME,0.5
NEQIT,100

!*solve*!
/STATUS,SOLU
/nerr,100,100,off
SOLVE
```

APPENDIX E ANSYS LOG FILE FOR THE HARMONIC ANALYSIS OF THE FEA MODEL

```
/CWD,'C:\Ansys_program\Molex_Auto_Model\Model2D_formal2'
RESUME,'model_LongBlade_static_LowE_step3','db','C:\Ansys_program\Molex_Auto_
Model\Model2D_formal2\',0,0

/SOLU
!*
ANTYPE,3
!*
!*
HROPT,FULL
HROUT,ON
LUMPM,0
!*
EQSLV,FRONT,1e-008,
PSTRES,0
!*
HARFRQ,10,75,
NSUBST,65,
KBC,1
!*
ALPHAD,0,
BETAD,0,
DMPRAT,0,
!*

FLST,2,3,1,ORDE,3
FITEM,2,1236
FITEM,2,2062
FITEM,2,2660
!*
/GO
D,P51X, ,0,0, , ,ALL, , , , ,

FLST,2,3,1,ORDE,3
```

```
FITEM,2,121
FITEM,2,131
FITEM,2,133
!*
/GO
D,P51X, ,0,0, , ,UX, , , , ,

FLST,2,3,1,ORDE,3
FITEM,2,121
FITEM,2,131
FITEM,2,133
!*
/GO
D,P51X, ,0.0005,0, , ,UY, , , , ,

/STATUS,SOLU
SOLVE
```